CANADIAN THESES

THÈSES CANADIENNES

NOTICE

The quality of this microfiche is heavily dependent upon the quality of the original thesis submitted for microfilming. Every effort has been made to ensure the highest quality of reproduction possible.

If pages are missing, contact the university which granted the degree.

Some pages may have indistinct print especially if the original pages were typed with a poor typewriter ribbon or if the university sent us an inferior photocopy.

Previously copyrighted materials (journal articles, published tests, etc.) are not filmed.

AVIS

La qualité de cette microfiche dépend grandement de la qualité de la thèse soumise au microfilmage. Nous avons tout fait pour assurer une qualité supérieure de reproduction.

S'il manque des pages, veuillez communiquer avec l'université qui a conféré le grade.

La qualité d'impression de certaines pages peut laisser à désirer, surtout si les pages originales ont été dactylographiées à l'aide d'un ruban usé ou si l'université nous a fait parvenir une photocopie de qualité inférieure.

Les documents qui font déjà l'objet d'un droit d'auteur (articles de revue. examens publiés. etc) ne sont pas microfilmés

THIS DISSERTATION HAS BEEN MICROFILMED EXACTLY AS RECEIVED

LA THÈSE A ÉTÉ MICROFILMÉE TELLE QUE NOUS L'AVONS REÇUE

Canada

THE UNIVERSITY OF ALBERTA

AN INVESTIGATION OF THE EFFECTS OF EXTERNAL CAVITY FEEDBACK

ON SEMICONDUCTOR LASERS

by

R. D. ANDERSON

A THESIS

SUBMITTED TO THE FACULTY OF GRADUATE STUDIES AND RESEARCH

IN PARTIAL FULFILMENT OF THE REQUIREMENTS FOR THE DEGREE

OF MASTER of SCIENCE

DEPARTMENT OF ELECTRICAL ENGINEERING

EDMONTON, ALBERTA

SPRING, 1986

Permission has been granted to the National Library of Canada to microfilm this thesis and to lend or sell copies of the film.

The author (copyright owner) has reserved other publication rights, and neither the thesis nor extensive extracts from it may be printed or otherwise reproduced without his/her written permission.

L'autorisation a été accordée à la Bibliothèque nationale du Canada de microfilmer cette thèse et de prêter ou de vendre des exemplaires du film.

L'auteur (titulaire du droit d'auteur) se réserve les autres droits de publication; ni la thèse ni de longs extraits de celle-ci ne doivent être imprimés ou autrement reproduits sans son autorisation écrite.

THE UNIVERSITY OF ALBERTA

RELEASE FORM

NAME OF AUTHOR   R. D. ANDERSON

TITLE OF THESIS   AN INVESTIGATION OF THE EFFECTS OF

EXTERNAL CAVITY FEEDBACK ON

SEMICONDUCTOR LASERS

DEGREE FOR WHICH THESIS WAS PRESENTED   MASTER of SCIENCE

YEAR THIS DEGREE GRANTED   SPRING, 1986

Permission is hereby granted to THE UNIVERSITY OF
ALBERTA LIBRARY to reproduce single copies of this
thesis and to lend or sell such copies for private,
scholarly or scientific research purposes only.

The author reserves other publication rights, and
neither the thesis nor extensive extracts from it may
be printed or otherwise reproduced without the author's
written permission.

(SIGNED) ....

PERMANENT ADDRESS:

....

....

....

DATED ....19 ..

THE UNIVERSITY OF ALBERTA

FACULTY OF GRADUATE STUDIES AND RESEARCH

The undersigned certify that they have read, and
recommend to the Faculty of Graduate Studies and Research,
for acceptance, a thesis entitled AN INVESTIGATION OF THE
EFFECTS OF EXTERNAL CAVITY FEEDBACK ON SEMICONDUCTOR LASERS
submitted by R. D. ANDERSON in partial fulfilment of the
requirements for the degree of MASTER of SCIENCE.

....
Supervisor
....
....
....

Date...March 6, 1986..........

Dedication

To Kelly

Abstract

Coherent optical communication systems require semiconductor lasers, which oscillate in a single longitudinal mode with an extremely narrow spectral width, as sources for the transmitter and local oscillator.

This thesis discusses the laser parameters which affect the spectral content of the output. It is shown that increasing the photon lifetime in the resonator causes the spontaneous emission content in the output to decrease and hence, the longitudinal mode spectral width to decrease. The theoretical aspects of external cavity feedback are developed.

Experimental results are presented which demonstrate:

1. Varying longitudinal mode spectral width with varying feedback levels.

2. A semiconductor laser, with external grating feedback, which oscillates in a single longitudinal mode and is tunable over a frequency range of approximately 1.8Thz.

Acknowledgement

I wish to express gratitude towards the following:

Amnon Yariv for writing "Optical Electronics". Without this valuable information source, the thesis would have been astronomically more difficult.

Randy Giles, Jann Binder, Dominique Jodoin, and Zongqiang Ge for the many illuminating theoretical discussions which we engaged in and also for their input to the experimental work.

Kees denHartigh for his technical assistance.

The gentlemen in the Electrical Engineering shop for their skillful fabrications of some of the equipment used in the experimental work.

Bell Northern Research; the principal funders of the thesis. The providers of additional funding:

    Natural Sciences and Engineering Research Council

    University of Alberta

    Alberta Government Telephones

Dr. G. Cormack for administering the project.

Table of Contents

List of Tables

x

List of Figures

1. INTRODUCTION

1.1 HISTORY OF COHERENT OPTICAL COMMUNICATIONS

Lasers, the prerequisite for the realization of coherent optical communication systems, were proposed by Schawlow and Townes [1] in 1958. Subsequently, in 1960, Maiman [2] succeeded in inducing stimulated emission of photons in a ruby crystal coated on two parallel faces with silver. This was the first actual demonstration of a laser.

The early 1960's were host to a great deal of research in the areas of lasers and detection of optical signals. This research provided a stimulus for research in the application of lasers to communications.

In 1965, Goodwin and Pedinoff [3] experimented with an optical heterodyne system. They demonstrated "that the sensitivity of the indium arsenide detector is improved in excess of four orders of magnitude by the heterodyne system.". Goodwin [4,5] followed up on this work with a 3.39um heterodyne system in 1967, and a $10.6\mu m$ CO_2 system in 1968. Due to their high power capabilities, the CO_2 systems were studied in detail in the late 1960's [6].

The development of these long wavelength systems was quite successful. However, since the systems involved communications over atmospheric links, the signals suffered from turbulent degradations which often rendered the signal unsuitable for heterodyne detection [7]. Delange and Dietrich [8] demonstrated that "nearly ideal performance is

1

possible" in an enclosed transmission path. It was evident that if a practical waveguide could be developed which would ensure little or no interference along the transmission path, the feasibility of the link would be greatly increased.

Proceeding at the same time as the development of the coherent systems was research on glass fibers as optical waveguides. In 1966, the best fibers had losses greater than 1000 dB/km. However, Kao and Hockman [9] at Standard Telecommunications Laboratories in England speculated that losses of 20 dB/km should be attainable. It was felt that such fibers would be viable for communication systems.

The major breakthrough needed for useful fiber transmission was announced by Corning Glass Works, New York, in 1970. Researchers Kapron, Keck, and Maurer [10] reported fibers with 7 dB/km radiation losses. More recently, fibers with losses less than 0.5 dB/km have been developed [11]. Hence, the medium for viable optical communication exists today.

Unfortunately, the operating wavelength of the CO_2 systems did not coincide with either the minimum attenuation or dispersion regions of the optical fibers. A union of the existing heterodyne systems with the newly developed fibers was not possible.

Extensive research was carried out on semiconductor lasers in the 1960's and the characteristics of most of the constituent materials were known by 1970 [12]. The fiber

optic communication systems developed during the 1970's were operated initially in the 0.8-0.9μm region with research advancing to the 1.3μm and 1.55μm regions where the fiber dispersion is a minimum for the former and losses are a minimum for the latter.

The early semiconductor lasers were appropriate for Intensity Modulated Direct Detection (IMDD) Systems. However, they were not sufficiently stable nor coherent to be utilized in heterodyne/homodyne systems. For this reason, IMDD systems were concentrated on throughout the 1970's and advanced to the point where the systems were approaching receiver noise limitations.

During the late 1970's, research on coherent optical systems which utilize semiconductor lasers and glass fiber began to increase. The first demonstration of such a system was in 1980 by NTT in Japan [13].

Research on coherent optical communications remains active today. A great deal of the recent work concentrates on improving the components of the system.

1.2 COHERENT COMMUNICATIONS / NARROW LINEWIDTH LASERS

The following discussion is meant only as an introduction to why the topic of external cavity feedback lasers was deemed important to study. It is not an exhaustive introduction to coherent optical communications. The interested reader is invited to read an excellent tutorial by I.W. Stanley [14]. The following discussion is

derived from Stanley's tutorial.

In conventional optical communication systems, the transmitting laser is simply turned off and on and the receiver detects only the presence or absence of an optical pulse. An analogy is often made between this intensity modulation technique and the transmission technique of early spark gap radio. Coherent optical communication systems, however, utilize the phase information of the transmitting laser in order to benefit from the inherent increase in system sensitivity. The increase in sensitivity, which is discussed in detail below, is due to the presence of a local oscillator field.

Consider Figure 1-1 which shows a transmitted optical field being combined with a local oscillator field and the summed field being incident on the detector. Assume the fields have identical states of polarization and that the summing process is 100% efficient.

The detector is sensitive to incident optical power which is proportional to the square of the optical field. Furthermore, the current output by the detector due to the incident optical field is given by

$$I = \frac{\eta q P}{h \nu} \qquad (1-1)$$

where η is the quantum efficiency of the detector, q is the electronic charge, P is the power of the incident field, h is Planck's constant, and ν is the frequency of the optical

Field Combining Element

E_R=Received Field

E_L=Local Oscillator Field

E_D=Detected Field
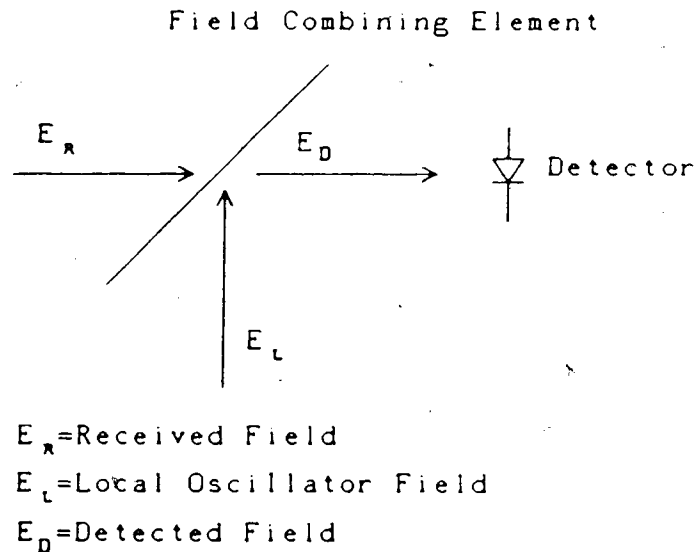
Figure 1-1 Summation of Received Optical Field with the Local Oscillator Field.

field. If the constant of proportionality between the power and the square of the amplitude of the incident electric field, E^2, is taken as K_0, then

$$P = K_0 E_R^2 \ . \tag{1-2}$$

Combining Equations 1-1 and 1-2 yields

$$I = \frac{K_0 \eta q E_R^2}{h\nu} \tag{1-3}$$

which shows that the detector current is proportional to the square of the total incident field.

Now, the electric field incident on the detector face is

$$\hat{E}_D = \hat{E}_R \cos(\omega_R t) + \hat{E}_L \cos(\omega_L t) \qquad (1-4)$$

where ω_L is the angular frequency of the local oscillator field and ω_R is the angular frequency of the received field. The circumflex above the field variable indicates absolute amplitude. Neglecting the high frequency components, which are not passed by the detector, the square of the total field is

$$\hat{E}_D^2 = \frac{1}{2}(\hat{E}_R^2 + \hat{E}_L^2) + \hat{E}_R \hat{E}_L \cos(\omega_R - \omega_L)t . \qquad (1-5)$$

There are two cases which arise from Equation 1-5 .

1. Homodyne: $\omega_L - \omega_R = 0$

2. Heterodyne: $\omega_L - \omega_R = \omega_F$ where ω_F is the intermediate frequency.

Case 1: Homodyne (Baseband filtered signal)

The component of the squared field which falls within the passband of the detector is

$$\hat{E}_D^2 = \frac{1}{2}(\hat{E}_R^2 + \hat{E}_L^2) + \hat{E}_R \hat{E}_L . \qquad (1-6)$$

In the case of modulation of the received field (frequency, phase, or amplitude), the information in the received field introduces time dependent changes to the $E \cos(\omega_R t)$ term in Equation 1-4. The net effect is that the last term in

Equation 1-6 becomes time dependent and the resulting detector signal current at the information signal frequency is

$$\hat{E}^2_D = 2E_R E_L \qquad (1-7)$$

where the peak values have been written in terms of rms values using

$$\hat{E} = \sqrt{2}\, E . \qquad (1-8)$$

The detector signal current becomes

$$I = \frac{2K_0 nq E_R E_L}{h\nu} . \qquad (1-9)$$

Case 2: Heterodyne (Intermediate frequency filtered signal)

The component of the squared field which falls within the passband is

$$\hat{E}^2_D = \hat{E}_R \hat{E}_L \cos(\omega_F t) . \qquad (1-10)$$

Writing Equation 1-10 in rms terms gives

$$\hat{E}^2_D = \sqrt{2}\, E_R E_L . \qquad (1-11)$$

The detector signal current becomes

$$I = \frac{\sqrt{2}\, K_0 \eta q E_R E_L}{h\nu} . \qquad (1-12)$$

The different factors of $\sqrt{2}$ which appear in the detector current for the heterodyne detection and homodyne detection cases are responsible for the 3db differences in receiver sensitivity associated with the two different modulation techniques. As will be shown, it is the product of the transmitted field and the received field which cause the reported [15] 15db to 20db improvement in receiver sensitivity over IMDD systems.

1.2.1 Detector Signal to Noise Ratio

The detector noise may be modelled by two terms. The first term is quantum noise or shot noise and is proportional to the received signal. The second term is thermal noise (Johnson noise) and is independent of the received signal.

The detector signal to noise ratio may be written as

$$SNR = \frac{I^2 R}{K_1 I^2 R + K_2} \qquad (1-13)$$

where K_1 is the shot noise proportionality constant, K_2 represents the thermal noise term and R is the input impedance of the receiver as seen by the detector diode.

Writing the signal to noise ratio in terms of the received field yields

$$SNR = \frac{KE_R^4 R}{KK_1 E_R^4 R + K_2} \qquad (1-14)$$

for the IMDD systems,

$$SNR = \frac{2KE_L^2 E_R^2 R}{2KK_1 E_L^2 E_R^2 R + K_2} \qquad (1-15)$$

for the heterodyne systems, and

$$SNR = \frac{4KE_L^2 E_R^2 R}{4KK_1 E_L^2 E_R^2 R + K_2} \qquad (1-16)$$

for the homodyne systems. K is given by

$$K = \frac{K_0 \eta q}{h\nu}^2 . \qquad (1-17)$$

From Equation 1-14, it is seen that, in IMDD systems, the acceptable minimum signal to noise ratio is limited by the thermal noise term, K_2. The thermal noise limitation to the signal to noise ratio limits the maximum transmission distance, since signal attenuation is proportional to fiber length. Using coherent detection schemes, Equations 1-15 and 1-16 show that the thermal noise limitation may be overcome by increasing the amplitude of the local oscillator signal E_L. The resulting increase in signal to noise ratio relates directly to an increase in receiver sensitivity which in turn relates directly to an increase in the maximum transmission distance.

The immediate advantage of coherent systems over IMDD systems lies in the improved receiver sensitivity due to overcoming thermal noise limitations. Another major advantage is the tremendous available bandwidth which may be utilized.

1.2.2 The Importance of the Laser Linewidth

There are four major requirements to be met for a successful coherent system which are not critically necessary for a conventional IMDD system. The requirements are:

1. Facility for modulating the phase, frequency, or amplitude of the laser.
2. A transmission path which maintains the temporal and spatial integrity of the phase.
3. A local oscillator at the receiver for heterodyne or homodyne mixing and detection.
4. A narrow linewidth single longitudinal mode laser.

This thesis concentrates on techniques for achieving narrow linewidth, single longitudinal mode operation of a semiconductor laser.

The necessity for stringent spectral properties of the laser is apparent when the following is considered. In a heterodyne system, the signal information is modulated onto an optical carrier which results in the signal information being present in the spectrum as bands on either side of the carrier frequency. First of all, assume that the carrier

center frequency is fixed. Then, from Figure 1-2, it is
seen that in order to avoid superimposing the laser spectrum
on top of the information spectrum (and losing the signal),
the linewidth of the laser must be considerably less than
the fundamental frequency (ie. 100Mhz) of the signal.

Jacobsen and Garret [16] have determined that the laser
linewidth in Hz must be less than 20% of the information
rate in bits/sec. Figure 1-2 conceptually illustrates the
above specification.

$$\Delta f_L < 0.2 \cdot f_s$$
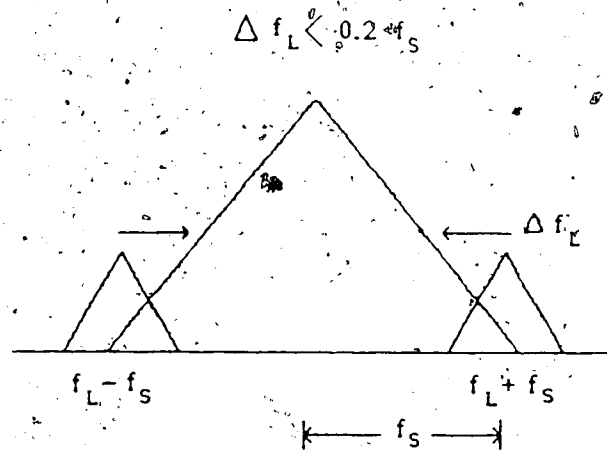
Figure 1-2 Signal Interference Effect of Excessive Laser
Linewidth

At 1.3μm and a bit rate of 100Mb/s, the requirement for
the laser linewidth to be 20% of the bit rate means that the
fractional stability, $\Delta f/f$, of the laser must be about 1

part in 10^-. Results have been reported where the
fractional stability was about 1 part in $10^{\cdot\,\circ}$ [17].

A related requirement is that the center frequency of
the laser must remain constant. In a homodyne system, the
difference of the transmitter and local oscillator center
frequencies must remain within the locking bandwidth of the
system controlling the local oscillator. In a heterodyne
system, the frequency difference must remain within the
control bandwidth of the feedback loop which controls the
local oscillator.

In summary, the two major requirements for the
semiconductor laser are that it exhibits a stable center
frequency and a narrow spectral linewidth.

1.2.3 Object of the Thesis

The purpose of the work reported in this thesis is to
gain an understanding of the properties of semiconductor
lasers which affect the laser spectrum.

Chapter 2 explores the theoretical origin of the
properties of, laser spectra. Chapter 3 introduces the
concept of external cavity feedback and the effect which
external feedback has on the laser spectrum. Chapter 4
presents and discusses the experimental investigation of the
properties of three external cavities. The three cavities
studied were:

1. Short external cavity with a mirror.

2. Long external cavity with a grin rod lens and a mirror.

3. Long external cavity with a grin rod lens and a diffraction grating.

Finally, Chapter 5 concludes with recommendations for furthering the study of external cavity feedback lasers at the University of Alberta.

2. THEORY OF LASER LINEWIDTH

2.1 ELECTRON TRANSITIONS

One of the hypotheses in the theory of quantum mechanics is that each of the electrons in an atom exist in one of a set of possible energy states. A narrow energy region, occupied by a number of allowed energy states, and bounded by regions essentially void of electronic activity (energy gaps), defines an energy band. Figure 2-1 illustrates two such bands separated by an energy gap. At at temperature of absolute zero, all energy states are occupied up to an energy known as the Fermi energy level. At temperatures above absolute zero, there is a well defined probability that some electrons are thermally excited into the band just above the Fermi energy level, known as the conduction band. The energy band immediately below the Fermi energy level is termed the valence band.
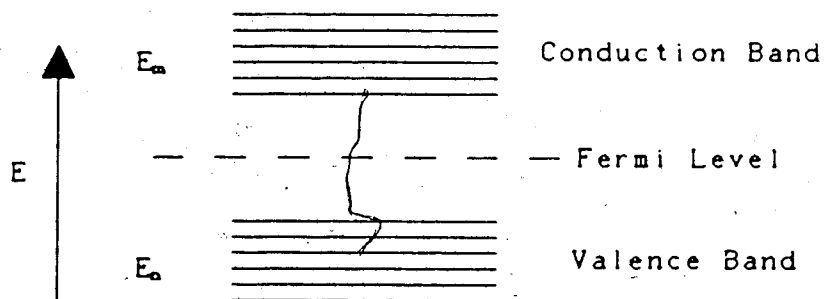
Figure 2-1 Energy Band Model of the Electrons in a Solid

Transitions from one energy state to another are characterized by the absorption or emission of an amount of energy equal to the energy difference between the two states. If the transition is radiative (ie. the energy transfer has been with an electromagnetic field), the frequency of the radiation emitted or absorbed is given by Bohr to be

$$\nu = \frac{\Delta E}{h} \qquad (2-1)$$

where $\Delta E = E_m - E_n$ is the nominal energy difference between the two states (typically the conduction and valence band edges), h is Planck's constant, and ν is the frequency of the radiation in Hz.

2.1.1 Spontaneous Transitions

An electron may undergo a non-induced transition, referred to as a spontaneous transition, from a high energy state to a lower energy state and, if the transition is radiative, emit a photon at a frequency given by Bohr's relation.

In an atomic system consisting of a large number of atoms, N_m of which are in the excited state designated by the quantum number m, the average number of these atoms undergoing a transition to level n per unit time is given by [18:pp.124]

$$\frac{dN_m}{dt} = A_{mn} N_m \qquad (2-2)$$

where A_{mn} is the spontaneous transition rate for the $m \to n$ transition.

The spontaneous transition rate implies a finite lifetime τ_{mn} associated with the transition $m \to n$. τ_{mn} represents the time required for the population to be reduced to e^{-1} times the original population.

Spontaneous emission is independent of direct electromagnetic field influences and hence is incoherent; there is no phase correlation to transitions that have occurred in the past or will occur in the future. Also, spontaneous transitions are strictly an emissive phenomena. Spontaneous absorption can not occur.

2.1.2 Lineshape Function

The idea that spontaneous emission is caused by a transition between two states representing two energy levels implies that the emitted radiation is monochromatic or, in other words, of single frequency. However, this is not strictly the case. Spectral analysis of the radiation yields a frequency distribution of non-zero width.

The lineshape function representing the spectral distribution of the radiation is denoted by $g(\nu)$. It is normalised so that

$$\int_{0}^{\infty} g(\nu)d\nu = 1 \qquad\blacksquare \qquad\qquad (2-3)$$

where $g(\nu)$ is a probability distribution function defining the probability that a spontaneous transition between levels m and n will release a photon in the frequency interval ν to $\nu+d\nu$. An example of a spectral lineshape function is illustrated in Figure 2-2.
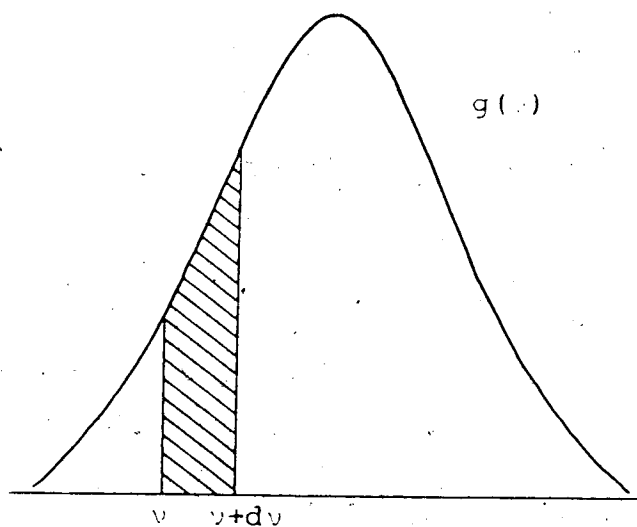
Figure 2-2 Spectral Lineshape Function

·The spectral distribution characterized by $g(\nu)$ is divided into the two categories of homogeneous and inhomogeneous broadening.

Homogeneous broadening describes the case where the spectral lineshape functions of the individual atoms are identical to the overall observed function $g(\nu)$. All transitions interact with the same 'pool' of electrons. It

is caused mostly by the finite lifetime τ of the excited state. It is also affected by atomic collisions which interrupt the relative phase between the atomic oscillations and the field in the crystal. Homogeneously broadened lineshape functions are typically modelled by a Lorentzian function of the type

$$g(\nu) = \frac{1}{(\nu-\nu_0)^2 + (\frac{1}{2\pi\tau})^2} \qquad (2-4)$$

which is the type of function illustrated in Figure 2-2.

Inhomogeneous broadening describes the case where the spectral lineshape functions of the individual atoms are different from the observed lineshape function, $g(\nu)$, of the system as a whole. In this case, the dominant mechanism is not the finite lifetime of the excited state. In gas lasers, one governing mechanism is Doppler shifting due to the velocity of the atoms in the gas. In crystal structures, inhomogeneous broadening may be due to crystal imperfections causing atomic neighbourhoods to vary. The imperfections have a variable effect on the spectral line profiles of photons from different regions in the crystal.

Under lasing conditions (Section 2.3), a medium which is inhomogeneously broadened will behave differently than a medium which is homogeneously broadened. An ideal homogeneously broadened medium will support only one lasing longitudinal mode due to the participation of all electrons in the single mode. The presence of the single mode results

in the onset of gain saturation at all frequencies. The mode which initially monopolizes the available gain will be the mode which requires the least gain to induce lasing. A medium which is inhomogeneously broadened can support several longitudinal modes since gain saturation due to oscillation at one frequency does not necessarily affect the available gain at another frequency.

2.1.3 Induced Transitions

When an atomic system is subjected to an electromagnetic field, the field may induce the electrons to change state. If the transition is from a lower energy level to a higher energy level, the atomic system absorbs energy from the field. If the opposite transition occurs, the atomic system emits energy to the field.

Induced transitions are characterized by a transition rate ω_i electrons/m^3 sec given by [18:pp.131]

$$\omega_i = \frac{c^3 \rho_\nu}{8\pi n^3 h\nu^3 t_s} g(\nu) \qquad (2-5)$$

where the suscript i indicates induced, c is the speed of light in free space, ρ is the mode energy density (joules/cm^3), η is the index of refraction in the medium, and t_s is the spontaneous lifetime of the excited state. It is important to note that w_i is proportional to the mode energy density and is "scaled" by the lineshape function $g(\nu)$.

Induced transitions differ from spontaneous transitions in two fundamental ways:

1. Induced transitions are both absorptive and emissive. Spontaneous transitions are emissive only.

2. Induced transition rates are proportional to the applied field. Spontaneous transition rates are independent of the applied field.

2.2 LIGHT AMPLIFICATION

Induced transitions make the phenomenon of light amplication possible under the proper conditions. A monochromatic wave travelling through an atomic medium will induce transitions provided the wave frequency is within the atomic resonance defined by the spectral lineshape function.

The net energy transfer, P, between the medium and the field (neglecting spontaneous transitions) is

$$\frac{P}{V} = (N_m - N_n)\omega_1 h\nu \tag{2-6}$$

where P/V is the net rate of energy transfer, per unit volume V, between the medium and the field. Neglecting any dissipation,

$$\frac{dI}{dz} = (N_m - N_n)\omega_1 h\nu \tag{2-7}$$

where I is the intensity of the field, and z is the displacement along the direction of propagation.

It is apparent that the monochromatic wave will increase in intensity as it propagates, through the medium whenever

$$N_m - N_n > 0 .$$ (2-8)

In semiconductor materials, the conventional gain condition $N_m - N_n > 0$ is governed by Fermi-Dirac statistics and becomes [18:pp.477]

$$f_c(E) \geq f_v(E)$$ (2-9)

where

$$f_c(E) = \frac{1}{e^{(E-E_{Fc})/KT} + 1}$$ (2-10)

and

$$f_v(E) = \frac{1}{e^{(E-E_{Fv})/KT} + 1} .$$ (2-11)

$f_c(E)$ represents the probability that a state in the conduction band is occupied. $f_v(E)$ represents the probability that the corresponding state in the valence band is occupied.

E_{Fc} and E_{Fv}, as shown in Figure 2-3, are known as quasi Fermi levels in the conduction and valence bands respectively. They are a steady state phenomena resulting

from a pumping mechanism which excites electrons into the
conduction band.

$$E_{Fc} - E_{Fv}$$ $$E_g$$ $$E_{FC}$$ $$E_F$$ $$E_{Fv}$$

o Unoccupied State (Holes)
● Occupied State   (Electrons)
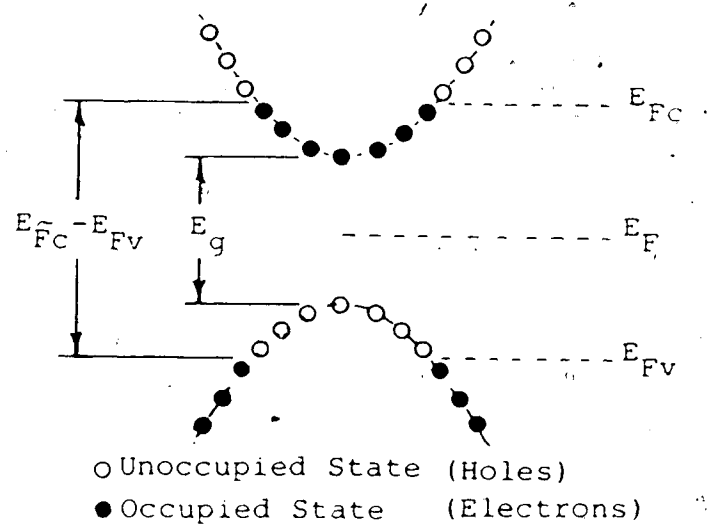
Figure 2-3   Quasi-Fermi Levels in the Conduction and Valence
Bands

Also, using the quasi Fermi levels, the range of
frequencies which are susceptible to gain then become

$$\frac{E_g}{h} < \nu < \frac{E_{Fc} - E_{Fv}}{h}$$ (2-12)

These limits define the boundaries of the spectral lineshape
function $g(\nu)$ as shown in Figure 2-4. (In light of the
previous discussion, the lineshape function is also known as
the gain curve.)

For photon energies less than E_g, no electron
transitions can occur between states in conduction and
valence bands. For photon energies greater than $E_{Fc} - E_{Fv}$,
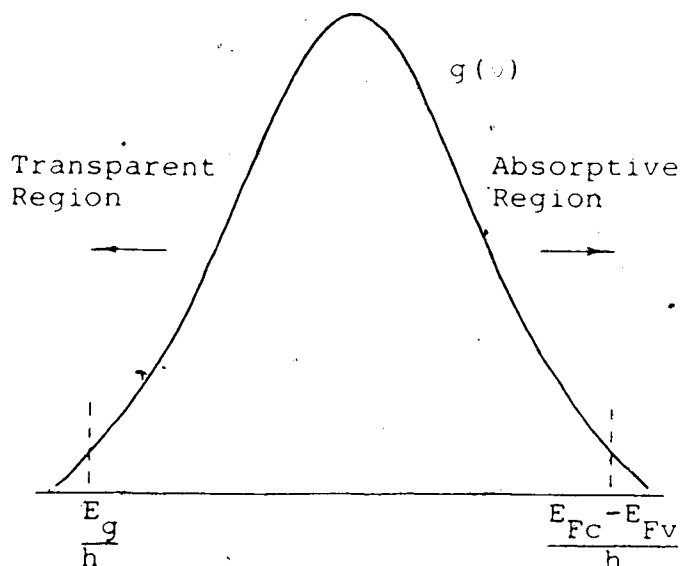
Figure 2-4   Boundaries of the Spectral Lineshape Function

the semiconductor extracts more radiative energy from the field than it is capable of providing and hence, it is absorptive.

2.3 LASER OSCILLATION

It has been stated that light amplification in a semiconductor material is possible provided an inversion condition is met and the incident light frequency is within the gain curve. Using feedback, it is possible to induce self-sustaining oscillations in the medium.

A semiconductor laser may be fabricated by cleaving a semiconductor crystal along two parallel planes which are orthogonal to the active region of the material. The active region is a junction between p-doped and n-doped semiconductor materials. The resulting interfaces act as mirrors and cause a portion of the emitted light to be fed

back into the laser. In the event that the fed back light is added in phase to the emitted light, oscillation is possible.

To analyse the laser system, the following parameters, which are illustrated in Figure 2-5, are necessary:

1. r_1, r_2 = amplitude reflectivities at the two interfaces.
2. α = intensity loss per unit length in the medium.
3. γ = intensity gain per unit length in the medium.
4. η = index of refraction of the medium.
5. l = cavity length.
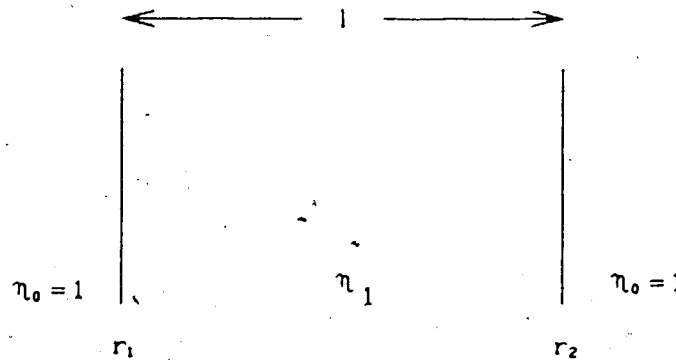
Figure 2-5 Laser Cavity Model

Oscillation will be sustained if a wave travelling through the medium is equal in amplitude and phase (within an integral multiple of 2π) to itself upon making one round trip through the cavity. In this case, the relationship

$$r_1 r_2 e^{(\gamma-\alpha)\ell} e^{-2jk_1\ell} = 1 \qquad (2-13)$$

must hold, where $k_1 = 2\pi/\lambda_1$ is the wavenumber in the medium and λ_1 is the wavelength in the medium. Solving for the phase and gain yields

$$k_1 = \frac{m\pi}{\ell} \qquad\qquad (2\text{-}14)$$

where m=1,2,3... and

$$\gamma = \alpha - \frac{1}{\ell}\ell n(r_1 r_2) \quad . \qquad\qquad (2\text{-}15)$$

Equations 2-14 and 2-15, respectively, are the phase and gain conditions required to sustain laser oscillation.

The allowable propagation constants k_1 are a discrete set characterized by a round trip phase, ϕ_1, in the cavity of an integral multiple of 2π. Figure 2-6 illustrates the allowed longitudinal modes superimposed on the gain curve.
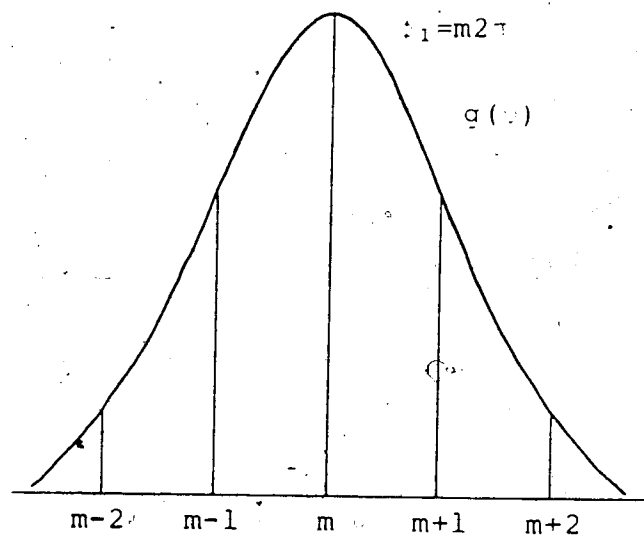
Figure 2-6 Solutions to Phase Condition Superimposed on the Gain Curve

The gain of the medium due to inversion must compensate for any distributed loss mechanisms in the cavity and the energy lost to transmission out of the cavity. Factors governing the required gain are discussed in more detail in Section 2.4.1 .

2.3.1 Fabry-Perot Resonator

The configuration of a semiconductor laser lends readily to modelling the laser as a Fabry-Perot resonator with an active medium.

The Fabry-Perot resonator was developed by Charles Fabry and Alfred Perot in 1899. The simplest form of the resonator is two plane parallel mirrors, with high reflectivities, separated by a distance d.

The important parameters of a Fabry-Perot resonator are:

1. Finesse

2. Free Spectral Range

3. Resolution

The resonator finesse is related to the q-factor of the resonator. It is determined by the flatness of the mirrors, stray light rejection, and mirror reflectivity. The reflectivity is the dominant contributor to the finesse. Therefore, an estimate of the finesse may be determined with knowledge of the reflectivity only. The finesse, , is given as [19:pp.309]

$$F = \frac{\pi}{2} \sqrt{F} \qquad (2-16)$$

where

$$F = \left(\frac{2r}{1-r^2}\right)^2 . \qquad (2-17)$$

F is the coefficient of finesse and r is the amplitude reflectivity.

The free spectral range (FSR) is the fundamental frequency (or wavelength) that will constructively interfere in the resonator. It is given by

$$\Delta\nu_{FSR} = \frac{c}{2L} \qquad (2-18)$$

or, expressed in terms of the wavelength,

$$\Delta\lambda_{FSR} = -\frac{\lambda^2}{2L} . \qquad (2-19)$$

The Fabry-Perot resonator causes constructive interference of the fundamental or any of its harmonics of integer order m. The FSR also represents the maximum frequency deviation $\Delta\nu$ that a signal component can vary from a primary signal, say ν_0, which interferes with order n (ie. m=n), and be distinguishable from the n+1 order of interference of the primary signal ν_0. Figure 2-7 illustrates the free spectral range.

a)Fundamental T/2=C/L
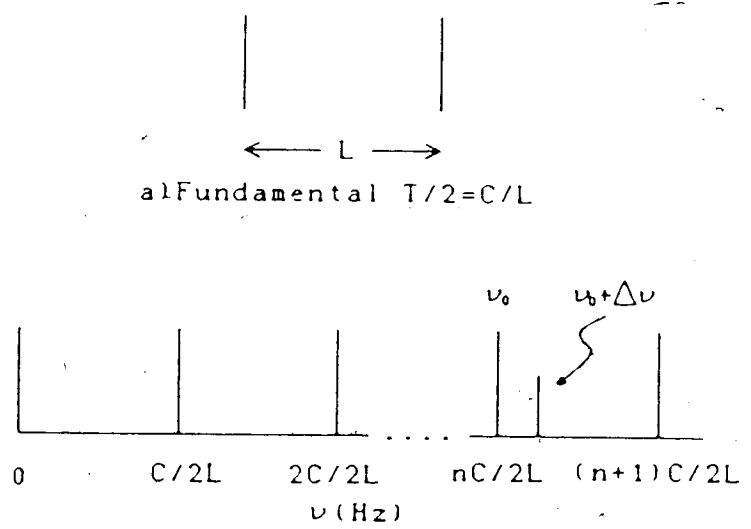
b)Primary signal ν_0 and component $\nu_0+\triangle\nu$.

Figure 2-7 Free Spectral Range of a Resonator

The longitudinal modes of a semiconductor laser are separated by the free spectral range of the laser cavity.

The resolution of the Fabry-Perot resonator is defined as the minimum separation of two components (ie. minimum $\Delta\nu$) that can be detected. The resolution is given by [19:pp.310]

$$\Delta\nu_{min} = \frac{C}{F2L} .$$

(2-20)

From equations 2-18 and 2-20, it is seen that the finesse is equivalent to the ratio of the free spectral range to the resolution;

$$F = \frac{\Delta\nu_{FSR}}{\Delta\nu_{min}} \quad . \qquad\qquad (2-21)$$

Figure 2-8 is a plot of the free spectral range and resolution versus cavity length l. The resolution is plotted for finesses equal to 100 and 50.

2.4 LONGITUDINAL MODE SPECTRAL WIDTH

The line width of the laser is defined here to be the full width half maximum (FWHM) wavelength spread of a single longitudinal mode. Figure 2-9 illustrates the FWHM of such a longitudinal mode.

The primary factors which govern the linewidth of the longitudinal modes are:

1. The photon lifetime in the resonator.

2. Degradation of coherence due to spontaneous emission.

3. Intensity to phase noise conversion.

4. Self pulsation or modulation of the laser.

5. Mode partition noise.

The photon lifetime in the resonator is dependant on the resonator type and quality. The semiconductor laser used for the experimental work can be modelled as a Fabry-Perot resonator.
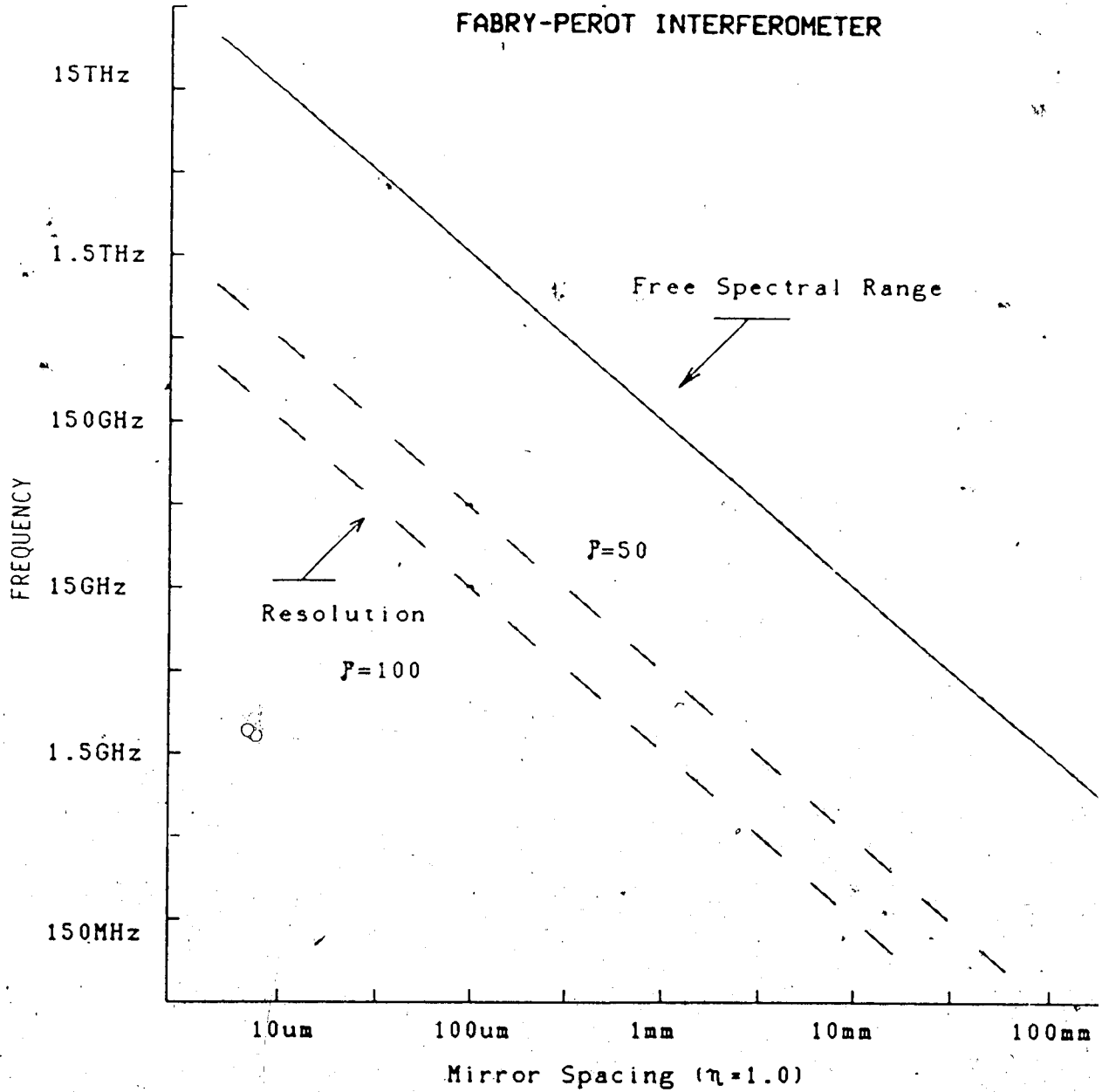
Figure 2-8 Fabry-Perot Resonator: Free Spectral Range and Resolution
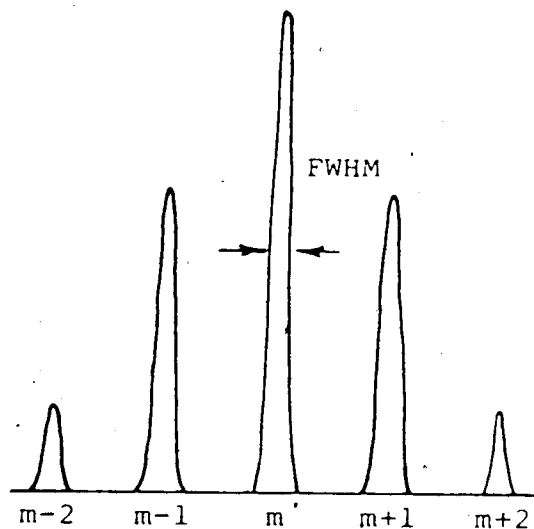
Figure 2-9   Full Width Half Maximum of a Longitudinal Mode

2.4.1 Photon Lifetime

The photon lifetime in the cavity is equivalent to the decay lifetime or the time it takes an electromagnetic field to decay to e^{-1} times its original value. In a simple Fabry-Perot resonator, the photon lifetime t_c is the time required for a field to decay to e^{-1} of its original value and is related to the cavity parameters by

$$t_c = \frac{n}{c\left[\alpha - \frac{1}{\ell}\ell n(r_1 r_2)\right]} \qquad (2-22)$$

where c is the free space velocity of light. The photon lifetime arises from the single pass losses

$$\left(\alpha - \frac{1}{\ell}\ell n(r_1 r_2)\right)\ell \qquad (2-23)$$

which occur in a time

$$t = \frac{n\ell}{C} \qquad (2-24)$$

The photon lifetime and FWHM are related by [18:pp.107]

$$\Delta\nu_{1/2} = \frac{1}{2\pi t_c} \qquad (2-25)$$

Equation 2-25 shows that an increase in the photon lifetime results in a decrease in the longitudinal mode width. An increase in the photon lifetime can be achieved by either increasing the cavity length 1 or increasing the reflectivities of the resonator mirrors. Photon lifetime is discussed in more detail in conjunction with spontaneous transitions in Section 2.4 .

2.4.2 Linewidth Degradation Due To Spontaneous Emission

Spontaneous transitions interrupt the phase of the cavity field. This phase interruption manifests itself as a limiting factor on attempts to decrease the FWHM of the longitudinal modes.

Schawlow and Townes [1] and later, using a different model, Henry [20], derived the expression

$$\Delta\nu_0 = \frac{2\pi h\nu_0(\Delta\nu_{1/2})^2}{P} \frac{N_2}{(N_2-N_1)_t} \qquad (2-26)$$

where $\Delta\nu_0$ is the FWHM of the longitudinal modes, ν_0 is the longitudinal mode centre frequency, $\Delta\nu_{1/2}$ is the FWHM of the

resonator, P is the mode power, and $(N_2-N_1)_t$ is the
threshold inversion density. The expression indicates an
inverse P relationship for the linewidth. Eventually, due
to the increase in N_2 with P, the FWHM approaches a constant
and becomes insensitive to further increases in optical
power. This residual linewidth, which is illustrated in
Figure 2-10, is due to the spontaneous transitions in the
cavity.
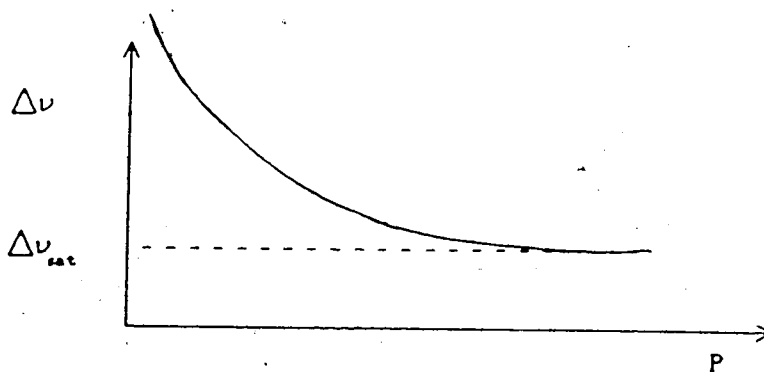
Figure 2-10   FWHM vs Optical Power

Typical values for spontaneous emission limited
linewidths are 2×10^{-3}Hz for HeNe lasers and 1.5×10^{6}Hz for
GaAs lasers [18:pp.334]. The large difference is due mainly
to the photon lifetime differences in the two lasers.

2:4.3 Linewidth Enhancement Factor

Further to the derivation of the basic relationship for
linewidth, Henry [20] included an additional term

$$\alpha = \frac{\Delta \eta'}{\Delta \eta''} \qquad\qquad (2-27)$$

which accounts for changes in the complex susceptibility of the semiconductor medium with respect to changes in the carrier density. $\Delta \eta'$ is the change in the real part of the index of refraction which is due to the presence of fewer electrons for "resonant" interaction with the field. $\Delta \eta''$ is the change in the imaginary part (gain) of the index of refraction due to a change in the electron inversion density.

The overall linewidth $\Delta \nu$ is altered by α according to

$$\Delta \nu = \Delta \nu_0 (1 + \alpha^2) \qquad\qquad (2-28)$$

where $\Delta \nu_0$ is the original line width derived by Schawlow and Townes.

For semiconductor lasers, α is typically 3 to 6 [20]. It represents a significant increase in linewidth over the linewidth predicted by the Schawlow-Townes formula.

2.5 INTERDEPENDANCE BETWEEN PHOTON LIFETIME AND SPONTANEOUS EMISSION

2.5.1 Rate Equation Model

The gross dynamics of a semiconductor laser can be understood by the use of a simple model and a series of associated rate equations.

Figure 2-11 is a four level model of a laser.
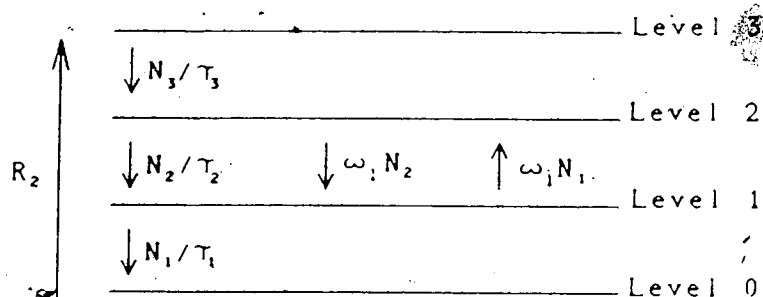
Figure 2-11 Simple Four Level Model of a Laser

Level 3 represents all energy levels into which electrons are pumped. Level 2 is the excited state of interest. In general, the spontaneous transition rate from level 3 to level 2, N_3/τ_3, occurs much faster than any other transition into or out of level 2. For this reason, the pumping may be thought of as being directly into level 2 and therefore, level 3 may be neglected. Level 1 represents the relaxed state. Levels 2 and 3 participate in the radiative emission processes. Level 0 is the ground state and is the electron source. R_2 is the rate of pumping of electrons into the excited states.

A set of coupled differential equations or rate equations can be written which describe the dynamics of the

electron populations at the various energy levels and the energy density in the laser cavity. The rate equations are

$$\frac{dN_2}{dt} = R_2 - \frac{N_2}{\tau_2} - \omega_1(N_2-N_1)_t \quad , \qquad (2-29)$$

$$\frac{dN_1}{dt} = \omega_1(N_2-N_1)_t - \frac{N_1}{\tau_1} + \frac{N_2}{\tau_2} \quad , \qquad (2-30)$$

and

$$\frac{d\rho_\nu}{dt} = \omega_1(N_2-N_1)_t \, h\nu - \frac{\rho_\nu}{t_c} \cdot \qquad (2-31)$$

where ω_1, the induced transition rate, is defined y Equation 2-5. Note that $(N_2-N_1)_t$ is the threshold inversion density and is constant when the laser current exceeds the threshold current. The subscript t is used to designate the threshold. All equations are functions of time. Under steady state conditions,

$$\frac{dN_2}{dt} = \frac{dN_1}{dt} = \frac{d\rho_\nu}{dt} = 0 \qquad (2-32)$$

and therefore

$$N_2 = (R_2 - \omega_1(N_2 - N_1)_t)\tau_2 \quad , \qquad (2-33)$$

$$N_1 = \omega_1(N_2 - N_1)\tau_1 + N_2 \frac{\tau_1}{\tau_2} , \qquad (2\text{-}34)$$

and

$$\rho_\nu = \Delta N_t \omega_1 h\nu t_c . \qquad (2\text{-}35)$$

where $\Delta N_t = (N_2 - N_1)_t$. Equations 2-32 to 2-35 are utilised in the following section.

2.5.2 Linewidth Degradation Ratio

The linewidth degradation ratio

$$\zeta = \frac{N_2}{\omega_1 \Delta N_t \tau_2} \qquad (2\text{-}36)$$

is here introduced. It is the ratio of the rate of spontaneous transitions

$$\frac{N_2}{\tau_2} \qquad (2\text{-}37)$$

to the rate of induced transitions

$$\omega_1 \Delta N_t . \qquad (2\text{-}38)$$

It is apparent from Section 2.4, which deals with the effect that spontaneous emission has on the laser linewidth, that minimizing ζ will result in a narrower saturated linewidth.

Equation 2-36 indicates four parameters which, if possible, may be varied in order to minimize ζ. The excited carrier lifetime τ_2 is a fixed physical property and is not readily altered. In an efficient laser system, an increase in ΔN_t can only be attained by a corresponding increase in N_2 ($N_1 \approx 0$) and therefore, increasing ΔN_t has no effect on ζ. Finally, since ω_i is proportional to the mode energy density (Equation 2-5), ω_i may be increased by increasing the pumping. However, increasing the pumping also causes a proportional increase in N_2 and therefore has no effect on ζ.

In order to decrease ζ, ω_i must be increased while simultaneously not incurring a proportional increase to N_2 at a fixed pumping rate R_2.

2.5.3 The Relationship Between Photon Lifetime and the Steady State Properties of the Laser

In terms of inversion density, the required gain for laser oscillation may be expressed as [18:pp.133]

$$\gamma = \frac{\Delta N_t c^2 g(\nu)}{8\pi\eta^2 \nu^2 \tau_2} \tag{2-39}$$

which shows that the inversion density ΔN_t is directly proportional to the gain. This expression may be written as

$$\gamma = \Delta N_t H_1 \tag{2-40}$$

where

$$H_1 = \frac{C^2 g(\nu)}{8\pi n^2 \nu^2 \tau_2} \cdot \qquad (2-41)$$

(Equation 2-39 is derived specifically for gas lasers. However, it is useful to make the following points.)

Equation 2-22 may be written as

$$\frac{n}{t_c C} = \alpha - \frac{1}{\ell} \ln(r_1 r_2) \cdot \qquad (2-42)$$

Equating Equation 2-42 to Equation 2-15 yields

$$\gamma = \frac{n}{C t_c} \cdot \qquad (2-43)$$

Finally, equating 2-43 with 2-40 yields

$$\Delta N_t = \frac{n}{H_1 C t_c} \qquad (2-44)$$

which shows that the threshold inversion density, ΔN_t, is inversely proportional to the photon lifetime t_c.

Since, at steady state, the rate of electron transitions N_1/τ_1, out of the lasing system must equal the rate of electrons entering the lasing system, R_2 (which remains constant), the population of the relaxed state, N_{r}, remains constant. Therefore, N_2 decreases with increasing t_c. From Equation 2-33, since R_2 is constant and ΔN_t decreases, ω_{ir} must increase to satisfy a decrease in N_2.

Returning to Equation 2-36 and noting that in an efficient
laser system $N_2/\Delta N_t \simeq 1$, it is observed that an increase in
the photon lifetime results in a decrease in the degradation
ratio, ζ, due to the increase in ω_i. Since ω_i increases
when the photon lifetime is increased, the ratio of the rate
of spontaneous transitions to the rate of induced
transitions is decreased. Therefore, since the saturation
linewidth is proportional to the spontaneous content of the
laser output, the saturation linewidth is decreased by
increasing the photon lifetime.

A more qualitative point of view is to examine the
total electron movement into and out of the excited state
N_2. The movement of electrons into the excited state is
constant and is equal to R_2 electrons/cm³ sec. The movement
of electrons out of the excited state is

$$\omega_1 \Delta N_t + \frac{N_2}{\tau_2} . \qquad (2\text{-}45)$$

Neglecting the spontaneous transitions, N_2/τ_2, leaves

$$R_2 = \omega_1 \Delta N_t . \qquad (2\text{-}46)$$

If ω_i is increased, by increasing the photon lifetime,
ΔN_t must decrease in order to satisfy Equation (2-45). ΔN_t
may be decreased by either decreasing N_2 or increasing N_1.
The following arguement proves that N_1 must remain constant,
and therefore, ΔN_t can only be reduced by reducing N_2.

Consider Figure 2-12.
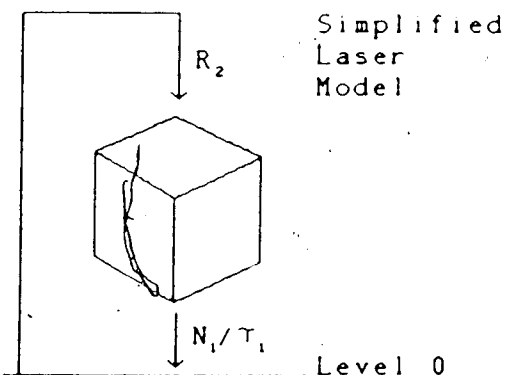
Figure 2-12   The Four Level Model is Represented by a Box

The detailed level model is replaced by a box [21]. The
rate of putting electrons into the box is R_2 and the rate of
taking electrons out of the box is N_1/τ_1, where R_2 and N_1/τ_1
are identical to the similar variables in the detailed
multi-level model. At steady state,

$$R_2 = N_1/\tau_1 \;.\qquad\qquad\qquad (2\text{-}47)$$

Since τ_1 is a physical constant, and R_2 remains constant, N_1
must also remain constant. Therefore, the population of the
excited state N_2 decreases to accomodate the decrease in the
required threshold inversion density ΔN_t . Figure 2-14 is a
flow chart which shows the chain of events following an
increase in the photon lifetime.

In summary, an increase in the photon lifetime results
in

Increase in photon lifetime

Decreased cavity losses   Increased energy density

Decreased required gain   Increased induced transition rate

                                 Decreased inversion density

                        Decreased excited level population

                Decreased spontaneous emission

        Decreased saturation linewidth
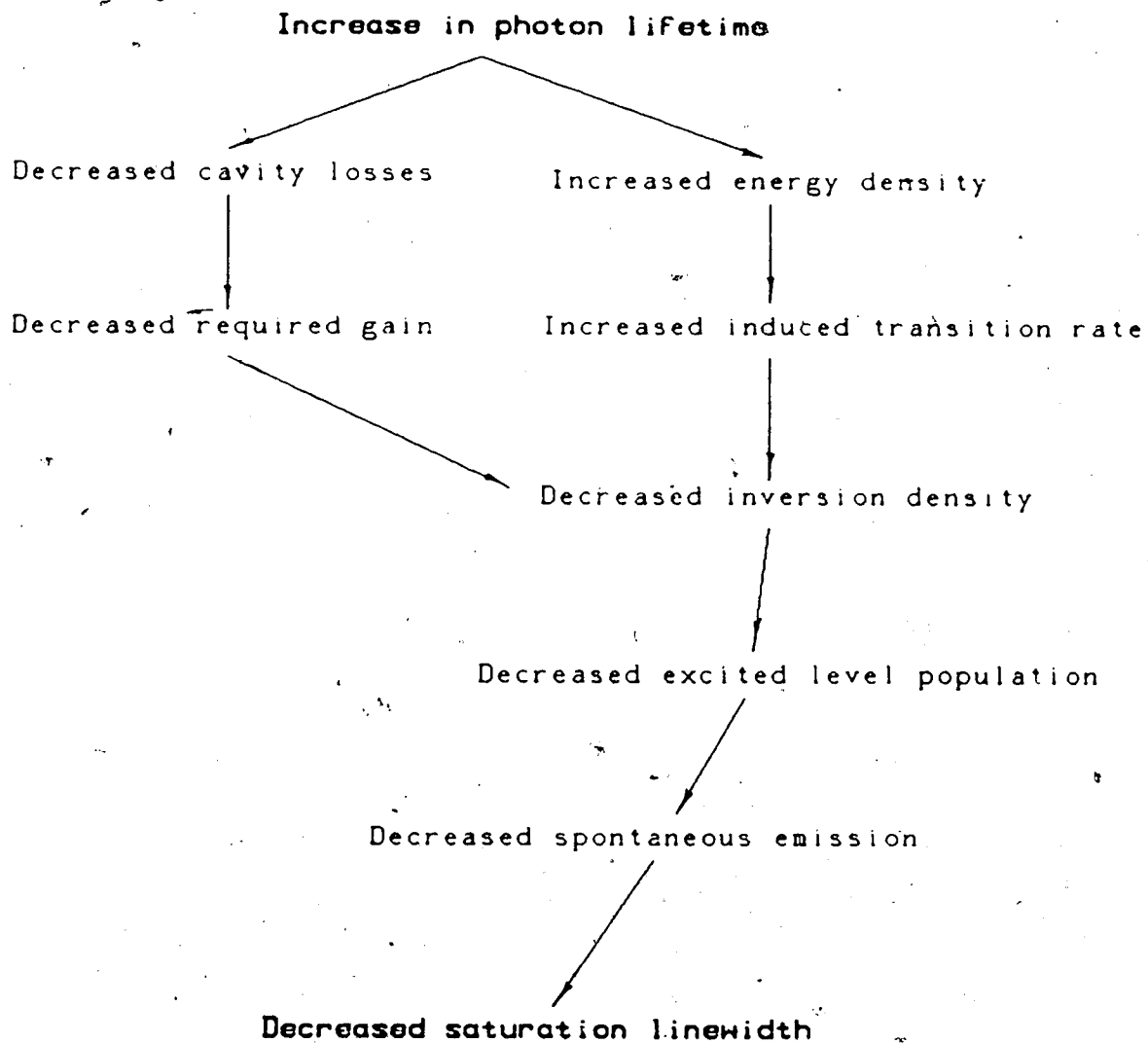
Figure 2-13 Chain of Events Caused by an Increase in the
Photon Lifetime

1. a lower threshold inversion density, ΔN_t , due to a

    decrease in the required medium gain and

2. a lower spontaneous emission limited linewidth due to a

    decrease in the population of the excited state.

Also, the increase in photon lifetime is associated with an

increase in the cavity resolution which in turn enhances

phase discrimination and narrows the FWHM.

A decrease in the longitudinal mode linewidth of a

semiconductor laser via an increase in the photon lifetime

of the resonator cavity is the object of the experimental

investigation of the thesis.

3. EXTERNAL CAVITY FEEDBACK

O

3.1 EXTERNAL CAVITY MODEL

An external cavity is created by placing a reflective object such that it causes a portion of the electromagnetic wave emitted by the laser to be fed back into the active region.

The coupled cavity system is studied using the model illustrated in Figure 3-1.

Figure 3-1 Compound Cavity Model

r_1, r_2, and r_3 are the amplitude reflection coefficients at the interfaces.
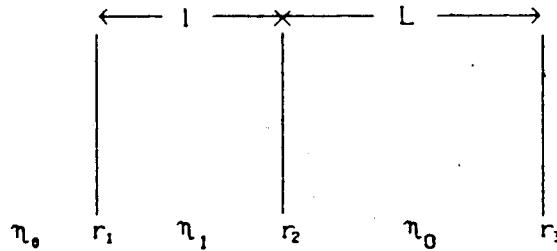
3.1.1 Eigenfrequencies of a Compound Cavity Resonator

The laser and external cavities may be modelled as Fabry-Perot Interferometers and as such, have free spectral ranges given by

$$FSR_\ell = \frac{c}{2n\ell} \qquad (3-1)$$

and

$$FSR_e = \frac{C}{2L} .$$ (3-2)

The ratio of the free spectral ranges is

$$\frac{FSR_\ell}{FSR_e} = \frac{L}{n\ell} .$$ (3-3)

If the ratio $L/\eta 1$ is equal to an integer, it is apparent that the eigenfrequencies of the two cavities will periodically be equal.

For example, consider a laser cavity with $\eta 1=500$um and an external cavity 2000um long so that $L/\eta 1=4$. The free spectral range of the laser cavity, FSR1, is 300Ghz. The free spectral range of the external cavity, FSRe, is 75Ghz. Figure 3-2 shows eigenfrequencies of both cavities.

a)

```
L        I        I        I        I        I
0      300      600      900     1200     1500  GHz
```

b)

```
L_L_L_L_L_L_L_L_L_L_L_L_L_L_L_L_L_L_L_L
0      300      600      900     1200     1500  GHz
```

a) $\eta 1=500$um FSR=300GHz

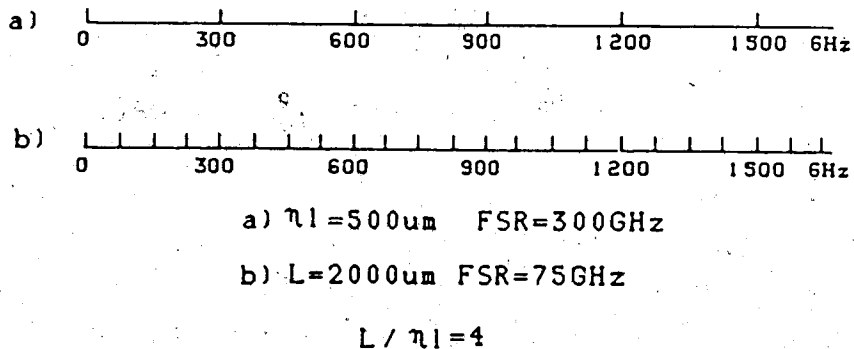b) L=2000um FSR=75GHz

L / $\eta 1$ =4

Figure 3-2 Eigenfrequencies of the Laser and External Cavities

The eigenfrequencies are periodically equal with the period equal to one laser cavity free spectral range.

The situation where $L/\eta 1$ is not equal to an integer is somewhat more complicated but is still well behaved. The following statement holds true for all cases.

If, in a compound cavity where $L > \eta 1$, an integer, x, can be found which satisfies the relationship

$$\frac{Lx}{n\ell} = m \qquad (3-4)$$

where m is also an integer, and if x is the smallest integer which satisfies the relationship, then x is the period of alignment, in free spectral ranges of the small cavity, between eigenfrequencies which are supported in both cavities. In the case where $L/\eta 1$ is irrational, the two cavities will have no eigenfrequencies in common.

Consider a cavity with $\eta 1 = 500um$. Table 3-1 contains the external cavity lengths corresponding to the row and column values of x and m. The underlined external cavity lengths are unique in that they do not occur with a smaller alignment ratio x. For example, when $L = 625\mu m$, the eigenfrequencies of the two cavities will be equivalent every fourth eigenfrequency of the small cavity.

3.1.2 Representation of Compound Cavity Resonance

The condition for sustained oscillation in the coupled cavity in Figure 3-1 is given by Olsson and Tang [22] to be

x\m	1	2	3	4	5	6	7	8	9	10
1	500	1000	1500	2000						
2		500	750	1000	1250					
3			500	666.7	833.2	1000				
4				500	625	750	875	1000		
5					500	600	700	800	900	1000

Table 3-1 Compound Cavity Alignment

$$e^{(\gamma-\alpha)\ell} = \frac{1+ r_2 r_3 e^{-j2k_0L}}{r_1 e^{-j2k_1\ell}\left(r_2 + r_3 e^{-j2k_0L}\right)} \quad (3-5)$$

This reduces to the standard oscillation equation

$$e^{(\gamma-\alpha)\ell} = \frac{1}{r_1 r_2 e^{-j2k_1\ell}} \quad (3-6)$$

when $r_3=0$.

Equation 3-5 takes into account the multiple reflections in the external cavity. It may be derived simply by replacing r_2 in Equation 3-6 with the expression for the effective reflectivity from a Fabry-Perot cavity

$$r_{eff} = \frac{E_r}{E_i} = \frac{r_2 + r_3 e^{-j2k_0L}}{1 + r_2 r_3 e^{-j2k_0L}} \quad (3-7)$$

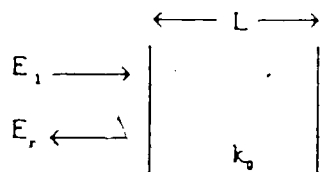where E_r and E_i are as shown in Figure 3-3.

Figure 3-3 Fabry-Perot Resonator Effective Reflectivity

In general, the effective reflectivity is complex. It greatly affects the phase and gain conditions of the solitary laser (a laser without external cavity feedback).

Equation 3-5 was first introduced by Olsson and Tang in 1981. They demonstrated the effect that the feedback had on the threshold gain of the laser and briefly, the effect it had on the spectrum of the laser. In 1983, Osmundsen and Gade [23] presented a detailed analysis of Olsson and Tang's "secular equation" (Equation 3-5). This analysis is the key to understanding the basic effects of optical feedback in a semiconductor laser. The following analysis is based upon the work of Osmundsen and Gade.

3.2 COMPLEX FEEDBACK PARAMETER

Osmundsen and Gade introduce the complex feedback parameter z. The complex feedback parameter enables the final phase and gain conditions to be represented as the sum of the solitary laser oscillating condition plus an additional term due to the feedback.

The complex feedback parameter z is defined here as

$$z = \frac{r_2}{r_{eff}} \qquad (3-8)$$

which is equivalent to

$$z = \frac{r_2(1 + r_2 r_3 e^{-j2k_0 L})}{r_2 + r_3 e^{-j2k_0 L}} \qquad (3-9)$$

where r_3 is the Fabry-Perot reflectivity.

The laser equation now becomes

$$e^{(\gamma-\alpha)\ell} = \frac{z e^{+j2k_1 \ell}}{r_1 r_2} \qquad (3-10)$$

In general, z is a complex number and may be represented as

$$z = |z| e^{j\varphi_z} \qquad (3-11)$$

where

$$|z|^2 = \frac{r_2^2(1 + 2r_2 r_3 \cos(2k_0 L) + r_2^2 r_3^2)}{r_2^2 + 2r_2 r_3 \cos(2k_0 L) + r_3^2} \qquad (3-12)$$

and

$$\varphi_z = \text{Tan}^{-1}\left(-\frac{r_2 r_3 \sin(2k_0 L)}{1 + r_2 r_3 \cos(2k_0 L)}\right) - \text{Tan}^{-1}\left(-\frac{r_3 \sin(2k_0 L)}{r_2 + r_3 \cos(2k_0 L)}\right) \qquad (3-13)$$

Similar to Equation (2-13), which describes the solitary laser, Equation 3-10 can be separated into gain and

phase conditions.

For oscillations to be sustained:
()

1. The round trip phase delay must be an integral multiple of 2π. The phase condition is

$$\varphi_z = m2\pi - 2k_1\ell .\qquad (3\text{-}14)$$

2. The round trip gain must be unity. The gain condition is

$$\gamma = \alpha - \frac{1}{\ell}\ln r_1 r_2 + \frac{1}{\ell}\ln|z| .\qquad (3\text{-}15).$$

In the case where the external cavity reflectivity, r_3, is 0 (no feedback), the phase and gain conditions reduce to the normal solitary laser feedback equations.

The phase, ϕ_z, represents the additional phase due to the external cavity and $(1/l)\ln|z|$ is the excess gain required for laser oscillation. ϕ_z and $|z|$ are periodic functions of the external cavity phase $\phi_0 = 2k_0 L$. For a fixed external cavity length L, a change in ϕ_0 of 2π represents a shift of one free spectral range in the eigenfrequency of the external cavity. For this reason, ϕ_z and $|z|$ may be thought of as also having a periodicity of one free spectral range of the external cavity.

Figures 3-4 and 3-5 are plots of one period of ϕ_z and $|z|$ respectively. In each case, curves are plotted for external cavity reflectivities, r_3, of .51, .256, .128, and

.064 as a parameter. The laser facet reflectivity, r_2 is fixed at 0.5 . These particular values are derived from experimental data. As the reflectivity increases, the peak magnitudes of both ϕ_z and $|z|$ also increase.
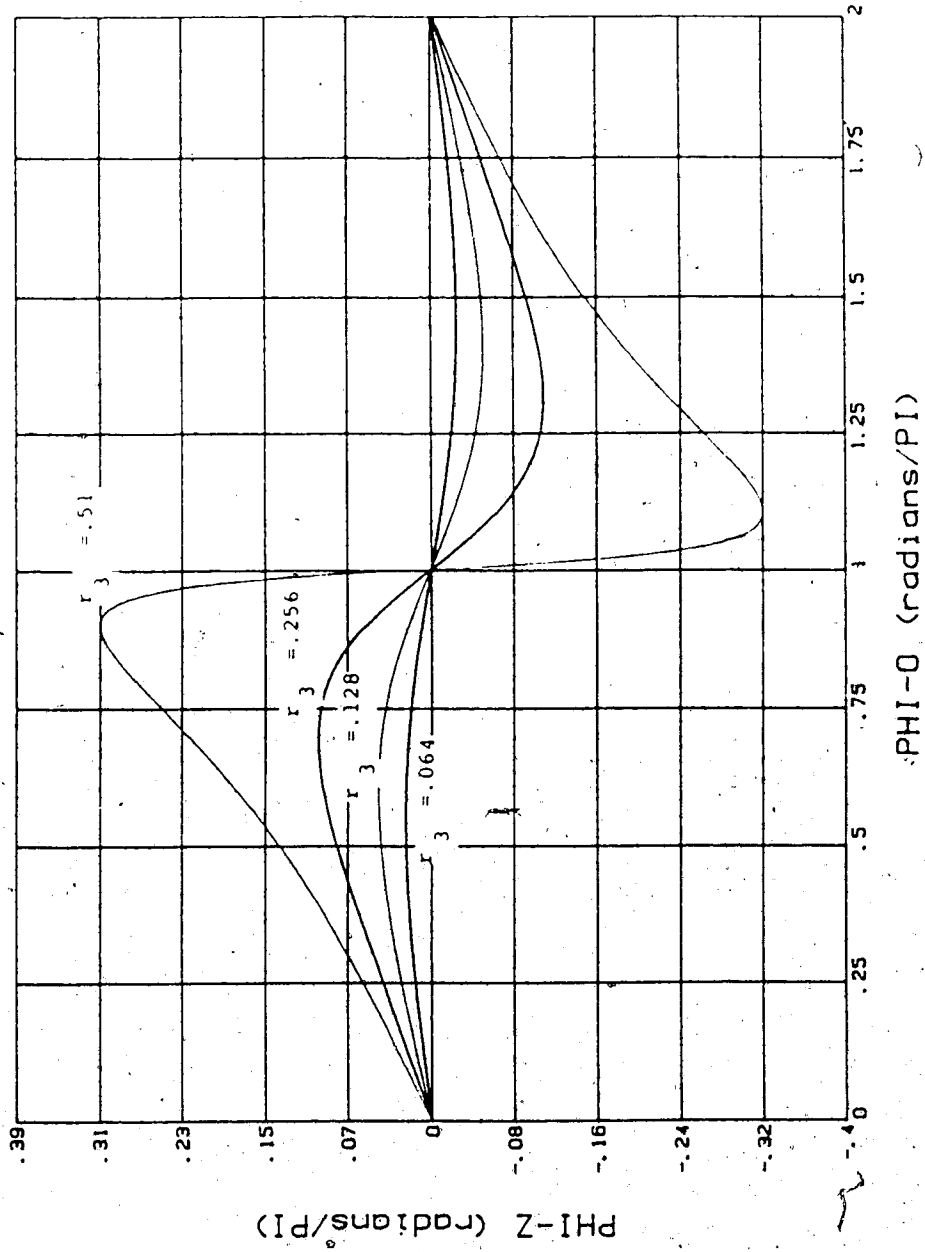
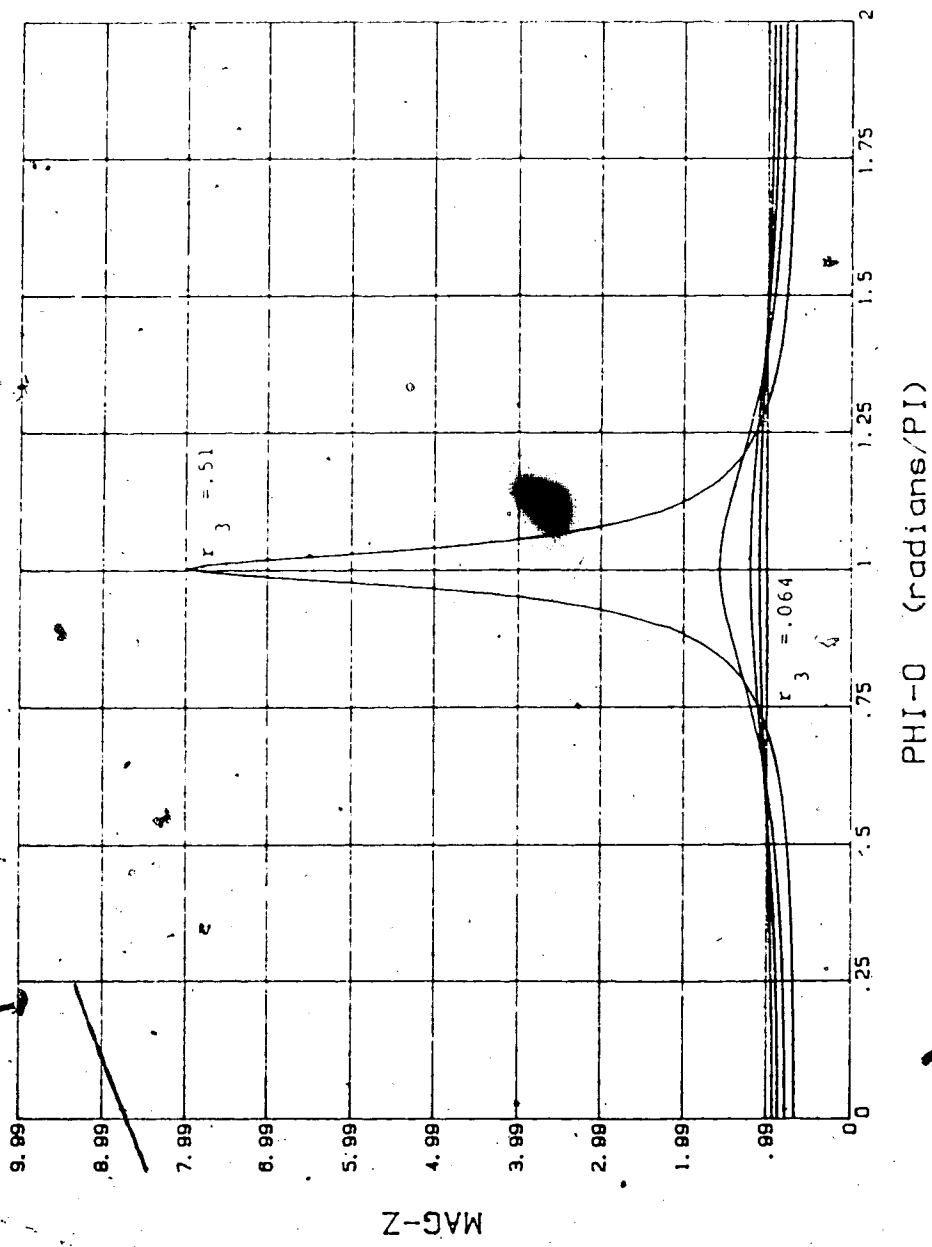Figure 3-4 Phase of the complex feedback parameter z.

53

Figure 3-5 Magnitude of the complex feedback parameter z.

3.2.1 Solutions to the Phase and Gain Conditions

The phase condition, Equation 3-14, may be written as

$$\varphi_z = m2\pi - \varphi_1 \qquad (3-16)$$

where

$$\varphi_1 = 2k_1 \ell \qquad (3-17)$$

is the phase in the laser cavity.

Since

$$\varphi_0 = 2k_0 L \qquad (3-18)$$

the ratio of the phase in the laser cavity to the phase in the external cavity is

$$\frac{\varphi_0}{\varphi_1} = \frac{L}{n\ell} \cdot \qquad (3-19)$$

Combining Equations 3-16 and 3-19, the phase condition becomes

$$\varphi_z = m2\pi - \frac{n\ell}{L} \varphi_0 \cdot \qquad (3-20)$$

Furthermore, the phase condition may be rewritten again as

$$\varphi_{z'} = \varphi_{rhs} \qquad (3-21)$$

where

$$\varphi_{rhs} = m2\pi - \frac{n\ell}{L}\varphi_0 . \qquad (3-22)$$

ϕ_{rhs} is a linear function of the external cavity phase ϕ_0.

Although the solutions to the phase condition will be a set of discrete wavelengths, corresponding to a set of discrete phases, the functions $|z|$, ϕ_z, and ϕ_{rhs} may be thought of as being functions of a continuous variable ϕ_0.

The points $\phi_{rhs} = 0$ correspond to

$$\varphi_1 = m2\pi \qquad (3-23)$$

which are solutions to the solitary laser phase condition. Figure 3-6 illustrates ϕ_{rhs} for several solitary laser phase solutions in the vicinity of the gain curve. The figure shows both the gain curve $g(\nu)$ and ϕ_{rhs}. Hence, the ordinate (not illustrated) is both radians (ϕ_{rhs}) and inverse frequency ($g(\nu)$). Differentiating Equation 3-19 yields

$$\frac{\Delta\varphi_0}{\Delta\varphi_1} = \frac{L}{n\ell} . \qquad (3-24)$$
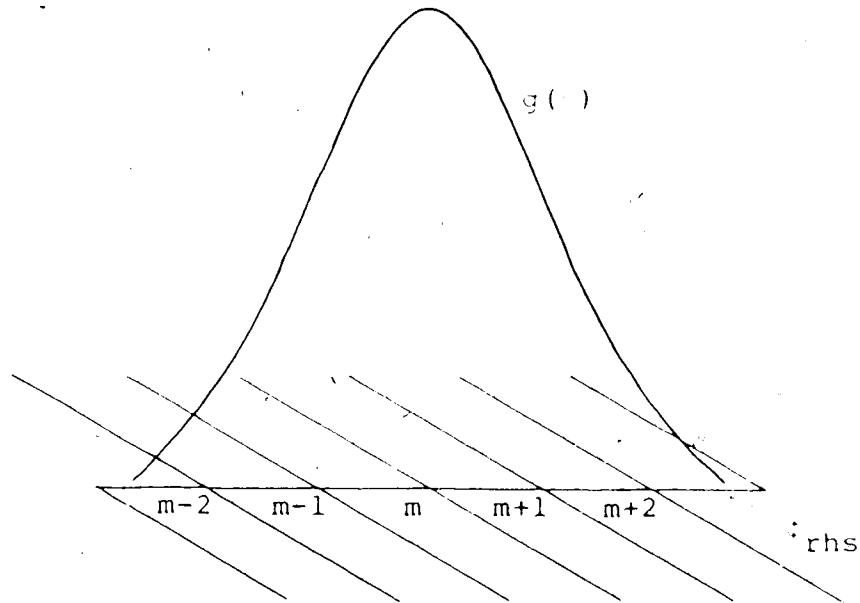
Now, if the phase in the laser cavity shifts by 2π (one free

Figure 3-6 ϕ vs ϕ_0

spectral range), then the phase in the external cavity will shift by

$$\Delta\phi_0 = \frac{L}{n\ell}\, 2\pi \; .$$
(3-25)

The phase shift indicated by Equation 3-25 is equivalent to a change in frequency of

$$\Delta f = \frac{L}{n\ell}\, FSR_e \; .$$
(3-26)

In the case where $L/\eta l$ is an integer, the free spectral range alignment coefficient of the resonators is equal to one, and the ϕ_z and ϕ_{rhs} curves will be coincident when the ϕ_{rhs} curve intersects the ϕ_0 axis.

Figure 3-7 shows the function ϕ_{rhs}, for m=n, superimposed on the function ϕ_z. (Four ϕ_z curves are shown

corresponding to external cavity reflectivities of .51,
.256, .128, and .064.)   All intersections of the two curves
are solutions to the phase condition.   The compound
resonator is capable of supporting longitudinal modes
corresponding to the graphical solutions, providing the
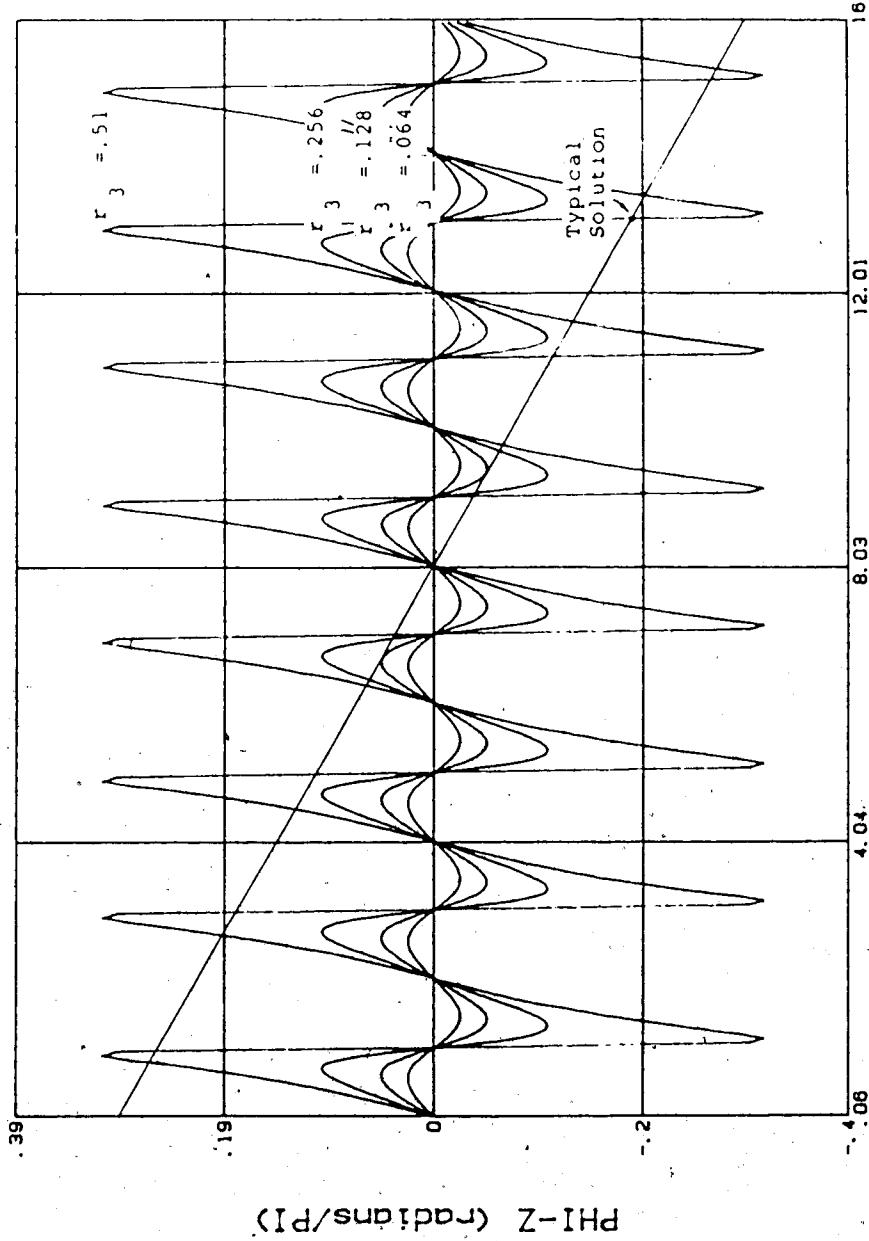excess gain can be accomodated by the laser medium.

Figure 3-7   Solution to the Phase Condition for Different Values of r_3

The following points can be made from Figure 4-7:

1. The solutions to the phase condition are situated in the neighbourhood of solitary laser longitudinal modes.

2. The number of solutions depends on the maximum magnitude of the ϕ_z curve. Strong feedback (large r_3) causes multiple solutions to the phase condition. The number of solutions can be decreased by decreasing the external cavity effective reflectivity.

3. The number of solutions also depends on the slope of the ϕ_{rhs} curve. The number of solutions can be decreased by decreasing the length of the external cavity.

With a proper combination of external cavity length and effective reflectivity, the compound resonator can be made to oscillate in a single longitudinal mode at each solitary laser mode solution.

In addition to causing oscillation in only one external cavity mode, it is also desirable to decrease the spectral linewidth of the radiation emitted from the compound resonator (Section 2.4).

For a fixed L, Equations (2-22) and (2-25) indicate that decreasing the spectral linewidth requires increasing the feedback by increasing r_3. This will increase the maximum value of ϕ_z and, as a result, the number of solutions to the phase condition will also increase.

For a fixed r_3, decreasing the spectral linewidth requires increasing the external cavity length L. This will decrease the slope on the linear curves and again will

increase the number of solutions to the phase condition.

Maximizing the photon lifetime and obtaining single external cavity mode oscillation are conflicting objectives and a compromise must be made.

3.3 STRONG FEEDBACK EFFECTS

To limit the phase solution to a single intersection at each solitary laser longitudinal mode, it has been demonstrated by Goldberg et al [24] that the external cavity reflectivity must be of the order of 10⁻⁴.

However, in contrast to the weak feedback theory, Wyatt et al [17] reported an operational grating feedback system in which the external cavity reflectivity is of the same order of magnitude as the laser facet reflectivity. This is strong feedback and, as indicated in Section 3.2 for a Fabry Perot reflector, should result in multiple solutions to the external cavity phase condition.

Sato et al. [25] proposed an explanation for the single mode oscillation under strong mirror feedback conditions.

The explanation is based upon coupling between external cavity modes. A detailed analysis of the nature of the coupling involves quantum mechanical perturbation theory and is beyond the scope of this thesis. The results of Sato's work are presented here for completeness.

Sato et al develop a mode coupling equation and, due to the difficulty of obtaining an exact solution for multi-longitudinal modes, treat two longitudinal modes in

the external cavity.

The differential equations for the modes are

$$\dot{E}_1 + j(\Omega_1 - \omega)E_1 + \Gamma_{11}E_1 + \Gamma_{12}E_2 = 0 \qquad (3-27)$$

and

$$\dot{E}_2 + j(\Omega_2 - \omega)E_2 + \Gamma_{22}E_2 + \Gamma_{21}E_{21} = 0 . \qquad (3-28)$$

where Ω_1 and Ω_2 are the angular frequencies of the electric fields E_1 and E_2. ω is taken as the average of Ω_1 and Ω_2, Γ_{11} and Γ_{22} are related to the mode losses and Γ_{12} and Γ_{21} are the coupling coefficients between the modes E_1 and E_2.

The relationships between the differential phase, $\Delta\Omega$, and gain, $\Delta\Gamma$, of the two modelled modes and the mode coupling, Γ_{12}, are illustrated in Figure 3-8. In the figure, $\Delta\Omega_0$ is the difference between the phase of the two modes when the coupling Γ_{12} is equal to zero.

The important feature of the figure is that above a critical value of the coupling Γ_{12}, the difference in mode losses $\Delta\Gamma$ is increased while the frequency difference $\Delta\Omega$ goes to zero. Essentially, a single longitudinal mode results.

In the case of strong optical feedback where several longitudinal modes satisfy the phase condition and where the differential gain between adjacent modes is not large enough for the cavity to make a selection, the single mode
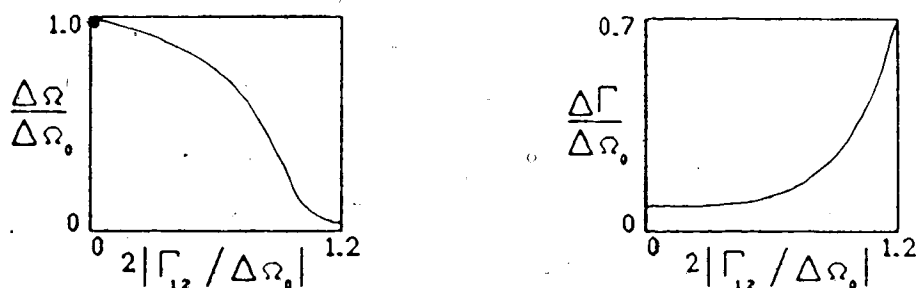
Figure 3-8   Differences Between Phases and Gains of Two
Modes as a Function of Mode Coupling for a Two Mode Model

oscillation is considered to be a result of strong coupling
between external cavity modes. This theory may provide an
explanation for the results of Wyatt et al [17] and Fujita
et al [25] where single external cavity mode oscillation
under strong grating feedback has been reported.

3.4 SELECTION OF A SINGLE LONGITUDINAL MODE

The external cavity is capable of altering the
longitudinal mode characteristics of the solitary laser.
The external mirror used in the model offers no means, other
than relying upon the degree of homogeneity in the gain
medium, by which a particular longitudinal mode can be
selected while discriminating against all others. This
selection can be done by using a diffraction grating in the

Littrow configuration as the feedback element. The two
properties of the grating which are important to the ability
to discriminate against longitudinal modes are the
dispersion and the resolution.

Figure 3-9 is a model of the external cavity using a
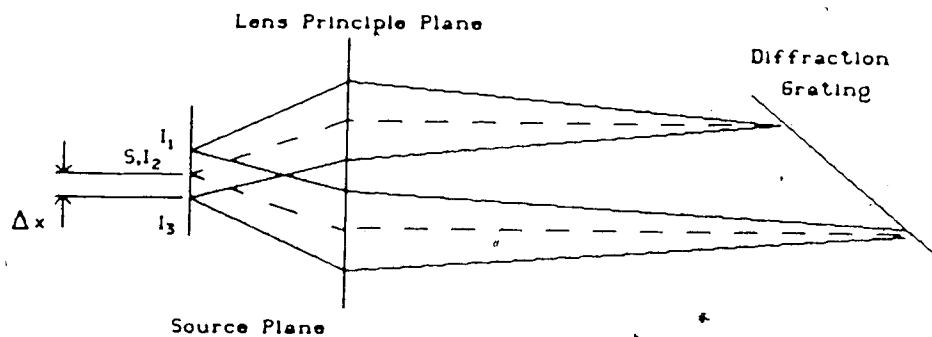diffraction grating in the Littrow configuration.

Figure 3-9 Diffraction Grating in the External Cavity

Point S is the laser. Points I_1, I_2, and I_3 are the
images of the laser after being reflected by the diffraction
grating. The image locations are wavelength dependent.
Each image is due to a different longitudinal mode.

In the Littrow configuration, the first order
diffraction is reflected back along the input beam axis.
The grating equation becomes

$$m\lambda = 2d \sin \varphi .$$
(3-29)

where m=1 for the first order, d=line spacing, and ϕ=angle

of dispersion with respect to an axis normal to the grating. The grating dispersion is

$$\frac{d\varphi}{d\lambda} = \frac{1}{2d \cos \varphi} \cdot \qquad (3-30)$$

The longitudinal mode image displacement along the laser face is of interest. The displacement is given by

$$\Delta x = f \Delta \varphi \qquad (3-31)$$

where f is the focal length of the lense and $\Delta \phi$ is the spatial angular separation between solitary laser longitudinal modes after being dispersed by the grating. Furthermore, the grating resolution is given as [27]

$$\Delta \theta = \frac{\lambda}{nd \cos \varphi_m} \qquad (3-32)$$

where $\Delta \theta$ is indicated in Figure 3-10 and n is the number of grating lines illuminated. The product, nd, is equal to the spot size on the grating.
Similar to equation 3-31, the spot size on the laser face is given by

$$\Delta s = f \Delta \theta \cdot \qquad (3-33)$$

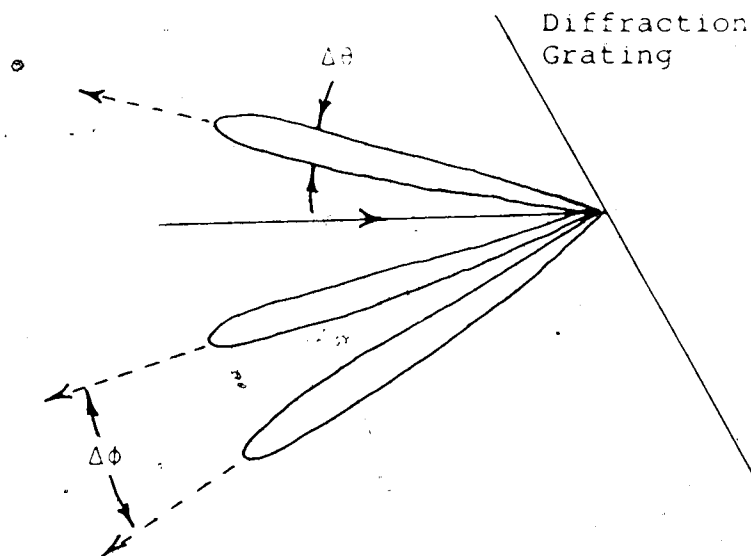A grin (graded index of refraction) rod lens was utilized in the experimental work. Determination of the

Figure 3-10 Diffraction Grating Resolution

diffracted beam image size and position on the laser face
requires the use of ABCD matrix ray propagation techniques.
Figure 3-11 is an enlarged illustration of the optical path
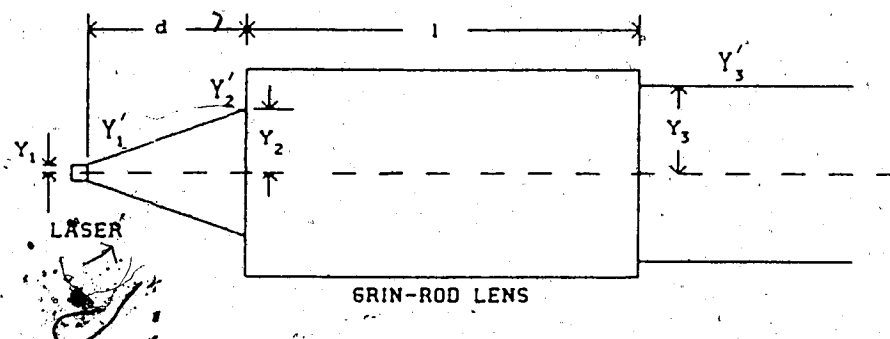from the laser through the grin rod lens.

Figure 3-11 Laser - Grin Rod Lens Optical Path

y and y' are the ray displacement from the optical axis and
slope respectively. The optical path is divided into two

sections. The first section is the gap between the laser and grin rod lens and the second section is the grin rod lens. The ABCD matrix for the first section is

$$\begin{bmatrix} 1 & d \\ 0 & 1 \end{bmatrix} \qquad (3-34)$$

The ABCD matrix for the grin rod lens is

$$\begin{bmatrix} \cos\left(\sqrt{\dfrac{k_2}{k}}\,\, 1\right) & \sqrt{\dfrac{k}{k_2}}\,\sin\left(\sqrt{\dfrac{k_2}{k}}\,\, 1\right) \\ -\sqrt{\dfrac{k_2}{k}}\,\sin\left(\sqrt{\dfrac{k_2}{k}}\,\, 1\right) & \cos\left(\sqrt{\dfrac{k_2}{k}}\,\, 1\right) \end{bmatrix} \qquad (3-35)$$

where k_2 is a lens constant, k is the propagation constant, and 1 is the length of the rod. For propagation from the laser through the grin rod lens, the matrix equation becomes

$$\begin{bmatrix} A & B \\ C & D \end{bmatrix}_{SYS} = \begin{bmatrix} A & B \\ C & D \end{bmatrix}_{LENS} \begin{bmatrix} A & B \\ C & D \end{bmatrix}_{GAP} \qquad (3-36)$$

The matrix equation can be solved to determine the spot size illuminating the grating by solving for the distance d which yields a slope equal to zero at the exit of the grin rod

lens. To determine the diffracted beam image size and location on the laser face, the above process must be reversed. The beams are propagated through the optical path at displacements and slopes given by the grating dispersion and resolution equations.

In order to ensure only a single longitudinal mode is being fed back into the active region, the spacing between spots should be greater than the dimension of the active region in the direction of the dispersion.

3.5 Applicability of Present Feedback Theory to the Diffraction Grating Case

It is important to note that the complex feedback theory of Osmundsen and Gade and the mode coupling theory of Sato have been developed using mirror feedback. To date, an analysis of the applicability of these theories to the diffraction grating feedback case has not been published. Furthermore, no paper has yet been published which reconciles these two seemingly conflicting theories.

4. EXPERIMENTAL INVESTIGATION OF FEEDBACK TECHNIQUES

4.1 APPARATUS

Figure 4-1 is a block diagram illustrating the configuration of the equipment used in the experiments. Figure 4-2 shows the actual experimental setup.
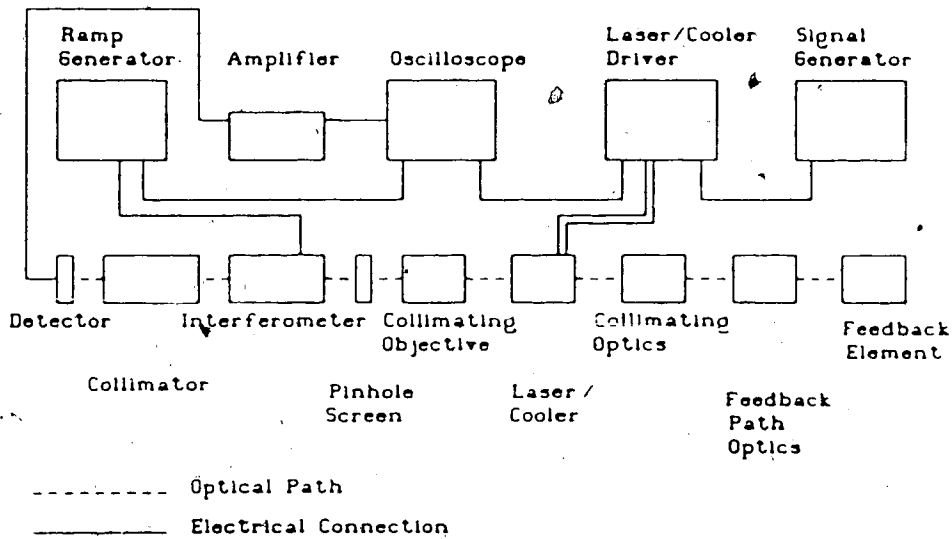

Figure 4-1   Block Diagram of Experimental Apparatus

4.1.1 Optics

The feedback optics and collimating objective (10X microscope objective) are mounted on Optikon MR50.16 three dimensional translation stages with 20μm per small division micrometers, which have an average accuracy, given by the manufacturer, of 3μm. The laser is mounted on a combination of an Optikon three dimensional MR50.16 translation stage, an in-house designed and built tilt stage, and an Optikon

Figure 4-2   Photograph of Experimental Apparatus

TR80S rotational micrometer. This combination of

positioning devices provided adequate positioning freedom

for the laser.

The 10X collimating objective is a standard microscope

objective coated for the visible region. It is mounted on

the xyz (3 dimensional) stage with a standard objective

mount. In addition, an extension tube is inserted between

the objective and the objective mount to provide clearance

over the laser mount. Only coarse θ_y adjustments were

possible by rotating the objective mount on top of the xyz

stage. θ_x adjustments were made by placing paper shims

between the objective mount and the xyz stage.

The Fabry-Perot Interferometer is a Burleigh Instruments Model RC-110 scanning interferometer. It is driven by a Burleigh Instruments RC-44 ramp generator. The plane mirrors are coated for the 1.3μm to 1.5μm region with reflectivities > 97.5%. The instrument finesse is estimated to be approximately 50. The output from the interferometer is collimated by a Burleigh Instruments Model RC-41 collimating lens system.

The detector and amplifier are a United Detector Model 351 unit, modified to provide pre-amp output to an oscillosccpe.

The feedback optics are described in Section 4.4 .

4.1.2 Laser Driver and Cooler

Figure 4-3 shows the laser and cooler mount.

The laser driver is a controllable current source with a current range of 4 mA to 25 mA. The driver has a modulation input which allows the current to be varied periodically. To assist alignment of the feedback, the current source was driven with a 5hz, 350mV triangular wave with a -500mV offset. The quiescent current was set at the laser driver to be 13mA. Applying the biased triangular wave resulted in a sweep from 7mA to 12mA. The current range begins 1mA below threshold and ends at 1.4 times the threshold current. All current values are approximate.

The cooler is a Melcor Model FC 0.6-18-06L thermoelectric cooler. It is driven by a pulse width
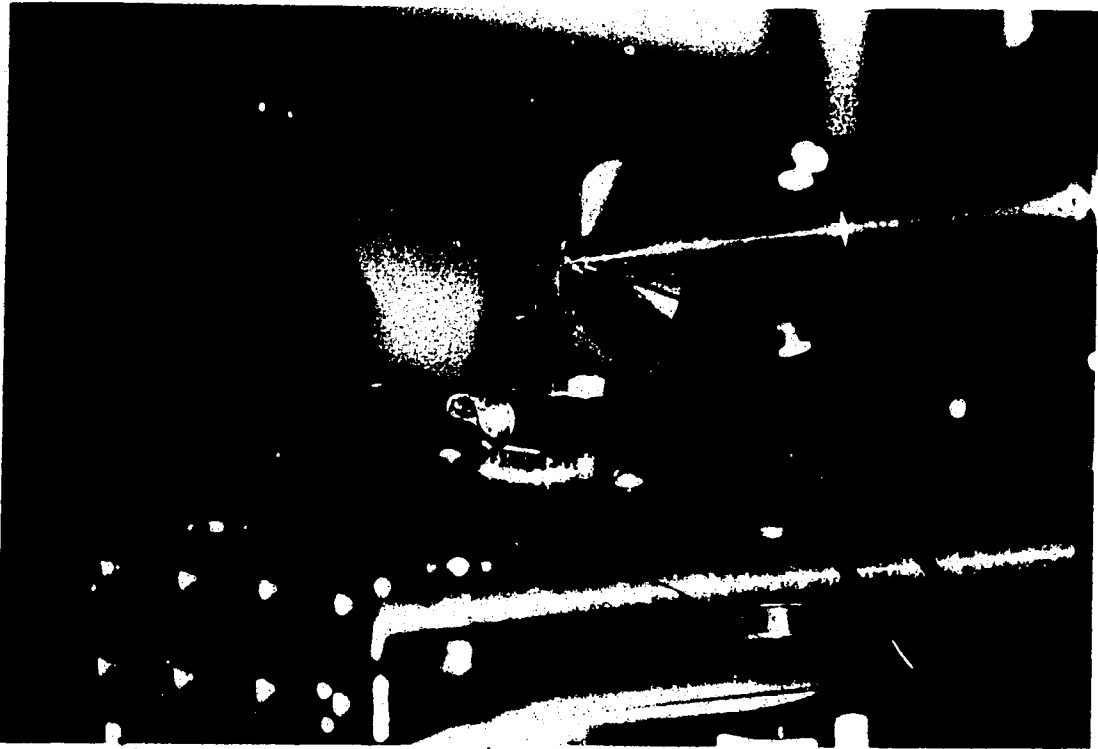
Figure 4-3   Laser and Cooler Mount

modulation control circuit. The laser mount temperature is
controlled to approximately 15°C.

4.2 LASER CHARACTERIZATION

The laser used for the experimental analysis was a
Mitsubishi Model ML7308 DH-Buried Crescent InGaAsP
semiconductor laser which emits radiation in the $1.3\mu m$
region.

The following characteristics of the laser were
measured:

1.   Optical Power vs Laser Current
2.   Laser Spectrum vs Laser Current

4.2.1 Optical Power vs Laser Current

Figure 4-4 shows the optical power as a function of the laser current.

The operating temperature of the laser was approximately 15°C. The threshold current of the laser is determined from Figure 4-4 to be 8.5mA.

Due to the mechanical construction of the detector mount, it was not possible to position the detector close enough to the laser to ensure all the radiation was captured. The curve labelled "Mitsubishi Data" in Figure 4-4 was obtained by laterally shifting the Power vs. Current curve, supplied by Mitsubishi, to coincide with the measured 8.5mA threshold current. The Mitsubishi curve is used in subsequent sections for transmission loss estimations in the feedback path.

The slope of the power vs current curve for I>Ith defines the external quantum efficiency which is given as

$$\eta_{ext} = \frac{e}{h\nu} \frac{\Delta P}{\Delta I} \qquad\qquad (4-1)$$

where e is the electronic charge, and $\Delta P/\Delta I$ is the slope for I>Ith.

4.2.2 Laser Spectrum

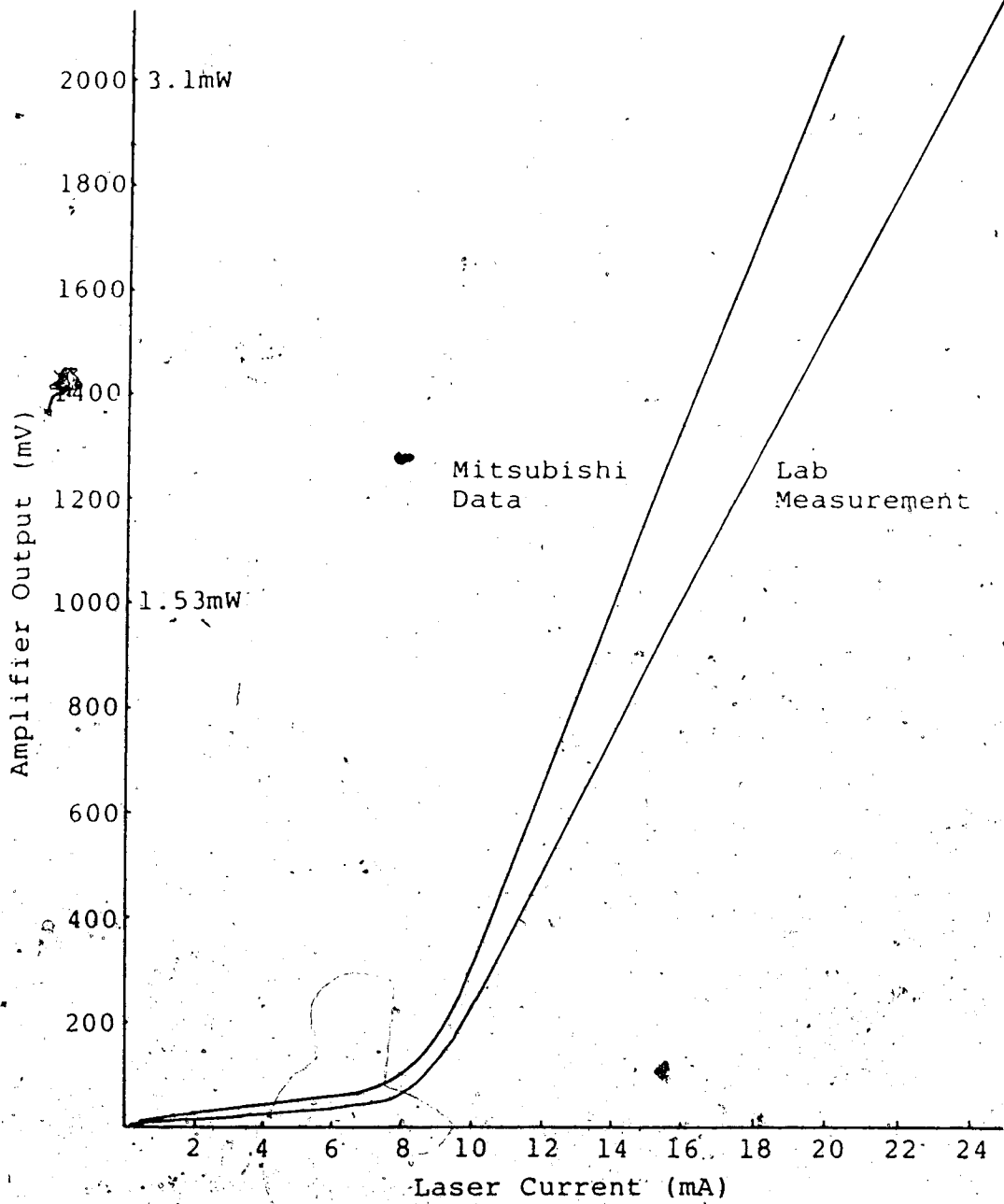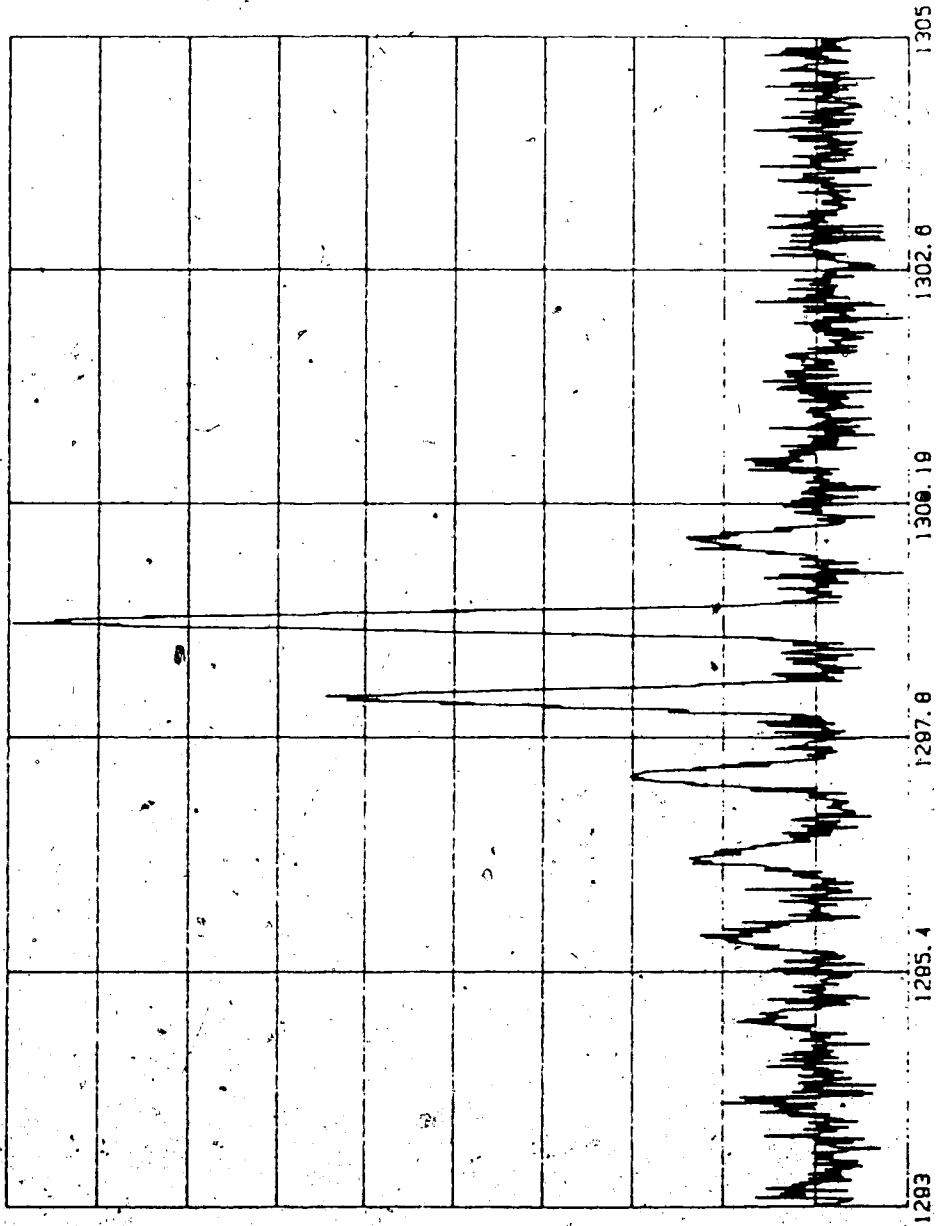Figures 4-5 to 4-10 show the laser spectrum for a current range of 10mA to 20mA.

Figure 4-4 Optical Power vs Laser Current

Figure 4-5   Laser Spectrum   I=10.0mA

MITSUBISHI LASER SPECTRUM (I=13.01mA)

Relative Intensity

Wavelength (nM)

1293   1295.4   1297.8   1300.19   1302.6   1305
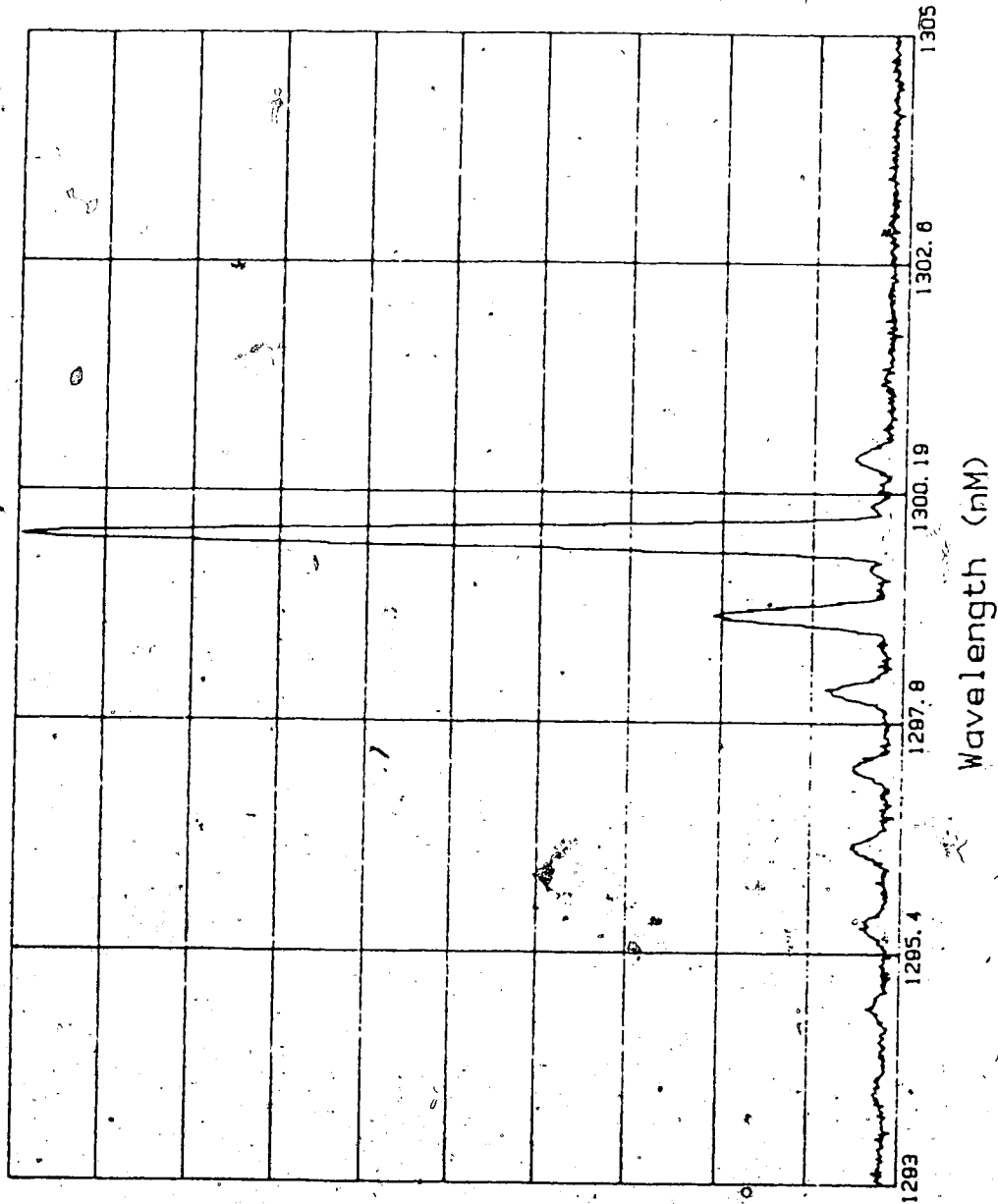
Figure 4-6   Laser Spectrum, I=13.01mA

Mitsubishi Laser Spectrum (I=15mA)

Relative Intensity

Wavelength (nM)

1293   1295.4   1297.8   1300.19   1302.6   1305
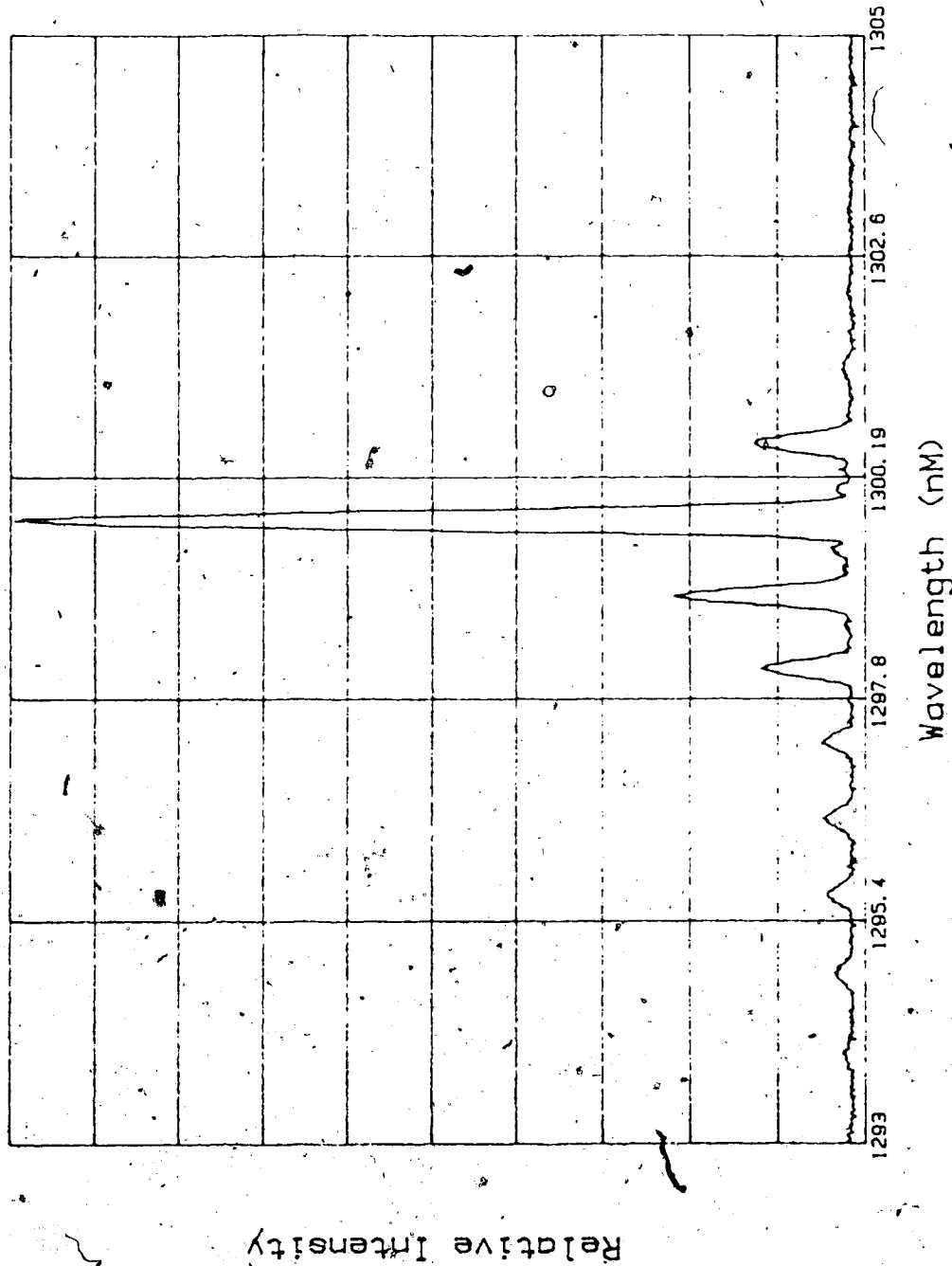
Figure 4-7   Laser Spectrum;   I=15.0mA.

Figure 4-8. Laser Spectrum, I=17.5mA

MITSUBISHI LASER SPECTRUM (I=20mA)

Relative Intensity

Wavelength (nM)

1293   1295.4   1297.8   1300.19   1302.6   1305
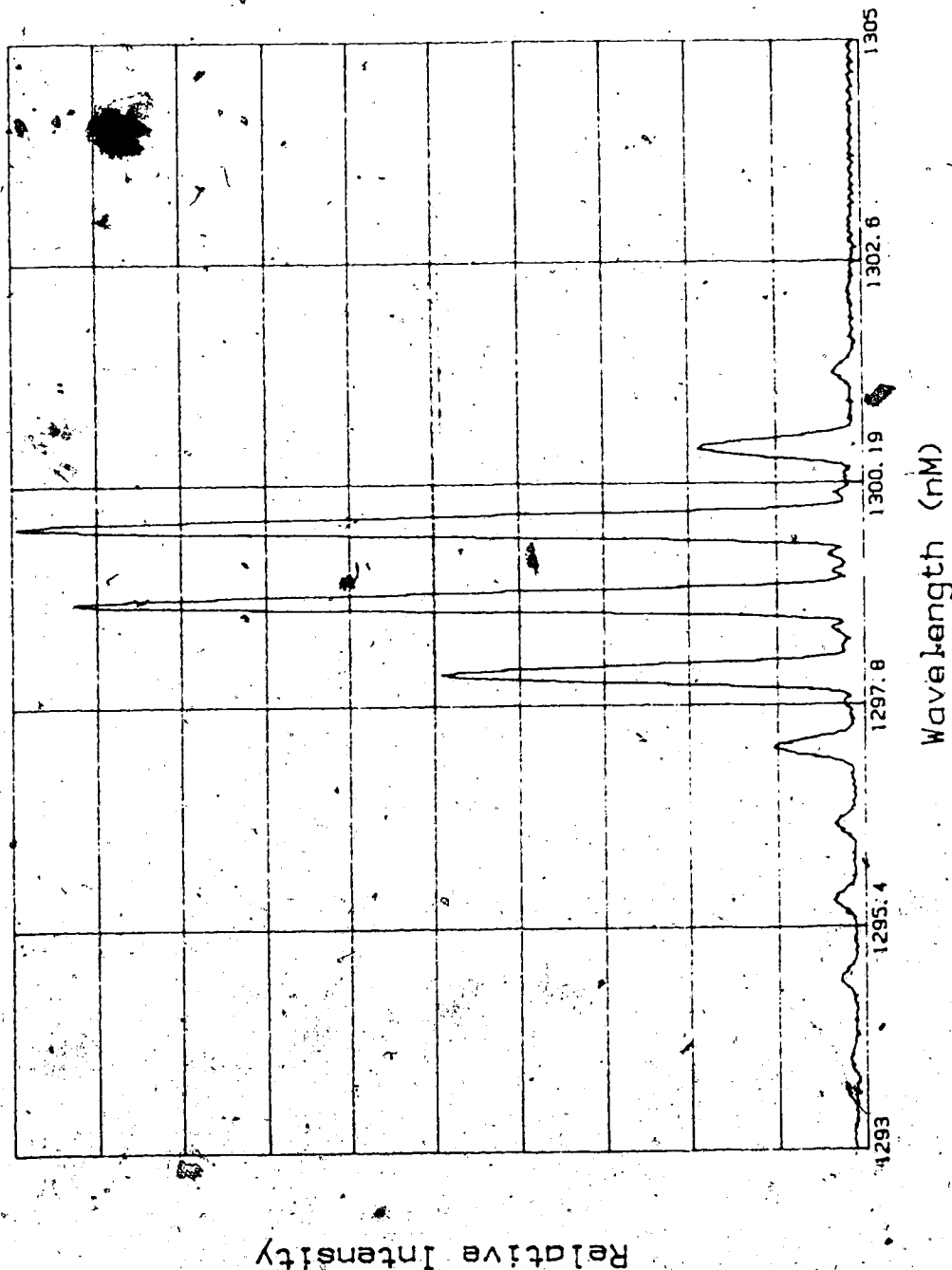
Figure 4-9   Laser Spectrum   I=20.0mA

MITSUBISHI LASER SPECTRUM (I=13.01mA)

Wavelength (nM)

Relative Intensity

Figure 4-10   Laser Spectrum.   I=13.01mA Monochromator Slit=25um
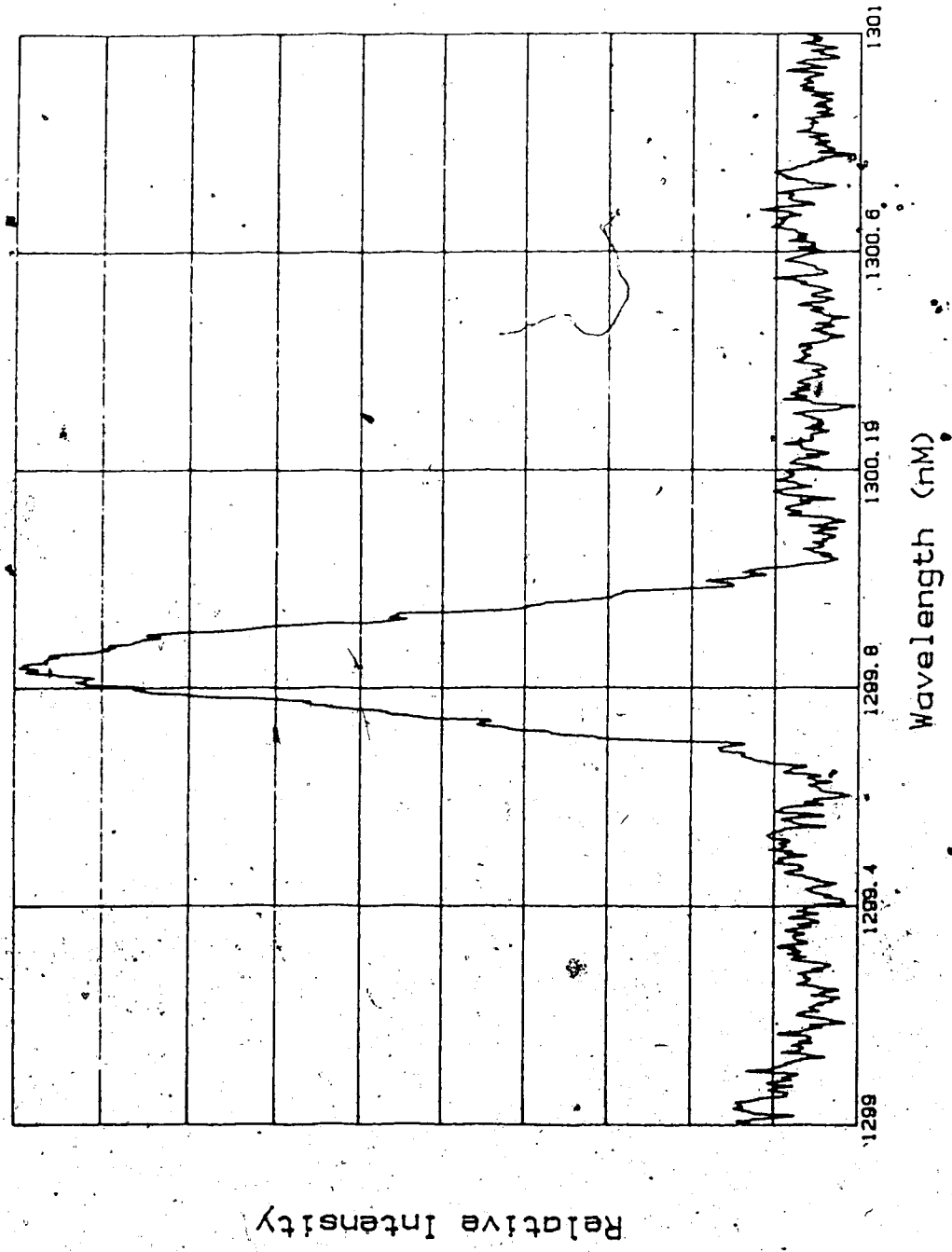
The spectra were measured with a McPherson Model 270, .35m, Monochromator. The monochromator parameters for Figures 4-5 to 4-9 are:

1. 50μm entrance and exit slits

2. 600 lines/mm diffraction grating

3. 2 Angstrom resolution

4. blaze wavelength

All spectra indicate the laser oscillates in the fundamental transverse mode.

The longitudinal mode spacing is measured to be 8.2Å. The laser exhibits the most pronounced single longitudinal mode oscillation at I=13.01mA.

The side mode suppression ratio of the laser spectrum is defined as the ratio of the intensity of the major longitudinal mode to the intensity of the longitudinal mode from the remaining modes which has the maximum intensity. The side mode suppression ratio from Figure 4-6 is 5.3/1.

Figure 4-10 shows the dominant longitudinal mode of the laser at I=13.01mA. The monochromator slit width is set to 25μm yielding a theoretical instrument resolution of 1Å. The FWHM linewidth is measured to be approximately 2Å.

4.3 EXTERNAL CAVITY EFFECTIVE REFLECTIVITY

An estimation of the external cavity reflectivity is necessary to obtain an estimation of the level of feedback.

Figure 4-11 shows the feedback optics of the long external cavity. The external cavity consists of all the

optics situated to the right of the center xyz translational
stage (the laser mount). The photograph is of the grating
feedback. However, the mirror, for the long external cavity
with mirror feedback, was taped onto the back of the grating
mounting plate. Except for the grating and mirror, the
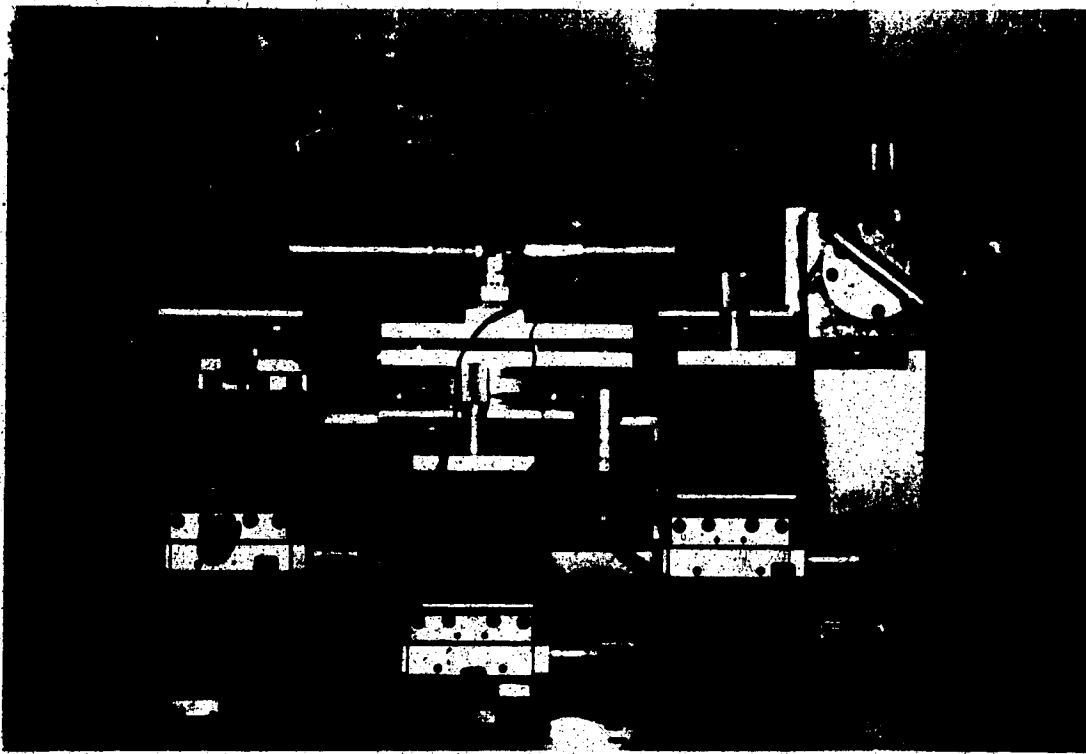equipment and layout of the two long external cavities was
identical.

Figure 4-11 Long External Cavity Optics

To determine the effective reflectivity, estimates of
the transmission losses through the grin rod (graded index
of refraction) lens, the transmission losses through the
neutral density filters, and the diffraction grating
efficiency are required.

Grin Rod Lens

Figure 4-12 is a plot of the Power vs Current curve, obtained with the power measurements taken after transmission through the grin rod lens, along with the Mitsubishi supplied Power vs Current curve (shifted to be compatible with experimental threshold current).

For I>Ith, the ratio of the two curves is, on the average, equal to 0.52. Hence, the amplitude transmission coefficient of the laser through grin rod lens optical path is $\sqrt{0.52}$ or .72 .

Diffraction Grating Efficiency

The incident power and the power diffracted into the zero and first orders were measured for the two laser currents 25mA and 13.01 mA. Figure 4-13 illustrates the geometry of the experimental configuration.

Table 4-1 lists the data obtained from measurements of the grating efficiency.

Column 5 in the table is the ratio of the power contained in the first order diffracted beam to the power transmitted through the grin rod lens. The mean value of the ratio is 0.545 . The grating amplitude reflectivity into the first order is approximately $\sqrt{0.545}$ or 0.74 .

Neutral Density Filters

A neutral density filter is used for the purpose of attenuating an optical field. The filter rating is defined
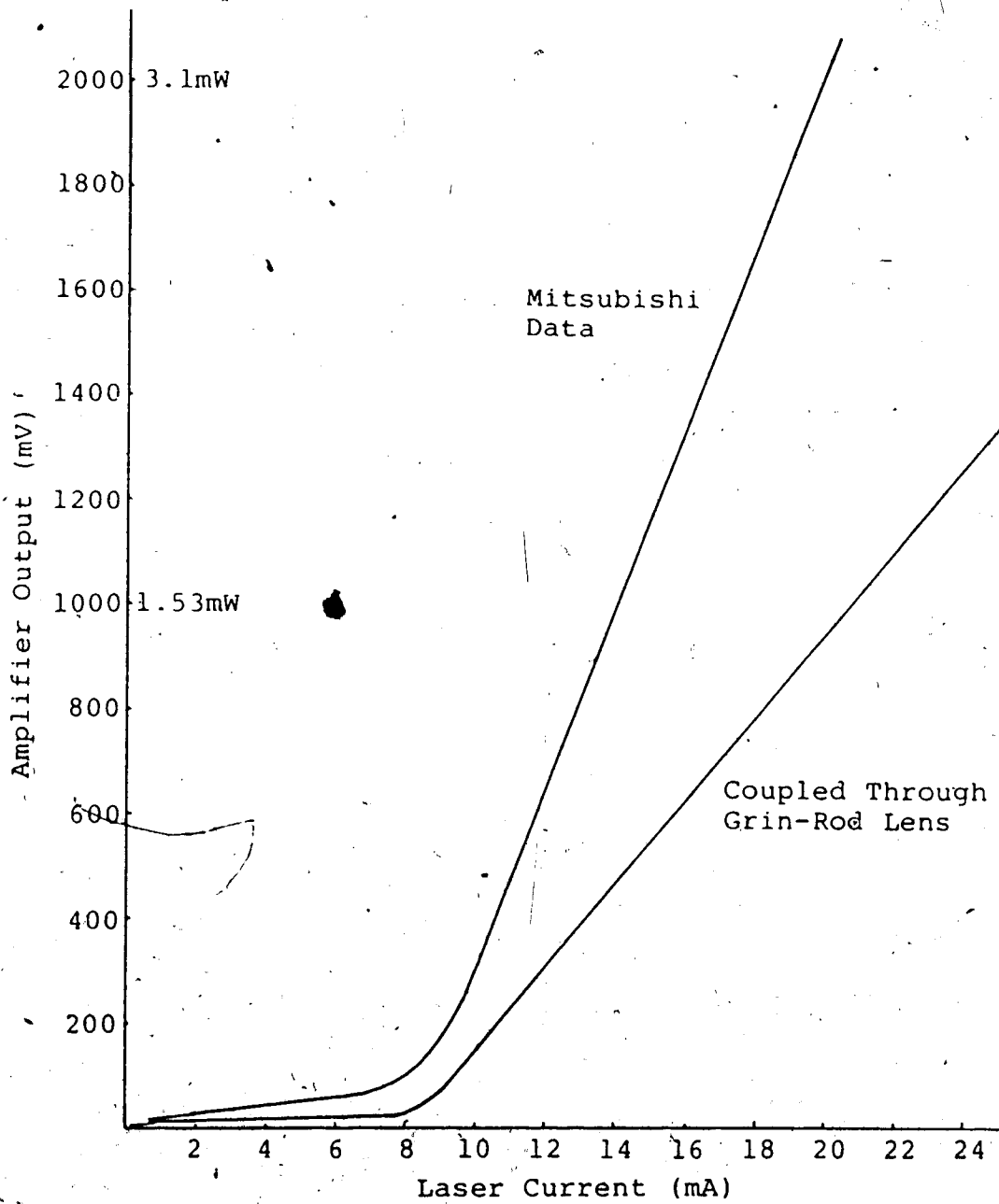
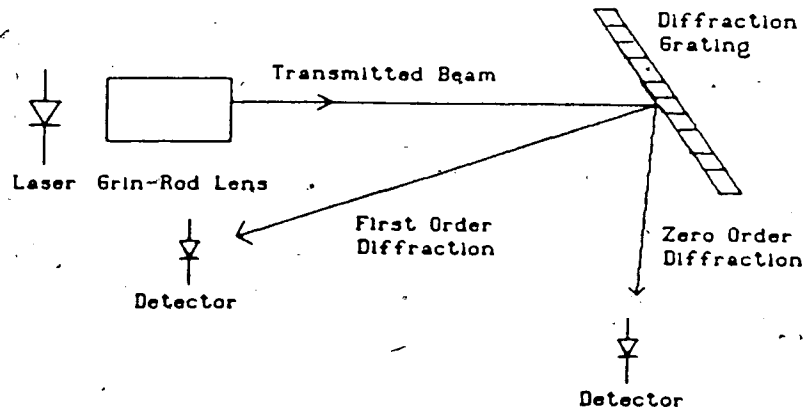**Figure 4-12   Grin Rod Lens Power Transmission**

Figure 4-13 Experimental Configuration for Grating Efficiency Measurements

Current	Transmitted	0 Order	1st Order	Ratio
(mA)	T (mW)	(mW)	(mW)	1st/T
25	1.997	0.086	1.067	0.53
13.01	0.597	0.030	0.334	0.56

Table 4-1 Diffraction Grating Efficiency Measurement Results

as the negative of the logarithim to the base 10 of the ratio of the transmitted optical power to the incident optical power.

The neutral density filters used were Kodak ND 0.7 films. The ND 0.7 rating is for the visible region. To

determine the transmission loss through the filters in the 1.3μm infrared region, Power vs Current measurements were made for a 1.3μm laser with and without two ND 0.7 neutral density filters between the laser and the detector. Figure 4-14 is a plot of the curves obtained with and without the filters in place.
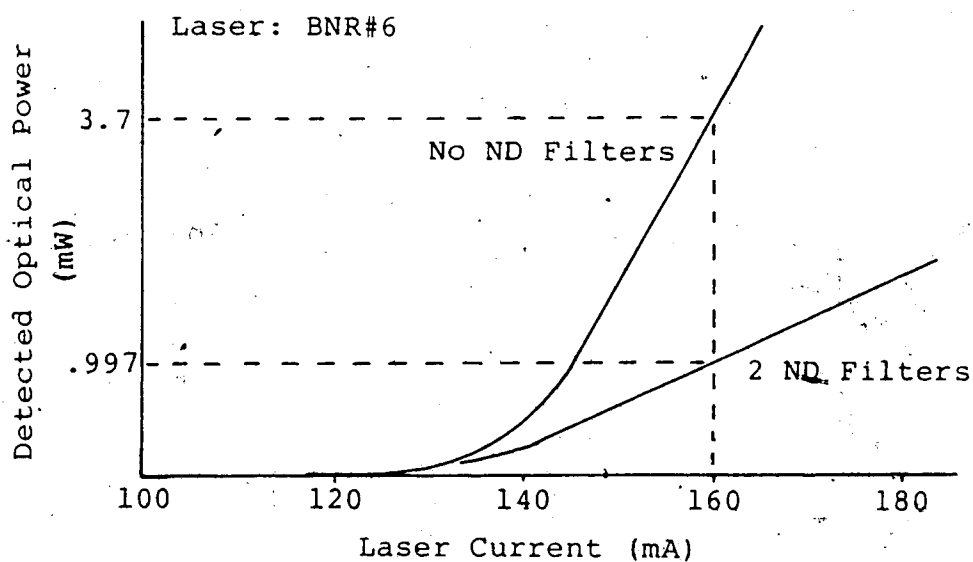

Figure 4-14 Power vs Current Measurements for Neutral Density Filter Analysis

For I>Ith, the ratio of the two curves is, on the average, 1/3.9 . The neutral density rating of the films is

$$ND = -\frac{1}{2} \log \frac{1}{3.9} = 0.3 \ . \qquad (4-2)$$

The factor of 1/2 accounts for two filters being used. The
amplitude attenuation of one filter is $10^{-.15}$ or 0.71 .

Effective Reflectivities

Table 4-2 lists the effective reflectivities of the
long external cavities utilizing grating and mirror
feedback.

	GRATING (.74)	MIRROR (1)
LENS (.51)	.38	.51
1 ND (.50)	.189	.256
2 ND (.25)	.094	.128
3 ND (.13)	.049	.064

Table 4-2 Estimated Effective Reflectivities

The entries in the table which are in parentheses are
two way amplitude transmission losses. Entries which are
not in parentheses are the effective reflectivities for the
associated combination of lens, neutral density filters, and
grating or mirror. For example, the entry which is at the

intersection of the Mirror column and the 2 ND row is the
effective reflectivity when the external cavity is made up
of the grin rod lens, two neutral density filters, and the
mirror. (The grin rod lens is included in all entries.)

4.4 FEEDBACK EXPERIMENTS

The experiments were conducted using the following
three feedback configurations:

1. Short external cavity with mirror

2. Long external cavity with grin rod lens and mirror

3. Long external cavity with grin rod lens and diffraction
   grating

4.4.1 Short External Cavity

4.4.1.1 Feedback Optics

Figure 4-15 illustrates the geometry of the short
external cavity.

The mirror was fabricated by silvering a polished
($\lambda/10$) end of a 2mm x 5in glass rod. The glass rod was
rigidly mounted on top of the xyz translation stage by using
a plexiglass clamping device originally designed for fibers.
Only course angular adjustments were possible. θ_y
adjustments were made by rotating the plexiglass block on
top of the xyz translation stage. θ_x adjustments were made
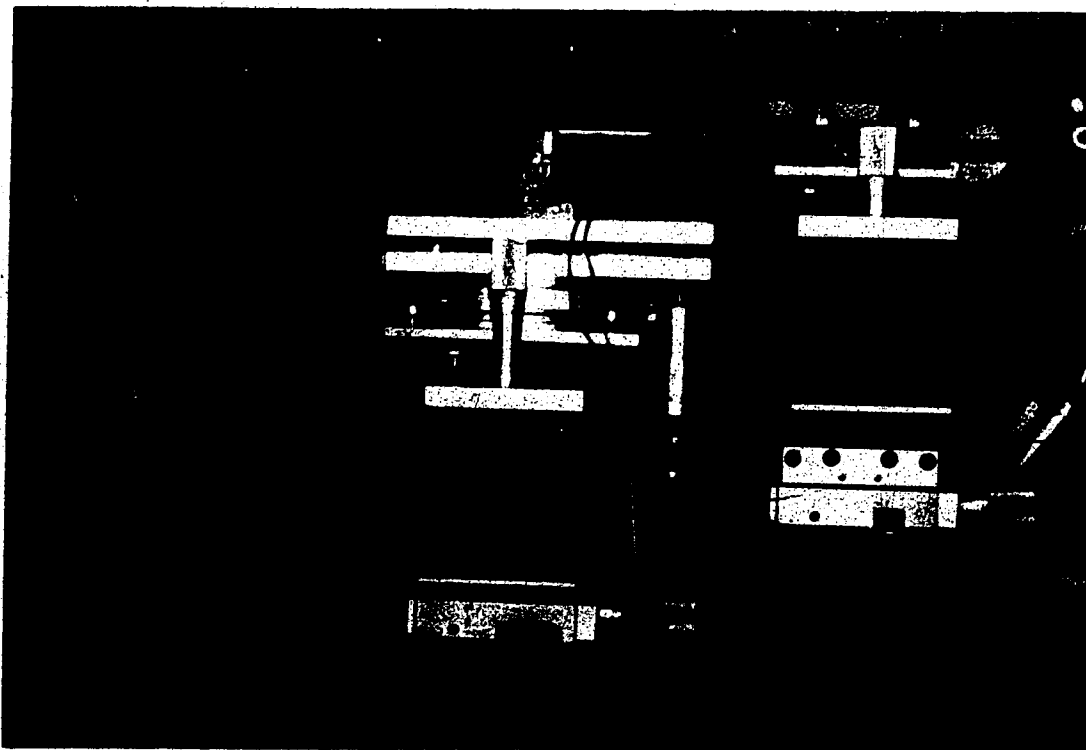by placing paper shims between the plexiglass block and the
xyz translation stage.

Figure 4-15   Short External Cavity Optics

The external cavity length was found to yield the
largest spectral control at approximately 20μm. Fine tuning
of the external cavity length was limited by the accuracy of
the z translation stage.

4.4.1.2 Experimental Results

Feedback Alignment

Since the threshold current is directly proportional to
the laser cavity losses, the threshold current will be
reduced when the external cavity is aligned. The external
cavity effectively increases the laser facet reflectivity.
From Equation 2-15, it is seen that increasing the

reflectivity will decrease the cavity losses. Figure 4-16
illustrates the geometry of the experimental set up used
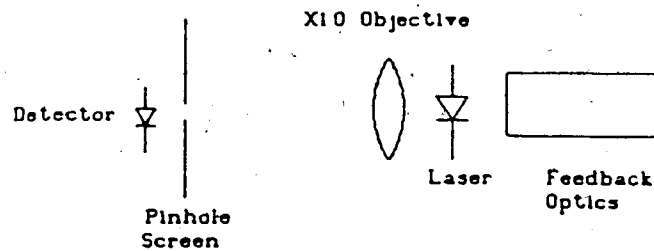while aligning the feedback.

Figure 4-16 Optical Configuration Used for Alignment

The laser was driven with the triangular wave described
in Section 4.1.2 . Figure 4-17 illustrates the expected
change in the detected optical power, ΔP, due to a decrease
in the threshold current, ΔI_{th}, caused by feedback. Figure
4-18 illustrates an undesired effect due to the detection of
radiation reflected back from the feedback path, but not
properly aligned to alter the threshold current. To prevent
incorrectly interpreting the back reflected radiation as an
increase in optical power due to correct alignment, the
output from the left facet of the laser was focused onto a
100μm pinhole and detected with the UDT detector. Any
radiation which is not properly focused onto the pinhole
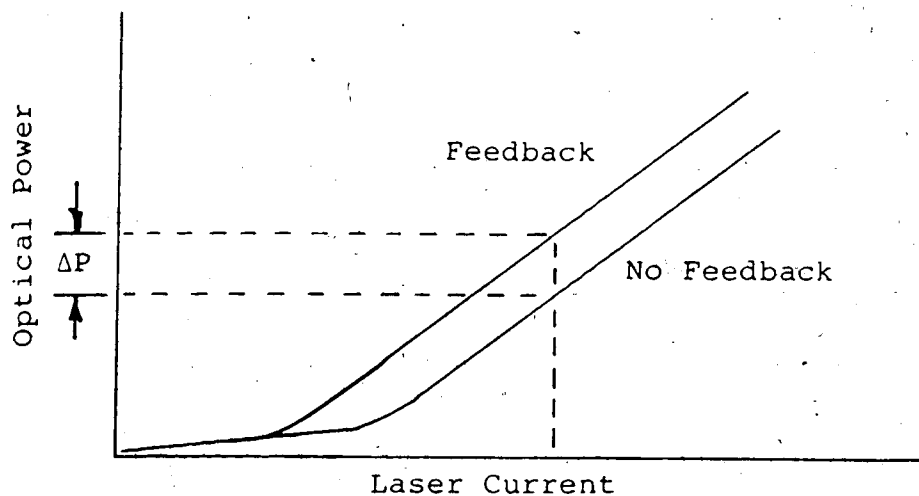would not contribute significantly to the detected optical
power.

Figure 4-17 Expected Change in Detected Optical Power Due to a Decrease in the Threshold Current with Feedback

Figure 4-19 shows actual results after aligning the mirror. Figure 4-20 shows the interpretation of Figure 4-19.

The threshold current decreases from 8.8mA to 8.2mA which is equivalent to a 6.8% reduction. It is also seen that the slope increases under feedback, indicating either an increase in the external quantum efficiency or detection of back reflected radiation.

There are two observations which preclude the detection of back reflected radiation as an explanation for the increase in the slope $\Delta P/\Delta I$.

1. The detected radiation, below threshold, is equal in both the feedback and non-feedback cases.
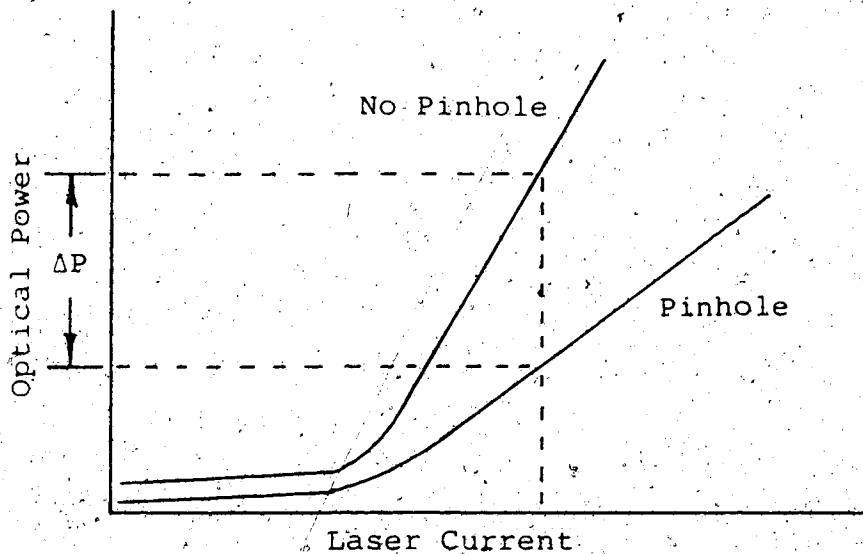
Figure 4-18 Expected Change in Detected Optical Power Due to Back Reflected Radiation

2. One experimental observation, to be outlined, shows an actual increase in the threshold current along with a decrease in the slope $\Delta P/\Delta I$.

Figures 4-21 and 4-22 are composite Power vs Current curves put together from data taken using different combinations of the pinhole and feedback.

Figure 4-21 shows the change in detected optical power when the pinhole is removed under feedback conditions. The feedback optics consist of the grin rod lens and the diffraction grating. Note that below threshold there is a significant increase in the detected optical power when the pinhole is removed. Figure 4-22 shows the change in detected optical power when radiation is fed back into the
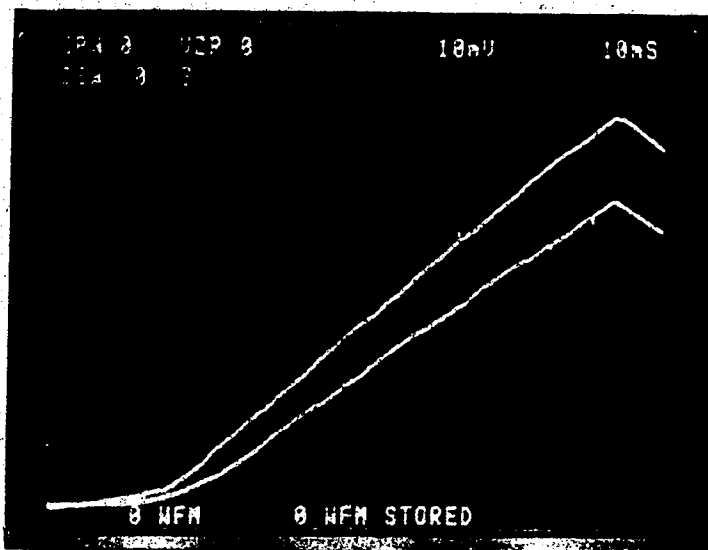
Figure 4-19 Power vs Current With (upper curve) and Without (lower curve) Feedback for Short External Cavity.
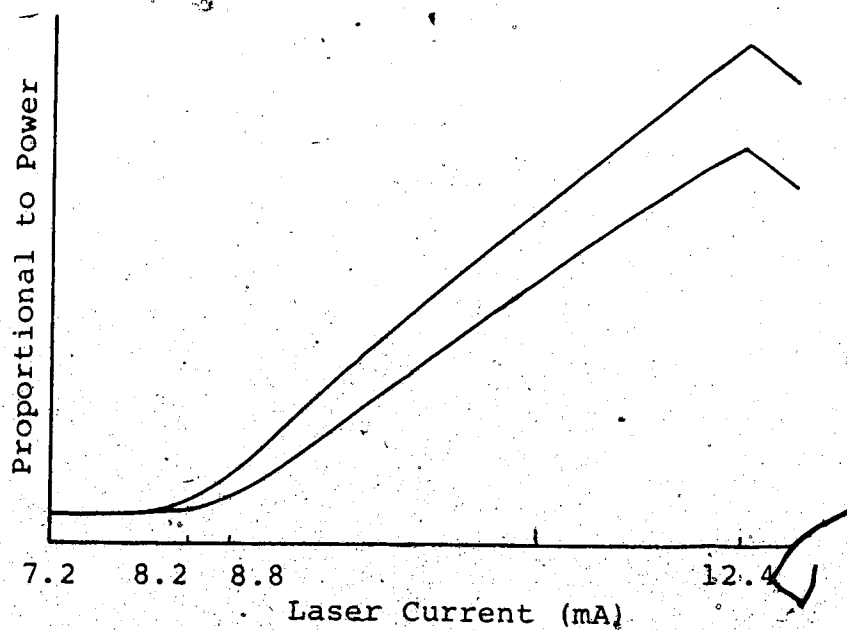

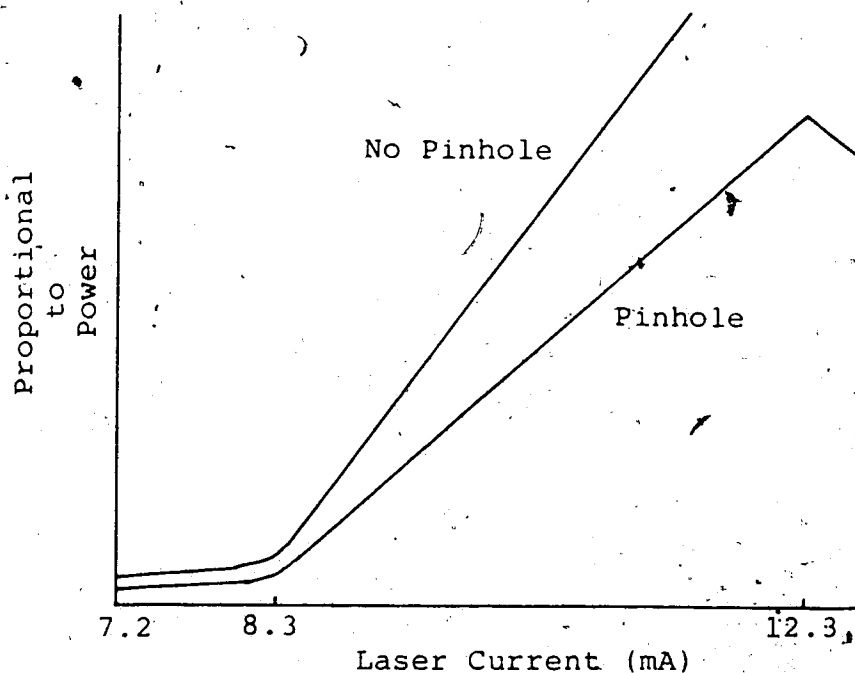**Figure 4-20** Analysis of Figure 4-19

Figure 4-21 Change in Detected Optical Power When Pinhole is Removed Under Feedback Conditions

laser with the pinhole in place. The lower curve (no feedback) defines the baseline for comparison. Since the detected power does not increase below threshold when radiation is fed back into the laser, it is concluded that the pinhole effectively filters out the back reflected radiation. It is unlikely that the change in $\Delta P/\Delta I$, above threshold, is caused by back-reflected radiation from the feedback optics.

Figure 4-23 shows Power vs Current curves for:

1. Upper curve - feedback adjusted (z translation) for minimum threshold
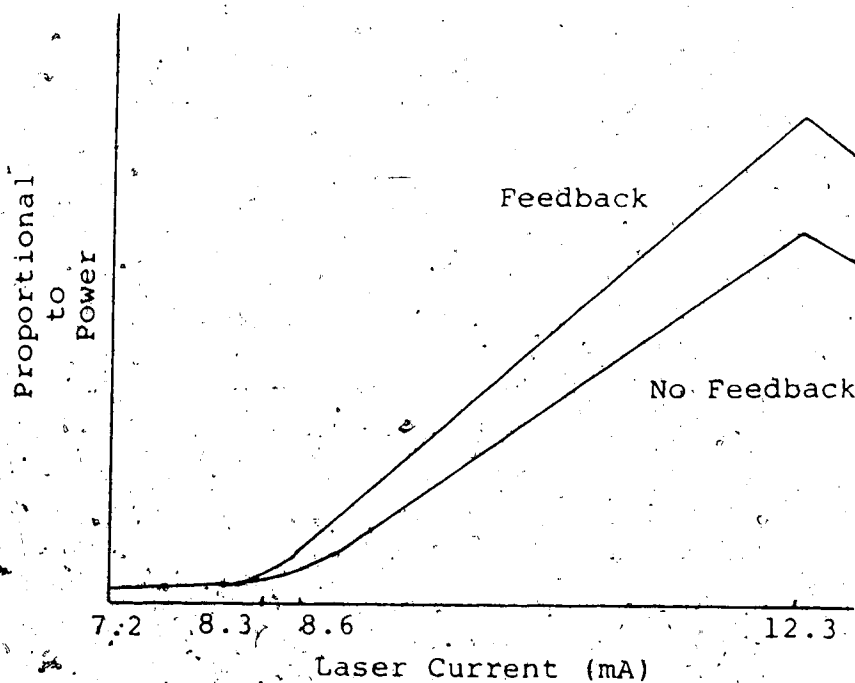
2. Middle curve - no feedback

Figure 4-22 Change in Detected Optical Power When Radiation is Fed Back into the Laser with the Pinhole in Place

3. Bottom curve - feedback adjusted for maximum threshold

The feedback is from the short external cavity with the mirror.

The bottom curve shows:

1. The detected optical power below threshold is equivalent to the detected optical power below threshold in the no feedback case.

2. The threshold current is greater than the threshold current in the no feedback case.

3. The slope $\Delta P/\Delta I$ is less than that in the feedback case. An increase in the threshold current combined with an apparent decrease in the external quantum efficiency can not
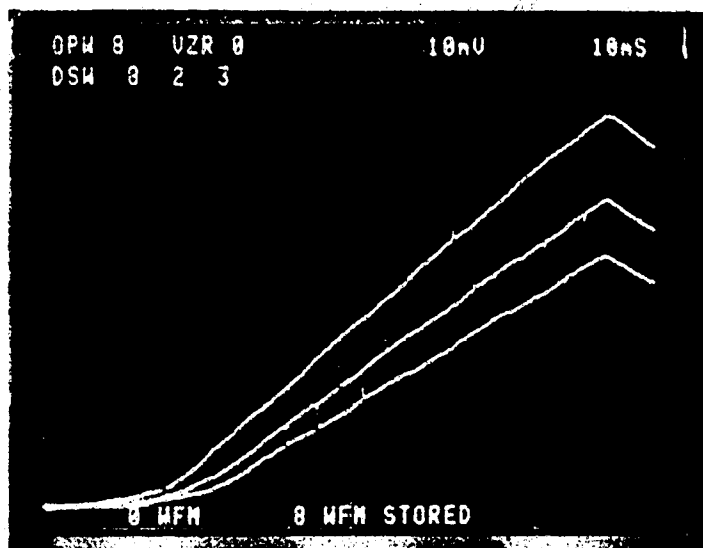
Figure 4-23 Power vs Current - Short External Cavity Feedback

be explained by the detection of back-reflected radiation. In summary, the apparent changes in the external quantum efficiency, whether an increase or a decrease, are not due to the detection of back-reflected radiation. The changes are conclusively real, and are caused by the external cavity feedback.

Laser Spectrum

Figure 4-24 shows the laser spectrum.

The spectrum was obtained after first adjusting the feedback for minimum threshold. The pinhole was then removed and the 10X objective was refocused to collimate the laser output for the Fabry-Perot Interferometer. The Fabry-Perot mirror spacing is 2.5mm giving a free spectral
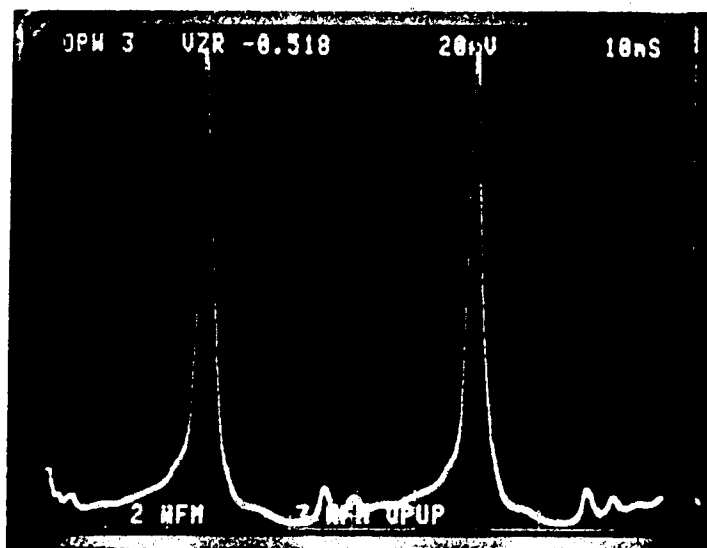
Figure 4-24   Spectrum - Short External Cavity Feedback

range of 60Ghz.   Assuming a finesse of 50, the instrument

resolution is approximately 1.2Ghz.

The FWHM of the spectrum is measured from Figure 4-24

to be 3.8Ghz.

4.4.2 Long External Cavity with Mirror Feedback

4.4.2.1 Feedback Optics

Figure 4-11 illustrates the geometry of the external

cavity.

The laser radiation was collimated using a .23P, 1.8mm

diameter, 4.4mm long grin rod lens.   It is mounted with an

in-house designed and fabricated holder attached to an

extension tube and standard microscope objective holder.

The entire assembly is attached to an xyz translation stage.

Only coarse θ_y adjustments were possible by rotating the objective holder on top of the xyz translation stage. θ_x adjustments were made by placing paper shims between the objective holder and the xyz translation stage. Due to the lack of proper mirror positioning equipment, a custom mounting stage which was fabricated for the diffraction grating, was utilized for the mirror by taping the mirror onto the back of the diffraction grating mounting plate. The external cavity length was approximately 15cm. Fine tuning of the external cavity length was limited by the accuracy of the $20\mu m$/small division micrometer, given by the manufacturer to be $3\mu m$.

4.4.2.2 Experimental Results

The external cavity was aligned for minimum threshold using the alignment technique outlined in Section 4.4.1.2 . Figure 4-25 shows the reduction in threshold current. Figure 4-26 shows the analysis of Figure 4-25.

The threshold current is reduced from 9.0mA to 8.4mA or 6.7%. The discrepancy in threshold currents between Figures 9 and 4-25 is likely due to slight changes in the laser operating temperature. The measurements were taken on different days and the ambient room temperature tended to vary over several degrees. The slopes, $\Delta P/\Delta I$ for I>Ith, are 0.7 for the short external cavity case and 0.66 for the long external cavity case. The external quantum efficiencies are approximately equivalent in the non-feedback cases. The similarity in external quantum efficiency indicates that the
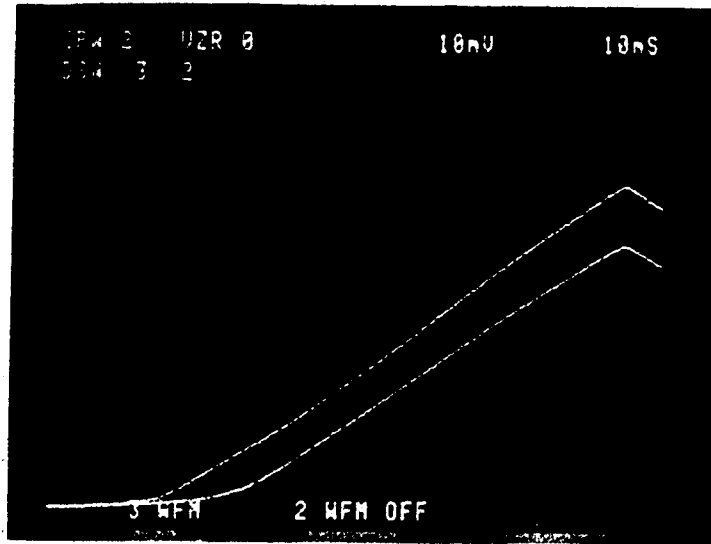
Figure 4-25 Power vs Current With (upper curve) and Without (lower curve) Feedback for Long External Cavity With Mirror Feedback.
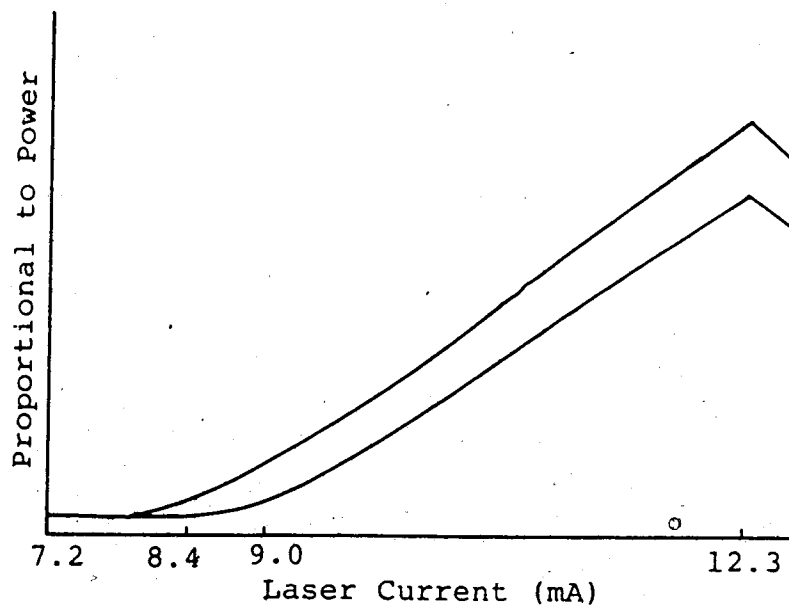

Figure 4-26 Analysis of Figure 4-25

difference in threshold current is probably due to temperature differences and not due to extraneous feedback (ie.from the 10X objective).

Laser Spectrum

Figure 4-27 shows two free spectral ranges of the laser spectrum measured by the Fabry-Perot Interferometer. The laser current is 25mA. The feedback path is blocked. It is important to note that the grin rod lens is positioned ~260μm from the laser and may have unwanted feedback effects on the laser as outlined in Section 4.5 . The interferometer mirror spacing is ~140μm giving a free spectral range of 1.1Thz. The instrument resolution is ~20Ghz. The FWHM of the dominant longitudinal mode is measured from Figure 4-27 to be ~21Ghz.

Figures 4-27 to 4-31 demonstrate consistency with the theory proposed by Osmundsen and Gade [23] and outlined in Chapter 3.

Figure 4-32 illustrates a concept which will be used to evaluate Figures 4-27 to 4-31.

The upper and lower envelopes of the spectra, as defined in Figure 4-32, indicate the effect that the varying levels of feedback have on the laser. Osmundsen and Gade [23] demonstrated that under strong feedback, the phase condition would be satisfied for a continuum of external cavity modes ranging across the entire frequency range between longitudinal mode solutions of the solitary laser.
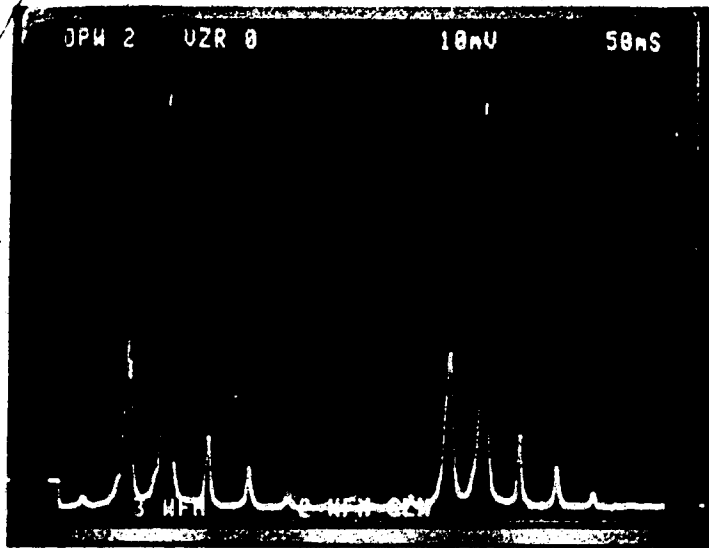
Figure 4-27   No Feedback
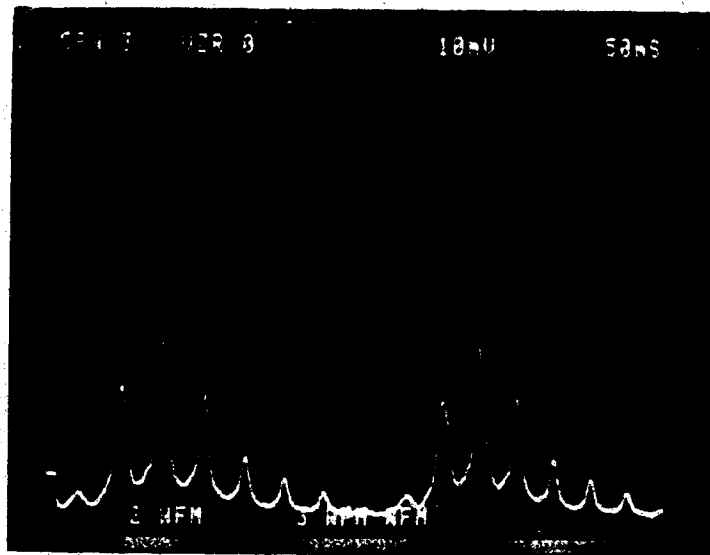
Figure 4-28   Feedback / No Neutral Density Filters

Under strong feedback, the expected spectrum is similar to Figure 4-32A. The amplitude of the bottom envelope will be
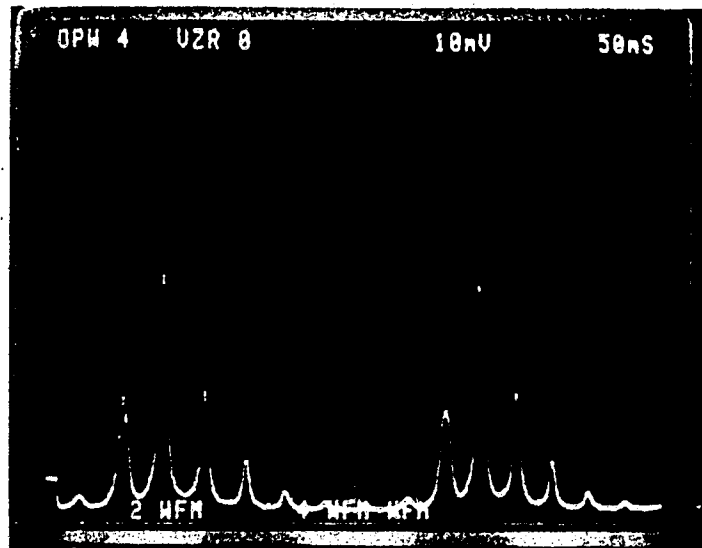
Figure 4-29 Feedback / One Neutral Density Filter

Figure 4-30 Feedback / Two Neutral Density Filters

increased due to the distribution of energy into external
cavity modes which are removed from the solitary laser

Figure 4-31 Feedback / Three Neutral Density Filters

A. Strong Feedback

B. Weak Feedback

Figure 4-32 Spectral Envelopes

modes. The amplitude of the upper envelope will be

decreased due to the finite amount of energy available for distribution amongst the competing longitudinal modes [26].

As the attenuation in the feedback path is increased, the number of solutions to the phase conditon will decrease. Only external cavity modes in the vicinity of solitary laser modes will participate in th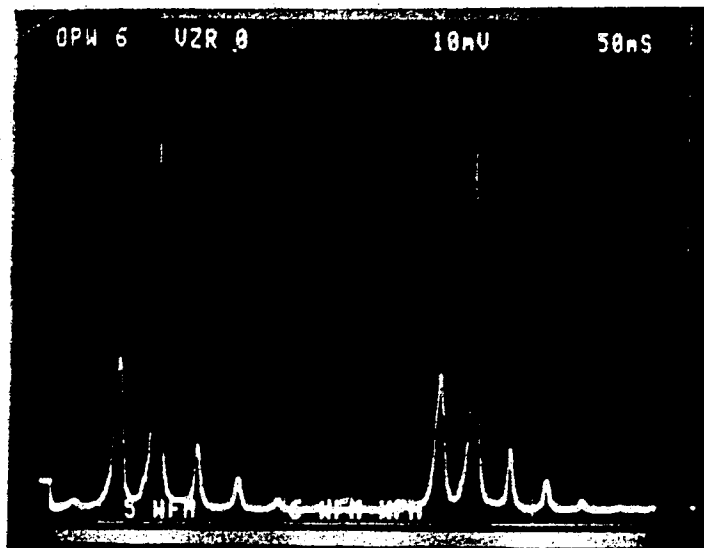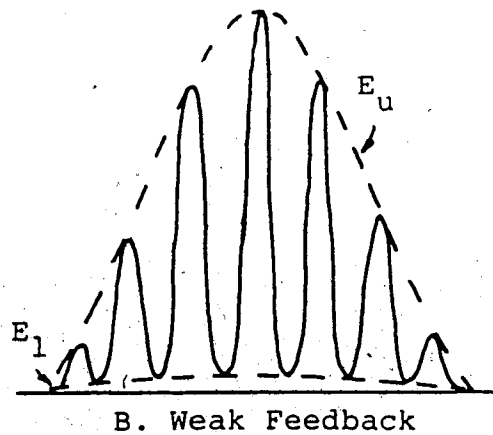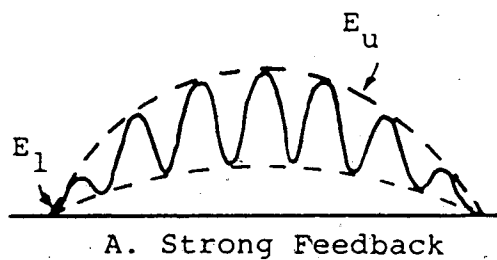e lasing. In this case, the expected spectrum will be similar to Figure 4-32B. The amplitude of the bottom envelope will decrease due to the absence of lasing modes between the solitary laser modes. The amplitude of the upper envelope will increase due the distribution of the available energy into a fewer number of longitudinal modes. Furthermore, the decrease in the number of external cavity modes, with increasing attenuation in the feedback path, causes the FWHM frequency range in the vicinity of the solitary laser longitudinal modes to decrease.

The changing envelope amplitudes and longitudinal mode FWHM with changing feedback levels are readily observable in Figures 4-27 to 4-31.

Figures 4-27 and 4-28 were obtained with infinite (blocked) and zero attenuation in the feedback path respectively. Figures 4-29 to 4-31 were obtained with one, two, and three neutral density filters (ND 0.3 1.3μm) in the feedback path respectively. Table 4-3 summarizes the results obtained from Figures 4-27 to 4-31. The reflectivities, r_3, listed in Table 4-3, were determined in Section 4.3 .

Figure	ND Filters	r_3	FWHM (Ghz)	Ratio
4-27	0	0	21 *	44
4-28	0	.51	41	9.7
4-29	1	.256	36	15.2
4-30	2	.128	26	25
4-31	3	.064	21 *	30.5

* Approximately equal to the resolution of the
interferometer.

Table 4-3 Summary of Long External Mirror Cavity Results

The maximum feedback case, shown in Figure 4-28, yields
the maximum FWHM and the minimum envelope ratio E_u/E_1. As
the attenuation is increased, the FWHM decreases and the
envelope ratio increases.

The number of solutions to the phase condition may be
estimated for different values of external cavity
reflectivity. Figure 4-33 shows a hypothetical graphical
solution to the phase condition. For weak feedback,
solutions to the phase condition will occur over a region
centered about the mode solutions to the solitary laser
phase condition.
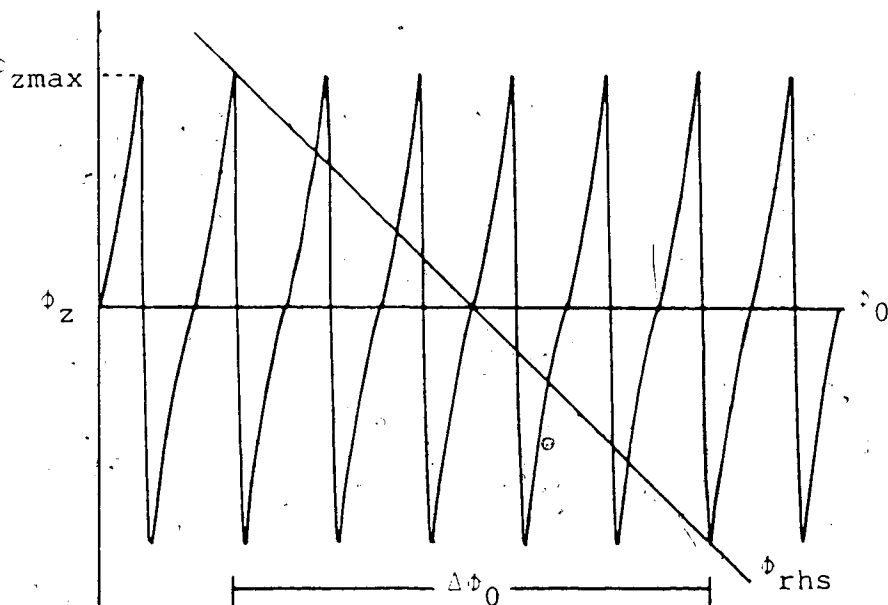
Figure 4-33   Solution Region of the Phase Condition

The solution region $\Delta\phi_0$ will be approximately

$$\Delta\varphi_0 = \frac{2\varphi_{z\ max}}{d\varphi_1/d\varphi_0} \qquad (4-3)$$

where ϕ_{zmax} is as given in Figure 3-3, and

$$\frac{d\varphi_1}{d\varphi_0} = \frac{n\ell}{L} \qquad (4-4)$$

is the slope of the line defining ϕ_{rhs}, ϕ_z goes through one period every 2π radians with 2 solutions to the phase condition per period. Therefore, an estimate of the number of solutions, S, is given by

$$S = \frac{2\varphi_{z\ max}\ L}{\pi n \ell} \cdot$$ <div align="right">(4-5)</div>

For an external cavity length of 15cm, a laser cavity length of 300μm, and laser index of refraction of 3.5 [28], the slope $\Delta\phi_1/\Delta\phi_0$ is determined, from Equation 4-4, to be .007.

Table 4-4 lists the number of solutions as a function of the external cavity reflectivity, r_3.

r_3	ϕ_z	Solutions
.51	.32	29
.256	.11	10
.128	.05	5
.064	.02	2

Table 4-4 Solutions to the Phase Condition

Data from Tables 4-3 and 4-4 are plotted in Figure 4-34 as a function of the external cavity reflectivity, r_3.

The FWHM decreases proportionately with decreases in the effective reflectivity for $r_3 < .25$. There is good indication that the FWHM can be further reduced with
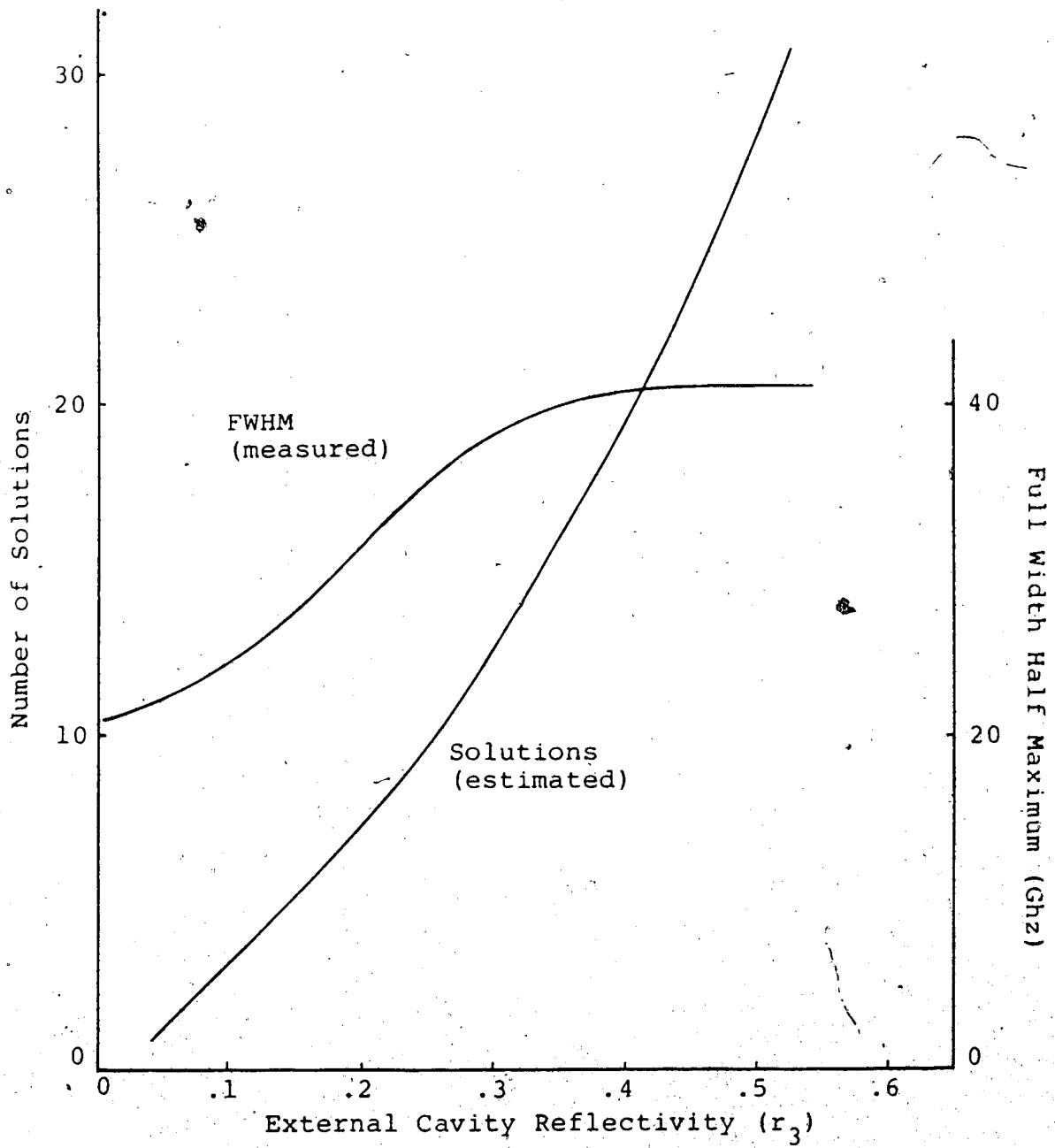
Figure 4-34 Relationship Between Solutions to the Phase Condition and FWHM

corresponding further reduction in the effective reflectivity. However, measurements were limited by the resolution of the Fabry-Perot Interferometer. It was not possible to increase the interferometer mirror spacing due to the multi-longitudinal mode full width of the laser spectrum being broader than the free spectral range of the interferometer. For $r_3 > .25$, the FWHM tends to saturate. The saturation is based upon 1 data point and may not be reliable. However, it is reasonable to expect the FWHM to saturate in the vicinity where $r_3 \simeq r_2$ since the number of solutions to the phase condition remains constant for $r_3 > r_2$.

Goldberg et al. [24] found that attenuation in the order of 10^{-4} was necessary to cause single external cavity mode oscillation resulting in linewidths in the order of 100Khz (The longitudinal mode FWHM of the solitary laser used in their experiments was ~17Mhz.). In the experimental work presented here, the laser spectrum appears to revert back to the solitary laser spectrum as the attenuation approaches 10^{-2}. However, for linewidths below the solitary laser linewidth, the measurements were limited by the resolution of the Fabry-Perot Interferometer.

Although the experimental work, with the long external cavity with mirror feedback, did not appear to yield single external cavity mode oscillation, the data obtained are, in general, consistent with theory put forth by Osmundsen and Gade [23].

4.4.3 Long External Cavity with Diffraction Grating Feedback

4.4.3.1 Feedback Optics

Figure 4-11 illustrates the geometry of the external cavity.

The grin rod lens and mount are described in Section 4.4.2.1 . The diffraction grating has 1200 lines/mm and is blazed for $0.75 \mu m$. It is oriented with its lines parallel to the junction plane to fully utilize the advantages of the small dimension of the active region which are:

1. Illumination of the maximum number of grating lines.
2. The active region aperture is smallest in the vertical direction, enhancing selection of a minimum wavelength range from the dispersed radiation from the grating.

The grating is mounted on a positioning device which provides y, z, θ_x, and $\Delta \theta_y$ movements. The angular motion about the y axis is differentiated from pure angular rotation by the Δ prefix since the motion is provided by a tilt stage, instead of a proper rotational micrometer. The precision of the rotational micrometer utilized for θ_x positioning is approximately .25°.

4.4.3.2 Experimental Results

The external cavity was aligned for minimum threshold using the alignment technique outlined in Section 4.4.1 . Figure 4-35 shows the reduction in threshold current. Figure 4-36 shows the analysis of Figure 4-35. The threshold current is reduced from 8.8mA to 8.3mA or 5.7%.
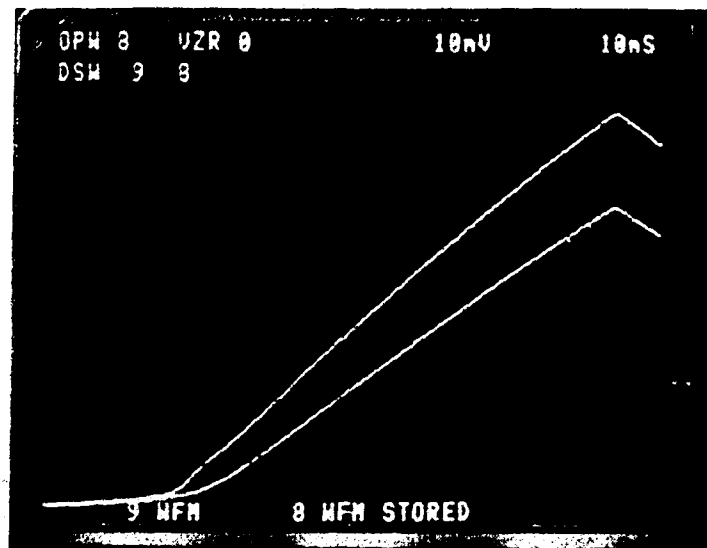
Figure 4-35 Power vs Current With (upper curve) and Without (lower curve) Feedback for Long External Cavity with Grating Feedback.
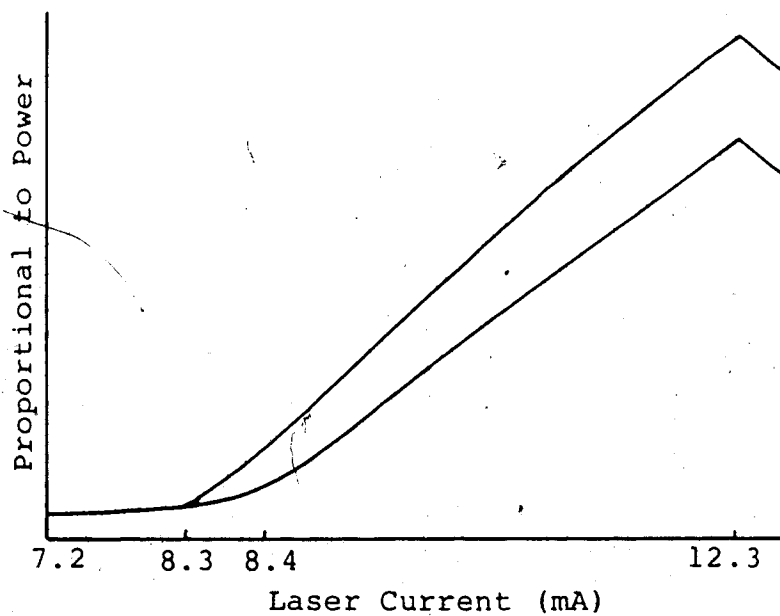
Figure 4-36 Analysis of Figure 4-35

Rotating the diffraction grating resulted in a periodic change in the laser output intensity with grating position. Figure 4-37 shows the amplifier output as a function of grating angle.
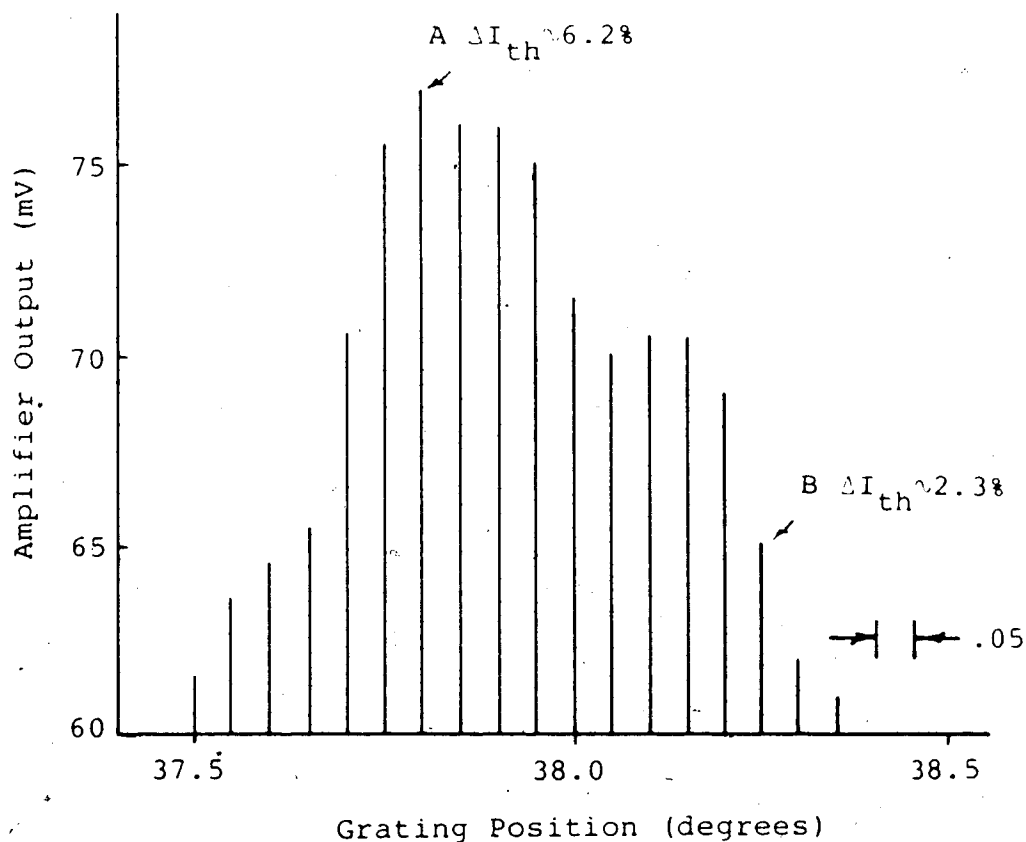
Figure 4-37 Detector Output as a Function of Grating Angle

The abscissa scale could only be estimated due to the low precision of the rotational micrometer. The abscissa increment between successive intensity peaks is approximately .05°. It is possible to verify the accuracy of this figure as it should be equivalent to the calculated angular separtion, between successive longitudinal modes, of

the diffraction grating.

The diffraction grating parameters are m=1, d=1/1200 mm, and λ=1.3μm. From equations 3-28 and 3-29, the angular separation for Δλ=8.2Å is .045°. The experimentally estimated value for the grating angular separation of .05° is in close agreement with the theoretical value of .045°. The resolution of the grating and the imaging of the radiation returned from the grating must also be estimated to ensure that the grating and lens will adequately separate the longitudinal modes. Each selected mode should affect the laser without interference from adjacent modes.

The manufacturer's specifications for the grin rod lens are:

1. Quadratic constant = .327

2. Numerical aperture = .46

3. Diameter = 1.8mm

4. Length = 4.4mm

5. Working distance (collimated output) =260μm

Using the above parameters and solving the ABCD matrix equation (Equation 3-40), given in section 3.4, for y_3 (Figure 3-11) yields a spot diameter on the grating of 3.2mm. 3.2mm is an unreasonable value for the spot size since the grin rod lens diameter is only 1.8mm. The ABCD matrix for the grin rod lens is not valid in this case. The spot size was estimated from experimental work to be approximately 750μm. Substituting a spot size of 750μm into equation 3-31 yields the FWHM angular divergence of the

dispersed rays to be ~.3°.

The estimated grating resolution of .3° is very poor. At a diffracted mode angular spacing of .05°, the diffracted beam from one mode will easily overlap four adjacent longitudinal modes. Due to the poor reliability of the ABCD transfer matrix for the grin rod lens, it is difficult to determine spot sizes and relative positioning on the laser face. However, due to the indicated overlap in the diffracted beams, the resultant spots on the grating face will overlap significantly. It is expected that this would increase the difficulties in obtaining single longitudinal mode oscillation due to the partial feed back of adjacent longitudinal modes.

However, it is evident that the observed periodic change in the output intensity with grating rotation is due to the feedback from consecutive longitudinal modes. The laser appears to be responding favourably to the feedback even though the estimation of the grating resolution indicates the optics are not optimum.

The peak indicated as A in Figure 4-37 corresponds to the maximum observed threshold reduction of 5.7%. Figure 4-38 shows the threshold reduction for the peak indicated as B in Figure 4-37. Figure 4-39 is the analysis of Figure 4-38. The threshold reduction is from 8.8mA to 8.5mA or 3.4%. For the case of peak B (Figure 4-37), the grating is tuned such that the feedback wavelength is situated near the long wavelength edge of the gain curve.
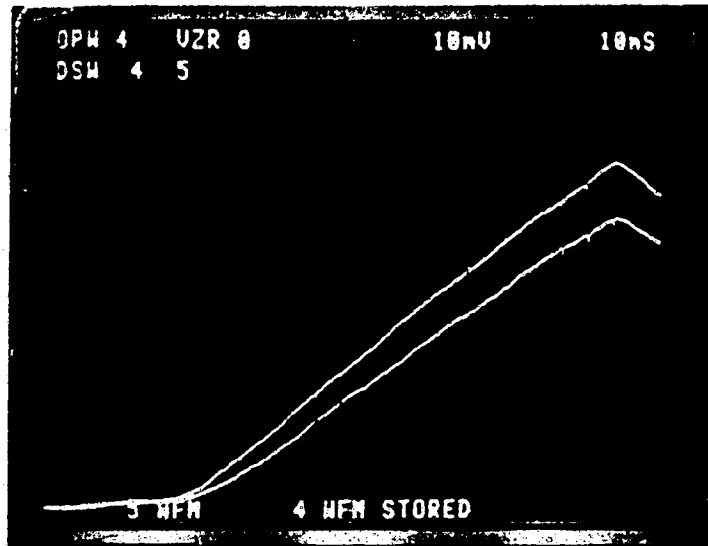
Figure 4-38 Power vs Current With (upper curve) and Without (lower curve) Feedback for External Grating Position B.
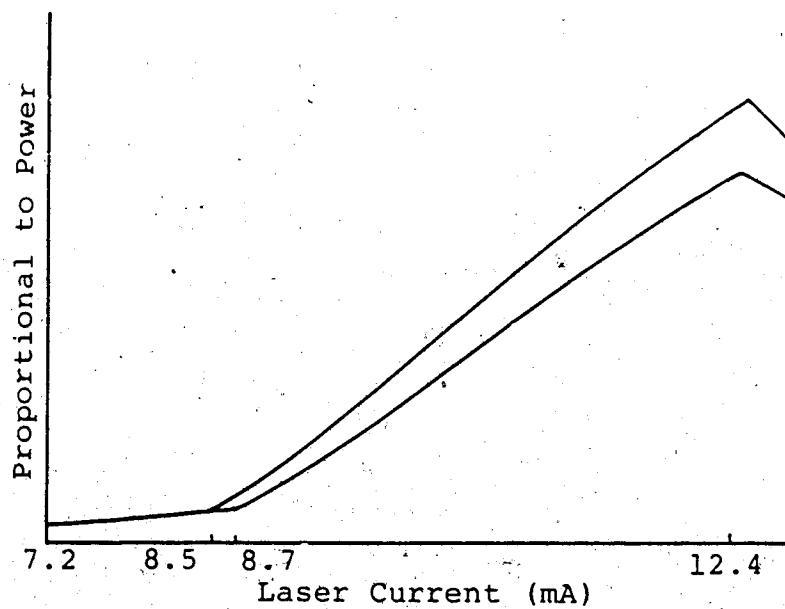
Figure 4-39 Analysis of Figure 4-38

Laser Spectrum

Figure 4-40 shows the spectrum of the laser when the
feedback is aligned for minimum threshold.
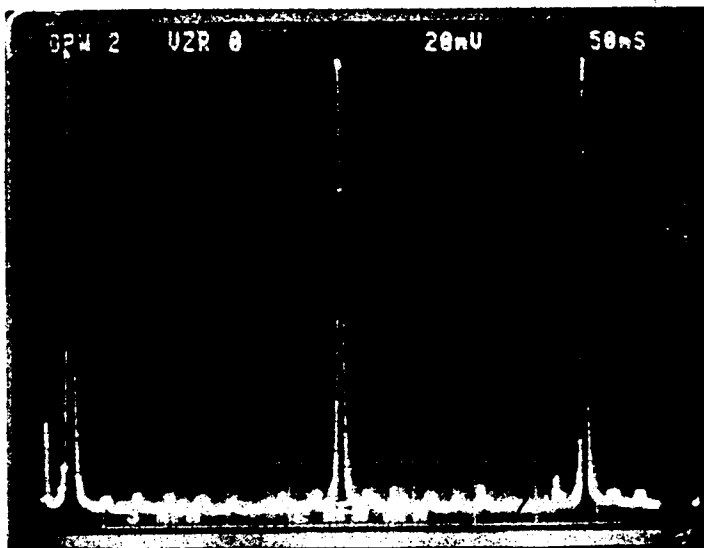
Figure 4-40 Laser Spectrum - Long External Cavity with
Grating Feedback

Approximately two free spectral ranges of the Fabry-Perot
Interferometer are shown. The laser current is 13.01mA.
The Fabry-Perot Interferometer mirror spacing is ~120μm
which gives a free spectral range of ~1.2Thz.

The side mode suppression ratio from Figure 4-40 is
36:1 or 15.6db. The side mode suppression ratio in the
non-feedback case is determined, from Figure 4-6, to be
5.1:1 or 7.1db. The external cavity results in an
improvement to the side mode suppression ratio of 8.5db.

Figures 4-41 to 4-43 show the tuning effect on the
spectrum as the grating is rotated. The figures show the

tuning of three separate longitudinal modes located near the

centre of the gain curve. The laser was similarly tuned to

twelve different longitudinal modes over a range of ~98Å or

1.8Thz.
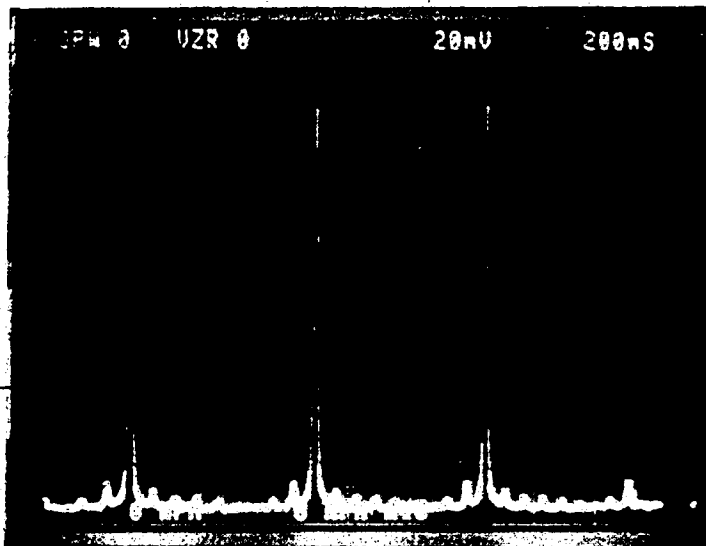
Figure 4-41   Spectrum Tuning - Grating Position m-1

Longitudinal Mode Linewidth

Figure 4-44 shows approximately three free spectral

ranges of the Fabry-Perot Interferometer output. The mirror

spacing is 3mm which gives a free spectral range of 50Ghz.

The instrument resolution is approximately 1Ghz. The FWHM

frequency spread of the longitudinal mode is measured from

Figure 4-44 to be 15.8Ghz. A FWHM of 15.8Ghz is broader

than the expected linewidth of the solitary laser

longitudinal modes which is in the megahertz range [17,24].
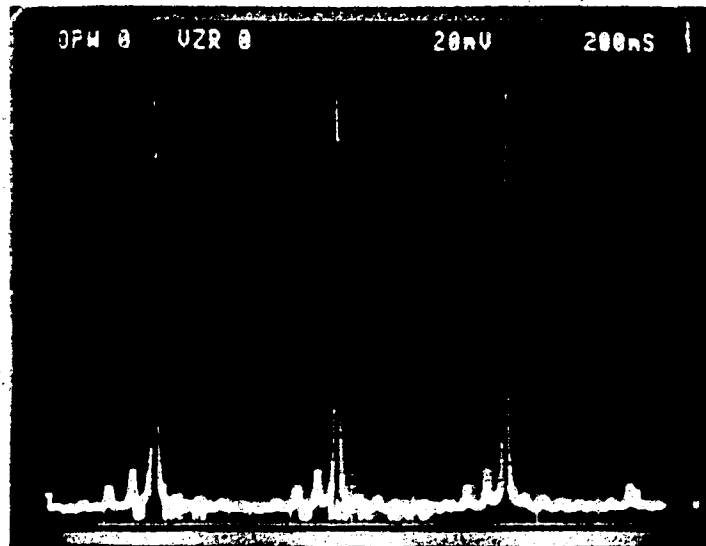
Figure 4-42   Spectrum Tuning - Grating Position m
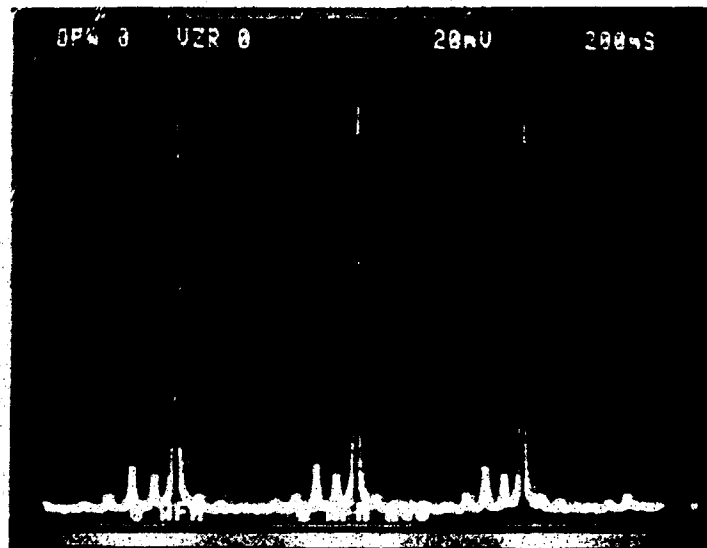
Figure 4-43   Spectrum Tuning - Grating Position m+1

From the results of Section 4.4.2, it was expected that placing neutral density filters in the feedback path would
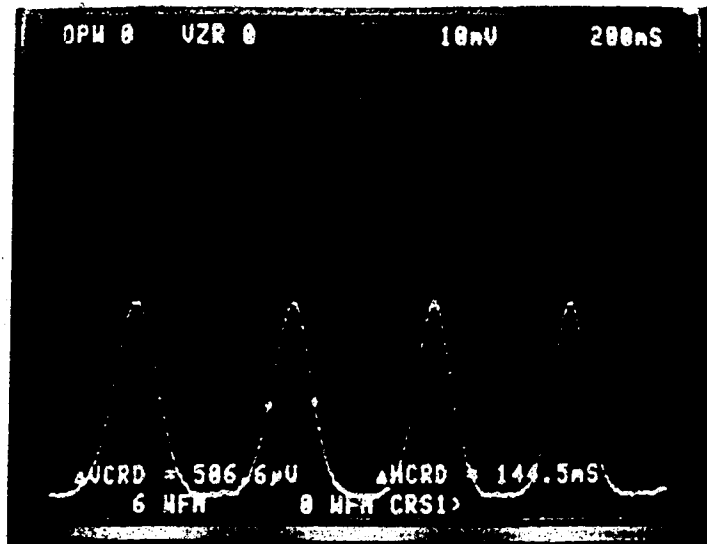
Figure 4-44 High Resolution Spectrum Measurement / FWHM
~16Ghz

decrease the FWHM of the longitudinal mode. However, as the
neutral density filters were placed in the feedback path,
two problems occurred.

First, the laser tended towards multi-longitudinal mode
oscillation. With the Fabry-Perot Interferometer adjusted
for maximum resolution, the corresponding small free
spectral range caused overlapping of adjacent orders and
resulted in the FWHM appearing to broaden. Attempts to
retune the laser were hindered due an inability to align for
minimum threshold while observing the spectrum.

The second problem preventing the FWHM from responding
as expected to increased attenuation in the feedback path is
shown in Figures 4-45 and 4-46. Figure 4-45 shows the
spectrum with three neutral density filters in the feedback
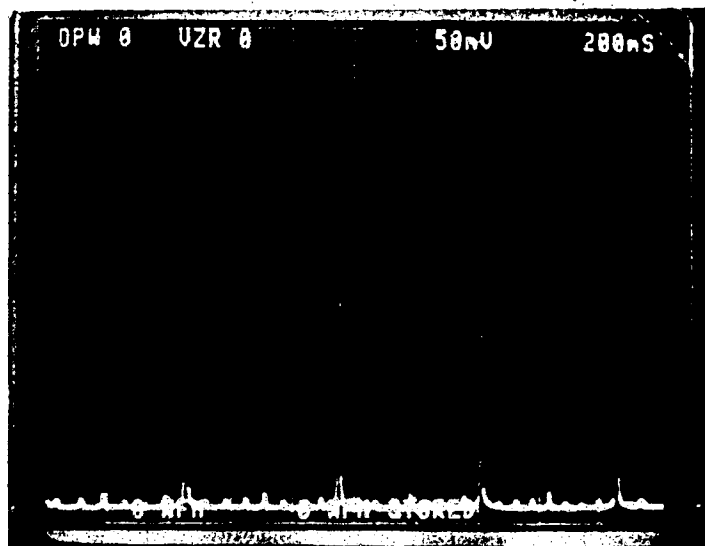
Figure 4-45 Spectrum Obtained With Three ND Filters in the Feedback Path and also With the Feedback Path Blocked
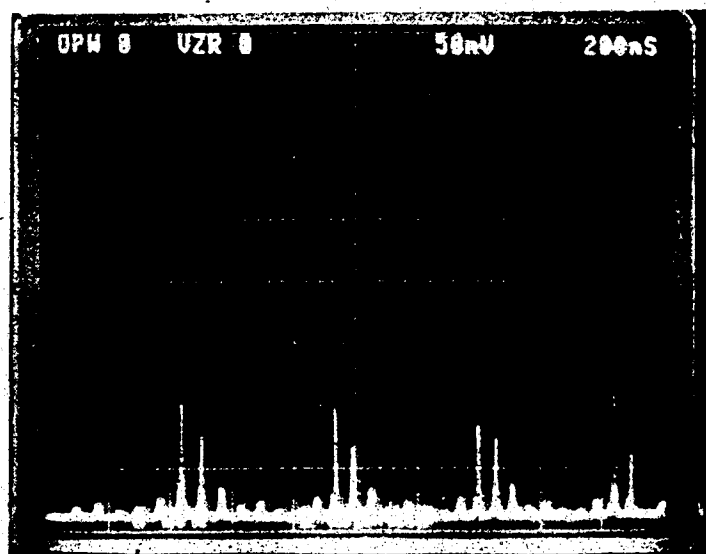
Figure 4-46 Spectrum After a Minor Adjustment to Position of the Grin Rod Lens.

path. (The Fabry-Perot Interferometer mirror spacing is

~125μm.) The spectrum in Figure 4-45 did not change when

the feedback path was blocked. Evidently, reflections from
the AR coated grin rod lens are causing tuning of the laser.
Verification of grin rod tuning is shown in Figure 4-46
where a slight (much less than 10μm) adjustment is made to
the z drive of the grin rod lens mount. This caused the
spectrum to change significantly. (Actually, the tuning is
caused by weak feedback from a short external cavity.)

4.4.3.3 Extraneous Feedback

In addition to the feedback from the grin rod lens,
extraneous feedback was also observed originating from the
optics on the output side of the laser. Figure 4-47 shows
two laser spectra.
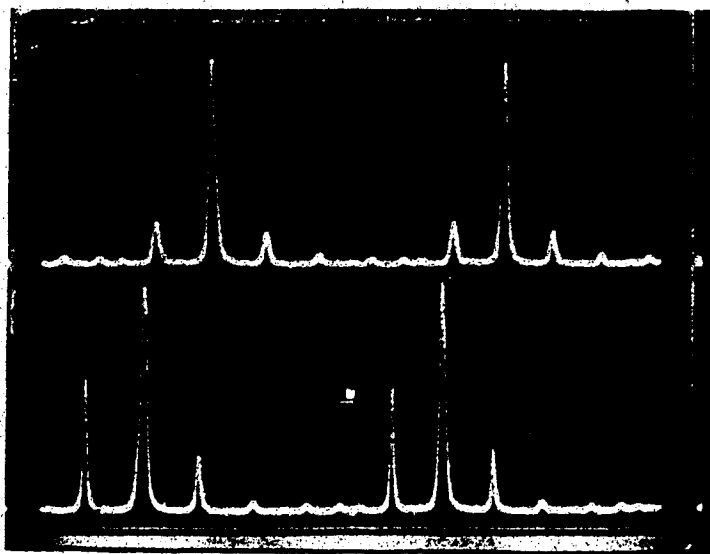
Figure 4-47 Extraneous Feedback Effect of Fabry-Perot
Interferometer

The only difference in the setup between the upper and lower

curves is an angular shift of the Fabry-Perot Interferometer with respect to the optical axis. The figures show a significant change in the spectrum. The side mode suppression ratio is 3.7/1 in the upper curve and 1.7/1 in the lower curve. The apparent lateral shift between the two spectra is due to the optical path length change caused by rotating the interferometer about an axis vertical to its optical axis.

In summary, the extraneous feedback from the grin rod lens made it not possible to verify the theory of Osmundsen and Gade using grating feedback. However, the laser did behave favourably to external grating feedback. It was possible to select a single longitudinal mode with an associated improvement in the side mode suppression ratio. In addition the laser was readily tuned by rotating the grating.

5. CONCLUSION

The experimental results obtained from investigations of the three external cavities:

1. short external cavity with a mirror,

2. long external cavity with a mirror, and

3. long external cavity with a diffraction grating

indicate very positively that the spectrum of the laser may be influenced and controlled with external feedback. The results of Section 4.4.2, which are in agreement with the weak feedback theory put forth by Osmundsen and Gade [23], in conjunction with the demonsration of single longitudinal mode selection and tuning in Section 4.4.3, indicate that it is feasible to proceed to develop a single longitudinal mode narrow linewidth laser using external cavity techniques.

The discrepancy raised by successful results reported for both strong and weak feedback remains unresolved. There is opportunity for a research program aimed at determining the reasons why both strong and weak feedback yield successful results. Furthermore, both weak and strong feedback theories should be formally extended to the case where the external reflector consists of a diffraction grating. Successful results using a diffraction grating are presented in this thesis as well as in published papers [17,30]. However, no theoretical analyses have been published which address the case where the external reflector is a diffraction grating.

In the continuing work on this project it is important to implement several changes to the experimental apparatus and procedures prior to undertaking an attempt to achieve narrow linewidth, single longitudinal mode oscillation of a semiconductor laser. The laser is extremely sensitive to perturbations in the external cavity. This extreme sensitivity places very stringent requirements on the mechanics of the compound cavity system. Many resources are generally dedicated towards obtaining a high degree of mechanical stability and precision [29].

The following points and recommendations, which arise from correspondence with an expert in the area of external cavity feedback (Appendix A) and from the author's experience, should be incorporated into subsequent attempts, by persons whose long term objectives require such a device, to develop a narrow linewidth laser using external cavity techniques:

1. Directly pursue the configuration used by Wyatt et al. in their successful external cavity feedback experiments. (No verification of the strong feedback theory put forth by Sato et al. [25] and discussed in Section 3.3 was obtained. However, according to Wyatt and Sato, compound cavity systems with strong feedback are more stable than weak feedback systems and hence, are more attractive.)

2. Utilize the long external cavity with diffraction grating.

3. The external cavity collimating lens must be anti-reflection coated and of such type that it may be located several millimeters away from the laser (ie. X20 .5 NA microscope objective) to minimize extraneous feedback influences.

4. Isolate all observation optics from the laser.

5. Use beam dividing devices (couplers or cube beam splitters) to allow simultaneous observation of optical output power, the laser spectrum, and the spectral linewidth.

6. Develop a technique for observing the feedback image on the laser face [30] to assist alignment.

7. Implement a high resolution technique for measuring the laser spectral width [31].

8. Use piezoelectric positioning devices for all optics which are to be used for tuning the laser.

9. Use optical mounting equipment which allows the necessary degrees of freedom for positioning without sacrificing rigidity and precision.

A narrow linewidth, single longitudinal mode, semiconductor laser is a necessary prerequisite for an economical coherent optical communication system. Such lasers have been developed in laboratories throughout the world. The same laboratories are proceeding with experimental coherent optical communication systems and are significantly further advanced than any similar projects, known to the author, which are being undertaken in Canada.

It is very important that the coherent optical
communications project be placed into an atmosphere of
strong theoretical knowledge, solid experimental background,
and substantial financial resources if it is to succeed.

REFERENCES

1. A.L. Schawlow and C.H. Townes, "Infrared and Optical Masers", Physical Review, Vol. 112, pp.1940-1949, 1958.

2. T.H. Maiman, "Stimulated Optical Radiation in Ruby", Nature, Vol. 187, pp.493-494, 1960.

3. F.E. Goodwin and M.E. Pendinoff, "Application of CCL_4 and CCL_4:CCL_2 Ultrasonic Modulators to Infrared Optical Heterodyne Experiments", Applied Physics Letters, Vol. 8, pp. 60-61, 1966.

4. F.E. Goodwin, "A 3.39μm Infrared Optical Heterodyne Communication System", IEEE Journal of Quantum Electronics, Vol. QE-3, pp. 524-531, 1967.

5. F.E. Goodwin and T.A. Nussmeier, "Optical Heterodyne Communications Experiments at 10.6μm", IEEE Journal of Electronics, Vol. QE-4, pp. 612-617, 1968.

6. Hans W. Mocker, "A 10.6μm Optical Heterodyne Communication System", Applied Optics, Vol. 8, pp. 677-684, 1969.

7. I. Goldstein, P.A. Miles, and A. Chabot, "Heterodyne Measurements of Light Propagation Through Atmospheric Turbulence", Proc. IEEE, 53, pp. 1172-1180, 1965.

8. O.E. Delange and A.F. Dietrich, "Optical Heterodyne With Enclosed Transmission Paths", Bell System Technical Journal, Vol.47, No.2, pp. 161-178, 1968.

9. K.C. Kao and G.A. Hockman, "Dielectric Fiber Surface Waveguides for Optical Frequencies", Proc. IEEE, Vol. 133, pp. 1151, 1966.

10. F.P. Kapron, D.B. Keck, and R.D. Maurer, "Radiation Losses in Glass Optical Waveguides", Applied Physics Letters Vol. 17, pp. 423-425, 1970.

11. T. Miya, Y. Terunma, T. Hosaka, and T. Miyashita, "Ultimate Low-Loss Single Mode Fiber at 1.55μm", Electronic Letters, Vol. 15(4), 1979.

12. J.E. Geusic, W.B. Bridges, and J.I. Parkove, "Coherent Optical Sources for Communications", Proc. IEEE, Vol 58, pp. 1419-1439, 1970.

13. S. Saito, Y. Yamamato, and T. Kimura, "Optical Heterodyne Detection of Directly Frequency Modulated Semiconductor Laser Signals", Electronics Letters, Vol. 16, No.22, 1980.

14. I.W. Stanley, "A Tutorial Review of Techniques for Coherent Optical Fiber Transmission Systems", IEEE Communications Magazine, Vol. 23, No.8, pp. 37-53, 1985.

15. T. Okoshi, "Heterodyne and Coherent Optical Fiber Communications: Recent Progress", IEEE Transactions on Microwave Theory and Techniques, Vol. MTT-30, No.8, 1982.

16. G. Jacobsen and I. Garrett, "A Theoretical Analysis of Coherent Optical Communication Receivers with Non-negligible Laser Linewidths", Electromagnetics Institute Report N.R297, Technical University of Denmark, 1984.

17. R. Wyatt and W.J. Devlin, "10KHz Linewidth 1.5μmInGaAsP External Cavity Laser With 55nm Tuning Range", Electronics Letters, Vol. 19, No.3, pp. 110-112, 1983.

18. A. Yariv, Quantum Electronics, 3d Ed. New York: Holt, Rinehart, and Winston, 1985.

19. E. Hecht and A. Zajac, Optics, 4th Ed. Massachusetts: Addison-Wesley Publishing Company, 1979.

20. C.H. Henry, "Theory of the Linewidth of Semiconductor Lasers", IEEE J.Q.E., Vol. QE-18, No.2, pp. 259-264, 1982.

21. J. McMullin, Quote, "You can model anything with anything.", Communication Summer Seminar Series, University of Alberta, June 1985., ,

22. A. Olsson and C.L. Tang, "Coherent Optical Interference Effects in External Cavity Semiconductor Lasers", IEEE J.Q.E., Vol. QE-17, No.8, pp. 1320-1323, 1981.

23. J.H. Osmundsen and N. Gade, "Influence of Optical Feedback on Laser Frequency Spectrum and Threshold Conditions", IEEE J.Q.E., Vol. QE-19, No.3, pp. 465-469, 1983.

24. L. Goldberg, H.F. Talor, A. Dandridge, J. Weller, and R.O. Miles, "Spectral Characteristics of Semiconductor Lasers with Optical Feedback", IEEE J.Q.E., Vol. QE-18, No.4, pp. 555-564, 1982.

25. H. Sato, T. Fujita, and J. Ohya, "Theoretical Analysis of Longitudinal Mode Coupling in External Cavity Semiconductor Lasers", IEEE J.Q.E., Vol. QE-21, No.4, pp. 284-291, 1985.

26. A.P. Bogatov, P.G. Eliseev, L.P. Ivanov, A.S. Logginov, M.A. Manko, and K. YA. Senatorov, "Study of the Single-Mode Injection Laser", IEEE J.Q.E., Vol. QE-9, No.2, pp. 392-394, 1973.

27. F.A.Jenkins and H.E.White, Fundamentals of Physical Optics, 1st Ed. New York: McGraw-Hill Book Company Inc., 1937.

28. H. Higuchi, H Namazaki, E. Oomura, R. Hirano, Y. Sakibara, W. Susaski, and K. Fujikawa, "Internal Loss of InGaAsP/InP Buried Crescent (1.3μm) Laser", Applied Physics Letters, Vol. 41, pp. 320-321, 1982.

29. M.W. Fleming and A. Moorandian, "Spectral Characteristics of External-Cavity Controlled Semiconductor Lasers", IEEE J.Q.E., Vol. QE-17, No.1, pp. 44-59, 1981.

30. T. Fujita, S. Ishizuka, K. Fujito, H. Serizawa, and
    H. Sato, "Intensity Noise Suppression and Modulation
    Characteristics of a Laser Diode Coupled to an External
    Cavity", IEEE J.Q.E., Vol. QE-20, No.5, 1984

31. T. Qkoshi, K. Kikuchi, and A. Nakayama, "Novel Method
    for High Resolution Measurement of Laser Output
    Spectrum", Electronic Letters, Vol.16, No.16,
    pp.630-631, 1980.

Appendix A: Correspondence with Dr.R.Wyatt from BTRL.

Following is a letter received from Dr.R.Wyatt at

British Telecom in Ipswich, England. His letter is in

response to a solicitation for assistance which was sent by

the author in May, 1985.

British Telecom Res.   Labs
Martlesham Heath
IPSWICH
IPS 7RE UK
5/6/85

Dear Mr. Anderson,

    Thank-you for your recent letter re: external cavity
lasers and line narrowing; I will try to answer your
queries.

    All lasers used for external cavity work have had AR
coatings, with reflectivities in the 1-10% range variously.
A very small number of uncoated lasers have been tried -
these were much more critical to align, but could still be
make to work. The coated lasers, when run above threshold,
would have a multi-longitudinal mode spectrum, with maybe
3-7 modes, so single-mode operation of the basic laser is
not at all necessary, provided feedback is high enough (see
later).

    As far as differences between lasers are concerned, we
have used altogether probably 50 lasers, of various types;
buried crescent, DCPBH, and ridge guide, all at 1.5μm.

    Line narrowing is successful with all lasers, but
better transverse mode stability (DCPBH) gives more stable,
less critical output. So, no selection is necessary, other
than fundamental transverse mode operation.

    As far as your experiemental configuration is concered,
I would recommend a much higher NA objective - we typically
use a X20/.54 NA, AR coated for 1.5μm. We have not got
consistently good results with X10 objectives. Attenuation
should be unnecessary, if alignment is correct -try aligning

130

for minimum threshold, you should get down below 15mA
easily. Isolation/attenuation between laser and
interferometer will also help stability. Temperature
control is not necessary, few °C is OK, and current control
to few mA is all that's needed.

      Osmundsen and Gade's work does not apply to our
situation. We have a grating cavity; they were considering
only a plane mirror, and the selectivity of our grating is
high enough to select one mode.

      I hope these points help - if you want more
information, please call/telex, and keep me informed.

Yours,

Richard Wyatt

Following is the body of the letter which Dr. Wyatt's letter was in reply to.

Dear Drs. Wyatt and Devlin,

I am presently a graduate student at the University of Alberta. My thesis project is to demonstrate and understand frequency control of semiconductor lasers using external grating feedback techniques. I will greatly appreciate your assistance with some questions which I have.

To date, I have experimented with two 1.3μm lasers with no success. The first laser was a rudimentary gain guided device with A.R. coating on one facet. This laser was inherently unstable and I was not particularly surprised with the poor results. The second laser is of the double channel planar buried heterostructure (DC-PBH) configuration, produced by Fermionics Corporation in Chatsworth, California.

This laser appears to be quite stable with only a minor noise component at 750Mhz, at 30 mA (Threshold = 18 mA). However, the spectrum does not respond to increasing current as expected. The laser does not tend towards oscillation in one longitudinal mode as the current increases, but instead, it continues to support five modes. It also does not respond favourably to feedback. I am able to influence the different longitudinal modes by rotating the grating. However, I am not able to select a single longitudinal mode with the associated high side mode suppression.

My first set of questions are:

Out of a group of 100 lasers of the type which you use in your systems (Electronic Letters: Feb. 1983, Jan. 1985), how many would you expect to respond satisfactorily to external feedback?

Do you have a set of criteria for selecting a laser based upon its properties without feedback?

Is the anti-reflection coating a critical requirement? The work of Goldberg et al (IEEE J.Q.E. Vol.18, April 1982, pp.555) implies A.R. coating is not essential.

My experimental configuration consists of a X10 .25 NA microscope objective for collimating the output beam onto a 1200 lines/mm grating. A pair of crossed polarizers with a half wavelength retarder for variable attenuation are inserted in the external cavity. (I have experimented with cavity lengths of 20 to 50 cm.). The spectrum is monitored with a scanning Fabry-Perot interferometer. There is no isolation between the interferometer and the laser. The temperature and current are feedback controlled. Neither exhibits large fluctuations over time. However, I do not have the equipment to measure very small fluctuations. I can only assume that the control is adequate.

My second set of questions are: .

Do you have an explanation for the behaviour of your lasers under strong optical feedback? You are not using any attenuation, other than losses in your cavity. The work of Osmundsen and Gade (IEEE J.Q.E. Vol.19, March 1983, pp.465) indicates that, under strong feedback, the multi-external cavity modes supported will result in line broadening.

Is it extremely important to have high precision current and temperature control? I realize this is important for fine tuning, but is it necessary for "first order" observations?

The answers to these questions will be invaluable. I feel I am following correct procedures. However, I am not able to achieve the desired results. I suspect my problem is that I do not have a laser that will respond favourably under feedback conditions. The answers to my questions will enable me to procede with more insight than I have in the past.
Thank-you for your assistance.

Sincerely,

Rod Anderson